

**R-08-107**

# **Complementary modelling of radionuclide retention in the near-surface system at Forsmark**

## **Development of a reactive transport model using Forsmark 1.2 data**

Clara Sena, Fidel Grandia, David Arcos,  
Jorge Molinero, Lara Duro  
Amphos XXI Consulting S.L.

October 2008

**Svensk Kärnbränslehantering AB**

Swedish Nuclear Fuel  
and Waste Management Co  
Box 250, SE-101 24 Stockholm  
Tel +46 8 459 84 00



# **Complementary modelling of radionuclide retention in the near-surface system at Forsmark**

## **Development of a reactive transport model using Forsmark 1.2 data**

Clara Sena, Fidel Grandia, David Arcos,  
Jorge Molinero, Lara Duro  
Amphos XXI Consulting S.L.

October 2008

This report concerns a study which was conducted for SKB. The conclusions and viewpoints presented in the report are those of the authors and do not necessarily coincide with those of the client.

A pdf version of this document can be downloaded from [www.skb.se](http://www.skb.se).

# Summary

The Swedish Nuclear Fuel and Waste Management Company (SKB) is conducting a comprehensive geoscientific characterization of two alternative sites to allocate a deep geological repository of high level nuclear waste. The Site Characterization Program also includes the near-surface systems, which are expected to constitute the last geological barrier between the repository system and the earth's surface. The evaluation of the retention capacity of the near-surface systems is, therefore, very relevant for the site characterization program.

From the geological point of view, near-surface systems in the Forsmark area consist of Quaternary deposits that overlay a granitic bedrock. Glacial till is the most abundant outcropping Quaternary deposit (~75% of surface extension) and the remainder is made up of clayey materials (glacial and post-glacial clays). These types of near-surface sediments show distinctive hydraulic and geochemical features. The main reactive mineral in the till deposits, for the time scale considered in this work, is calcium carbonate (calcite). This mineral is found along with clay minerals (e.g. illite) and Fe(III) hydroxides. In contrast, glacial and post-glacial clays are basically composed of illite with minor amounts of calcium carbonate, and containing organic matter-rich levels (*gyttja*) which can promote reducing conditions in the system.

The assessment of the migration behaviour of selected long-lived radionuclides through the near-surface system of Forsmark was developed in /Grandia et al. 2007/, that focused on the evaluation of the capacity of the Quaternary deposits for radionuclide retention. The work reported here is an improvement of the geochemical conceptual and numerical model presented in /Grandia et al. 2007/, based on data available in the Site Descriptive Model v 1.2 (Forsmark).

Regarding the geochemical variability of the Quaternary deposits present at Forsmark and its implications on radionuclide mobility through the near-surface systems, a sensitivity analysis of the more relevant parameters considered in the reactive transport numerical models built in /Grandia et al. 2007/ is also presented here.

From the main report of the SR-Can project /SKB 2006/ it is stated that Ra is one of the radionuclides with greater contribution to the radioactive doses that might be transferred to the biosphere in the context of repository release. For this reason, Ra was added to the set of radionuclides selected in /Grandia et al. 2007/ (Sr, Cs, and U).

Another improvement in the numerical simulations presented here is the calculation of the hydrogeochemical steady state of the near-surface system, prior to repository release. This is done to approach the present-day conditions at Forsmark. In addition, radionuclides derived from repository release have been discriminated from those of natural origin, already present in the groundwaters. Radionuclides coming from repository were labelled as <sup>RD</sup>Cs, <sup>RD</sup>Sr, and <sup>RD</sup>U (RD stands for repository-derived). Ra was not labelled since the presence of this radionuclide in the modelled domain is exclusively attributed to repository release due to the extremely low concentrations observed in the natural waters of Forsmark.

The results attained in the reactive transport models built in this work show that the near-surface systems at Forsmark constitute a geochemical reactive barrier able to retain radionuclides by several key processes, namely cation exchange, adsorption on mineral surfaces and precipitation of pure phases and solid solutions.

The reactive transport simulations predict that repository-derived Sr, U, and Cs are retained in the solid phase of both Quaternary deposits under study, while Ra is effectively retained in the till deposit only. Ra is not retained in the glacial clay deposit since saturation of barite, which is the only retention mechanism considered in the simulations for this radionuclide, is not reached in this system.

The simulations indicate that, in the till deposit, Sr is retained via cation exchange and co-precipitation with calcite, U is retained due to the adsorption on ferrihydrite, Cs is retained via cation exchange and Ra is retained due to its co-precipitation with barite. On the other hand, in the glacial clay deposit, the simulations indicate that both Sr and Cs are retained by the same processes as identified for the till deposit, while U is retained by precipitation of amorphous uraninite.

# Contents

<b>1</b>	<b>Introduction</b>	7
1.1	Motivation and context	7
1.2	Objectives	7
1.3	Scope	8
1.4	Selection of radionuclides	9
<b>2</b>	<b>Description of conceptual models</b>	11
<b>3</b>	<b>Description of numerical models</b>	15
3.1	Hydrodynamic processes and parameters	15
3.2	Geochemical processes and parameters	16
3.2.1	Reference case #1: The till system	16
3.2.2	Reference case #2: The clay system	21
3.3	Numerical tool and thermodynamic database	22
<b>4</b>	<b>Numerical models setup</b>	23
4.1	Refinement of geochemical initial and boundary conditions	23
4.1.1	Reference case #1: The till system	23
4.1.2	Reference case #2: The clay system	25
4.2	Spatial and time discretisation	26
4.2.1	Reference case #1: The till system	26
4.2.2	Reference case #2: The clay system	27
4.3	Initial and boundary conditions	28
4.3.1	Reference case #1: The till system	28
4.3.2	Reference case #2: The clay system	34
4.4	Set-up of the sensitivity analysis	37
4.4.1	Reference case #1: The till system	37
4.4.2	Reference case #2: The clay system	38
<b>5</b>	<b>Numerical model results</b>	41
5.1	Reference case #1: The till system	41
5.1.1	Conservative transport	41
5.1.2	Reactive transport prior to repository release	42
5.1.3	Reactive transport after repository release	45
5.1.4	Conservative transport versus reactive transport	49
5.1.5	Quantitative assessment of the retention efficiency	51
5.1.6	Sensitivity analysis	55
5.2	Reference case #2: The clay system	56
5.2.1	Conservative transport	56
5.2.2	Reactive transport prior to repository release	58
5.2.3	Reactive transport after repository release	59
5.2.4	Conservative transport versus reactive transport	62
5.2.5	Quantitative assessment of the retention efficiency	64
5.2.6	Sensitivity analysis	66
<b>6</b>	<b>Distribution coefficient (<math>K_d</math>)</b>	69
6.1	Applicability of $K_d$ models	69
6.2	$K_d$ values from model outputs	69
6.2.1	Reference case #1: The till system	70
6.2.2	Reference case #2: The clay system	74
6.3	Application of $K_d$ -based numerical models in the near-surface deposits at Forsmark	77
6.3.1	Reference case #1: The till deposit	77
6.3.2	Reference case #2: The clay deposit	79
<b>7</b>	<b>Conclusions</b>	81
<b>8</b>	<b>References</b>	85

# 1 Introduction

## 1.1 Motivation and context

The Swedish Nuclear Fuel and Waste Management Company (SKB) is investigating two alternative sites to allocate a deep geological repository for the disposal of high level radioactive waste. SKB's intention is to assemble all the information that is required to choose one of the sites, and to submit a license application for a deep repository. In this context, SKB is conducting a comprehensive geoscientific characterization and modelling work. The results from the investigations at the sites are used as a basic input to the site descriptive modelling, which will summarise the current state of knowledge of the site, and will provide parameters and models to be used in further analyses within Safety Assessment, Repository Design and Environmental Impact Assessment.

One important component of the site description modelling approach is the so-called near-surface system, mainly composed of Quaternary deposits. The near-surface system is actually the transitional zone between the bedrock (also referred to as geosphere) and the surface system (also referred to as biosphere).

Near-surface systems (Quaternary deposits) would be the last natural barrier for an eventual radionuclide release from the repository to the surface. In this context, the evaluation of the radionuclide retention capacity of the near-surface system was developed in /Grandia et al. 2007/. From this evaluation it was possible to identify the main processes that affect the mobility of each studied radionuclide.

In order to improve the numerical models developed in /Grandia et al. 2007/ with respect to site specific features of the till and glacial clay deposits at Forsmark, the geochemical initial and boundary conditions were refined in the present work. Due to the natural geochemical variability of the modelled Quaternary deposits, a sensitivity analysis for key geochemical parameters that affect radionuclide mobility has been developed.

From the main report of the SR-Can Project /SKB 2006/ it is stated that Ra may be responsible for most of the radioactive doses transferred to the biosphere due to repository release, after long periods of time. Therefore this radionuclide was added to the radionuclide selection made in /Grandia et al. 2007/ (Cs, Sr, and U), and incorporated in the reactive transport numerical models developed in the present work.

The numerical approach has also been improved by attaining a hydrogeochemical steady state (of till and glacial clay deposits), which reflects the present day geochemical conditions of the near-surface systems at Forsmark, prior to the release of radionuclides from the repository. The radionuclides released from the repository in the next stage were labelled as follows:  $^{RD}Cs$ ,  $^{RD}Sr$ , and  $^{RD}U$  (RD standing for repository-derived, see section 4.3.1), to discriminate them from those naturally occurring in the near-surface systems at Forsmark. Ra concentration in the numerical models prior to repository release is considered to be below detection limit and therefore the presence of this radionuclide in the modelled domains is attributed exclusively to repository release.

## 1.2 Objectives

This work has two main objectives:

1. To improve the geochemical conceptual and numerical models of the till and glacial clay deposits based on the available data of Forsmark, and therefore achieve more realistic results.
2. To evaluate the impact of considering distinct geochemical scenarios on radionuclide mobility, reflecting the natural geochemical variability.

### 1.3 Scope

The work reported here is based on “datafreeze” 1.2 and the corresponding Site Descriptive Model version 1.2 of Forsmark site, as it is described in /SKB 2005b/. It is worth mentioning that major conceptual updates have been produced recently in Forsmark, mainly concerning the bedrock hydrogeological model. This fact could lead to some discrepancies with the hydrogeological assumptions adopted here. It must be clarified that the outcomes of this work are intended to be quantitative and realistic but not “site descriptive” for a particular catchment or place in the Forsmark candidate site.

The behaviour of selected long-lived radionuclides in the near-surface Quaternary deposits of the Forsmark site was evaluated and numerically modelled in /Grandia et al. 2007/. Due to their particular chemical nature, these elements will be selectively retained by distinct mechanisms. From the available data and comparing with other examples in similar environments, the more favourable retention mechanisms were determined.

As shown in /Grandia et al. 2007/, the evaluation of the retention capacity of the Quaternary deposits is made considering that radionuclides would migrate from deep bedrock to the surface so that the near-surface deposits will eventually interact with these radionuclides (Figure 1-1).

The report starts with a summary of the conceptual and numerical models described in /Grandia et al. 2007/ (Chapters 2 and 3). Chapter 4 shows the refinement of the geochemical conceptual models that represent the reference cases for the till and glacial clay deposits, and the setup of the sensitivity analysis. Chapter 5 deals with the numerical model results, and the evaluation of the retention capacity for the different geochemical scenarios considered. In Chapter 6, a study of the distribution coefficients ( $K_d$ ) of the studied radionuclides in the modelled domains is developed, together with the application of  $K_d$  models as an alternative methodology to the reactive transport simulations developed in the reference cases. Finally, the main conclusions are summarized in Chapter 7 of the report.

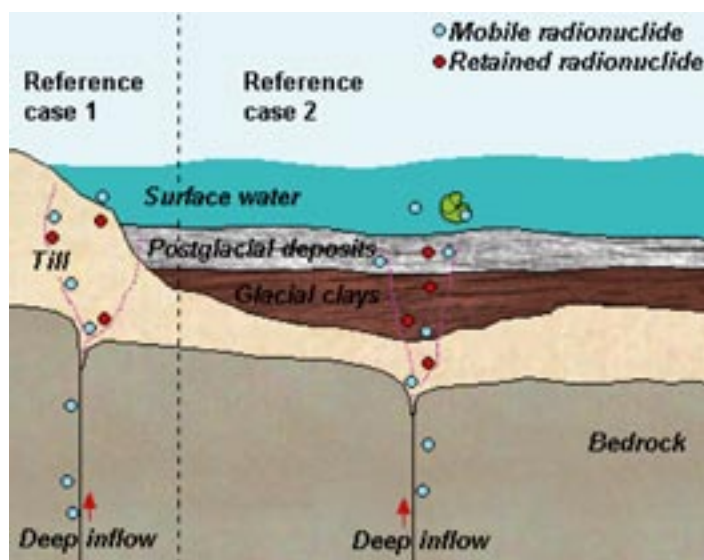


*Figure 1-1. Transition zones between bedrock and surface systems in the Forsmark area. Glacial (till and lacustrine clays) and post-glacial deposits are interface zones where radionuclides migration can be retarded.*

## 1.4 Selection of radionuclides

Concepts of deep geological disposal are designed to retard for long periods of time the migration of radionuclides to the surface. During this retention time, the concentration of many radionuclides decreases to negligible levels since their half lives are relatively short. In performance and safety assessment of deep repositories of high-level nuclear waste, only radionuclides with long half lives are expected to access the surface. Among these long-lived radionuclides, we select four for modelling purposes, based on the following considerations:

- Uranium as a redox-sensitive actinide.
- Radium as the main contributor of radioactive doses to the surface systems /SKB 2006/.
- Caesium as monovalent cation radionuclide that participates in cation exchange in the illite interlayer. This radionuclide is also an important dose contributor /SKB 2006/.
- Strontium as divalent cation radionuclide that interacts with carbonate minerals and participates in cation exchange in the illite interlayer.



## 2 Description of conceptual models

The retention capacity of the near-surface system in the Quaternary deposits was evaluated by means of reactive solute transport simulations in /Grandia et al. 2007/, considering two distinct domains.

The first reference case simulates a Quaternary till deposit overlying a granite bedrock. In this model deep groundwater containing dissolved radionuclides is assumed to migrate upwards through a fracture in the granite rock and eventually transfer these radionuclides to the Quaternary deposits (through the bottom boundary of the modelled domain, Figure 2-1). The Quaternary deposits are assumed to be hydraulically connected to a surface discharge zone. Figure 2-1 shows the conceptual sketch of the first reference case.

The second reference case simulates a glacial clay that is present at the bottom of a discharge zone (such as a lake or the Baltic Sea), and is overlying the till deposit. In order to evaluate the retention capacity of the glacial clay, it is assumed that deep groundwater can flow through a preferential path in the till, that contacts directly with the bottom of the clay layer. Figure 2-2 shows the conceptual sketch of the second reference case.

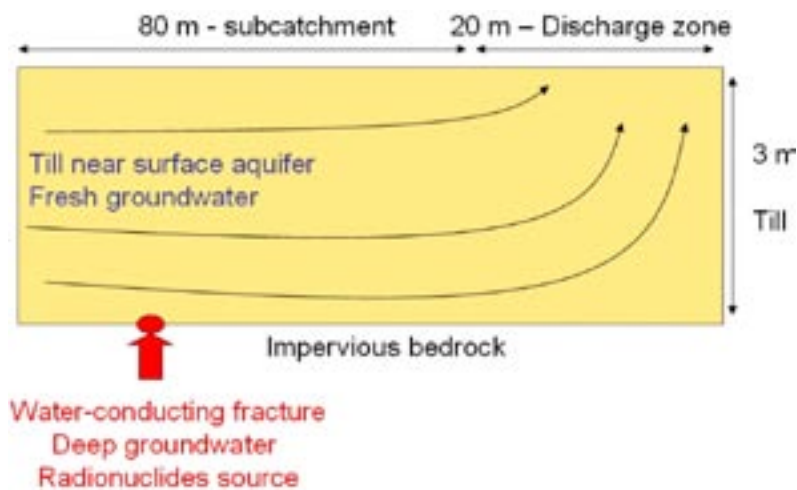


Figure 2-1. Sketch of reference case #1.

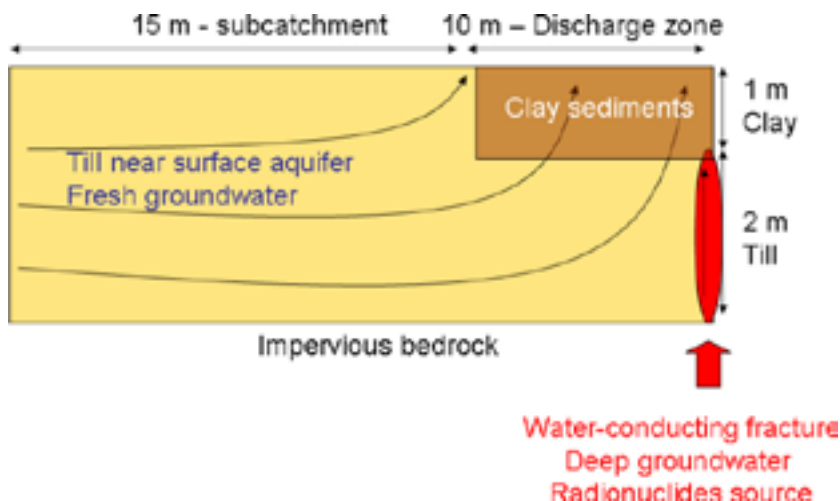


Figure 2-2. Sketch of reference case #2.

Three different waters are considered in the numerical models:

*Till shallow groundwater:* Overall, the chemistry of shallow groundwaters flowing through till is fairly constant, with a predominance of  $\text{Ca}^{2+}$  and  $\text{HCO}_3^-$  that reflects the equilibrium with the solid phase. The average composition of water sampled in well SFM0002 /Tröjbom and Söderbäck 2006/ has been selected as the till reference water for numerical calculations /Grandia et al. 2007/. This selection is made according to the following considerations: (1) This soil pipe has been repeatedly sampled (11 measurements), (2) it shows small seasonal changes, (3) it is saturated with calcite (i.e. equilibrium with the till), (4) it provides analytical data on redox sensitive elements (Fe, Mn, U), and (5) data on other elements of interest in the present work (Sr, Cs, Ba,  $\text{NH}_4^+$ ) are available. Points 2 and 3 provide evidence that the residence time of this groundwater in the till is relatively long. The availability of data on redox sensitive elements is especially relevant to determine the redox state of the water since little information on the redox potential is provided. The reference water for the till shallow groundwater, used for the numerical simulations, has been calculated by averaging the concentrations in the data available from the water samples collected in the well SFM0002. The complete chemical composition of the water taken from the SFM0002 soil pipe is listed in Table 2-1.

*Glacial clay porewater:* In contrast to the till groundwaters, the glacial clay porewater composition in the Forsmark area was not reported at the time for the start of the present work. The chemical composition though, is expected to be similar to lake bottom waters, perhaps with some modification due to biologic activity and water-sediments interaction. Therefore, water samples collected at the bottom of a lake (Lake Eckarfjärden, sampling point PFM117 /Andersson et al. 2003/) have been selected in /Grandia et al. 2007/ to set up the initial conditions of the glacial clay sediments (Table 2-1). These waters are relatively diluted (ionic strength  $\sim 6.0 \times 10^{-3} \text{ mol} \cdot \text{L}^{-1}$ ) Ca- $\text{HCO}_3$  waters. Characteristically, they show high contents of organic compounds, either dissolved or as suspended particulate ( $[\text{DOC}] \sim 1.50 \times 10^{-3} \text{ mol} \cdot \text{L}^{-1}$ ). In order to approach the composition of a glacial clay porewater at Forsmark, the water sample collected from the sampling point PFM117 has been equilibrated with the reactive minerals considered for the simulation of the glacial clay, using the code PHREEQC /Parkhurst and Appelo 1999/. The reactive minerals used for this calculation are pyrite, calcite and siderite, as shown in section 4.1.2.

*Radionuclide-bearing deep groundwater:* It is difficult to select a single sample for the bottom boundary condition since several chemically different waters occur underground in the Forsmark area. For the calculations, we have selected the average composition of groundwater sampled in soil pipe SFM0023 /Tröjbom and Söderbäck 2006/. The selected composition is obtained by averaging the available data from the water samples collected in soil pipe SFM0023. Despite its relatively shallow occurrence, this groundwater shares many geochemical features with deep groundwaters: It is a Na-Cl water with a moderate salinity (ionic strength =  $0.2 \text{ mol} \cdot \text{L}^{-1}$ ) (Table 2-1) and long residence time according to  $^3\text{H}$  and  $^{14}\text{C}$  data.

In /Grandia et al. 2007/ three radionuclides have been selected for numerical modelling: U, Cs and Sr. The reason for this selection is related to the fact that experimental data for the retention mechanisms (mainly cation exchange and surface complexation) are available in scientific literature, so that it can be implemented properly in the calculations.

In the present report, an additional radionuclide is selected for numerical modelling purposes:  $^{226}\text{Ra}$ . This modification with respect to the previous radionuclides selection (reported in /Grandia et al. 2007/) is related to the fact that the main safety assessment report of SKB reveals that  $^{226}\text{Ra}$  may be the main dose contributor from a repository release /SKB 2006, cf. Figure 10-14/.

**Table 2-1. Chemistry of the selected waters for numerical calculations. Concentrations in mol·L<sup>-1</sup>. Data taken from: (1) /Tröjbom and Söderbäck 2006/, and (2) /Andersson et al. 2003/.**

	SFM0002 <sup>(1)</sup>	PFM117 bottom <sup>(2)</sup>	SFM0023 <sup>(1)</sup>
pH	7.20	8.00	6.68
[Na] <sub>total</sub>	$1.22 \times 10^{-3}$	$2.65 \times 10^{-4}$	$6.93 \times 10^{-2}$
[K] <sub>total</sub>	$1.22 \times 10^{-4}$	$5.20 \times 10^{-5}$	$1.67 \times 10^{-3}$
[Ca] <sub>total</sub>	$2.89 \times 10^{-3}$	$1.19 \times 10^{-3}$	$1.32 \times 10^{-2}$
[Mg] <sub>total</sub>	$3.53 \times 10^{-4}$	$1.17 \times 10^{-4}$	$7.18 \times 10^{-3}$
[C] <sub>total</sub>	$5.66 \times 10^{-3}$	$2.51 \times 10^{-3}$	$2.14 \times 10^{-3}$
[Cl] <sub>total</sub>	$1.90 \times 10^{-3}$	$1.53 \times 10^{-4}$	$1.07 \times 10^{-1}$
[S] <sub>total</sub>	$2.41 \times 10^{-4}$	$6.39 \times 10^{-5}$	$3.73 \times 10^{-3}$
[Si] <sub>total</sub>	$9.74 \times 10^{-5}$	$4.63 \times 10^{-5}$	$7.56 \times 10^{-5}$
[Fe] <sub>total</sub>	$3.46 \times 10^{-5}$	$8.34 \times 10^{-7}$	$4.91 \times 10^{-4}$
[Fe(II)]	$3.44 \times 10^{-5}$	–	–
[Mn] <sub>total</sub>	$3.86 \times 10^{-6}$	–	$1.56 \times 10^{-5}$
[Sr] <sub>total</sub>	$2.09 \times 10^{-6}$	$6.23 \times 10^{-7}$	$4.13 \times 10^{-5}$
[U] <sub>total</sub>	$2.27 \times 10^{-8}$	$5.02 \times 10^{-9}$	$4.62 \times 10^{-10}$
[Cs] <sub>total</sub>	$6.47 \times 10^{-11}$	$4.51 \times 10^{-11}$	$1.62 \times 10^{-8}$ (*)
[NH <sub>4</sub> <sup>+</sup> ]	$6.61 \times 10^{-6}$	$1.82 \times 10^{-5}$	$1.95 \times 10^{-4}$
[PO <sub>4</sub> <sup>3-</sup> ]	$1.39 \times 10^{-7}$	$4.80 \times 10^{-8}$	$3.80 \times 10^{-8}$
[O <sub>2</sub> ]	$4.27 \times 10^{-5}$	–	–
DOC	$1.22 \times 10^{-3}$	$1.49 \times 10^{-3}$	$3.29 \times 10^{-4}$
[Ba] <sub>total</sub>	$7.28 \times 10^{-7}$	$1.44 \times 10^{-7}$	$1.94 \times 10^{-7}$

(\*) Taken from maximum Cs concentration in water sample of KFM01A soil pipe.

### 3 Description of numerical models

#### 3.1 Hydrodynamic processes and parameters

As shown in /Grandia et al. 2007/, for numerical modelling purposes groundwater flow through porous media is assumed to be governed by Darcy's Law. The code used for the numerical simulations solves the groundwater flow equation that combines Darcy's law and the mass balance equation of water. In addition, the solute transport processes considered in the model are: (1) advection, (2) molecular diffusion and (3) hydrodynamic dispersion. The equation governing solute transport through porous media is derived from the principle of mass conservation accounting for the mass fluxes due to the three above-mentioned processes.

In the current models it is assumed that the till deposits host a near-surface aquifer with an average recharge of 66 mm/year. In addition, from the fracture in the underlying granitic bedrock 2 mm/year of deep groundwater is transferred into the till phreatic aquifer. All these values are interpreted from water balance calculations in the MIKE SHE modelling of the Forsmark area reported in /Johansson et al. 2005/. According to available characterization data of the Quaternary deposits a thickness of 3 m has been assumed in the model for the till /Johansson et al. 2005/. The modelled till domain was divided along the vertical axis into three layers. The top 0.8 m-layer and the bottom 0.8 m-layer are more conductive than the intermediate layer (1.4 m) of lower permeability (Figure 3-1).

The whole till domain is assumed anisotropic with a vertical hydraulic conductivity 10 times lower than the horizontal hydraulic conductivity. The effective porosity is also stratified with higher porosity values in the surface layer, reflecting a higher level of weathering and physical degradation closer to the surface /Johansson et al. 2005/. Table 3-1 shows all the hydrodynamic parameters used in the numerical simulations. Hydraulic conductivity and porosity values have been taken from /Johansson et al. 2005/.

The values of transverse and longitudinal dispersivities used in the numerical simulations have been attributed according to realistic values for the dimension of the modelled domain that do not lead to a significant numerical dispersion. The diffusion coefficient has been set according to characteristic values of clayey sediments, while for the till system it is considered negligible.

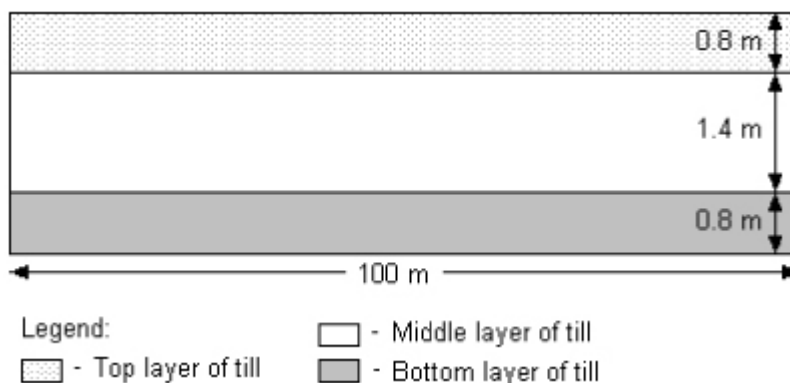


**Figure 3-1.** Layering of the till domain, from /Johansson et al. 2005/. The till is composed of three layers that show distinct hydraulic properties (Y axis magnified 15 times).

**Table 3-1. Values of the hydrodynamic parameters used in the numerical models. (1) /Johansson et al. 2005/, (2) attributed values.**

Material		$K_{\text{horizontal}}^{(1)}$ (m/s)	$K_{\text{vertical}}^{(1)}$ (m/s)	$\alpha_{\text{longitudinal}}^{(2)}$ (m)	$\alpha_{\text{transverse}}^{(2)}$ (m)	Porosity <sup>(1)</sup> (-)	Diffusion coefficient <sup>(2)</sup> (m <sup>2</sup> /s)
Till	Layer 1	$1.5 \times 10^{-5}$	$1.5 \times 10^{-6}$	0.5	0.2	0.15	negligible
	Layer 2	$1.5 \times 10^{-6}$	$1.5 \times 10^{-7}$	0.5	0.2	0.05	negligible
	Layer 3	$1.5 \times 10^{-5}$	$1.5 \times 10^{-6}$	0.5	0.2	0.05	negligible
Clay		$1.0 \times 10^{-8}$	$1.0 \times 10^{-9}$	0.5	0.2	0.2	$5 \times 10^{-10}$

## 3.2 Geochemical processes and parameters

### 3.2.1 Reference case #1: The till system

#### *Aqueous speciation*

Solute speciation in the groundwaters has been calculated by considering the chemical composition of each water type at the different conditions (i.e. Eh and pH) for each domain considered. The thermodynamic database used in the calculations is described in section 3.3. Since the studied groundwaters are rich in aqueous carbonate, Fe(III) carbonate complexes have been added in the thermodynamic database. These species are  $\text{Fe}(\text{CO}_3)_3^{3-}$  and  $\text{FeOHCO}_3$ . The complexation reactions for these species with the corresponding constants are shown in Table 3-2. Constants are obtained from /Grivé 2005/.

Activity coefficients for charged species have been calculated by using the Davies equation:

$$\log \gamma_{a_i} = -Az_i^2 \left( \frac{I^{1/2}}{1+I^{1/2}} - 0.31 \right) \quad (\text{equation 3-1})$$

where  $I$  is the ionic strength of the solution,  $z_i$  is the electric charge of the species in solution.  $A$  is a constant that depends on temperature.

For uncharged species, the Extended Debye-Hückel equation has been used:

$$\log \gamma_{a_i} = -\frac{Az_i^2(I)^{1/2}}{1+Ba_i(I)^{1/2}} + bI \quad (\text{equation 3-2})$$

where  $a_i$  is the ionic radius of the species in solution.  $A$  and  $B$  are constants that depend on temperature and dielectric water constant. Unless otherwise specified,  $b$  is assumed to be 0.1 for all uncharged species.

**Table 3-2. Complexation reaction of aqueous Fe(III) carbonates and corresponding thermodynamic constants from /Grivé 2005/.**

Reaction	LogK (25°C)
$3\text{HCO}_3^- + \text{Fe}^{2+} \leftrightarrow \text{Fe}(\text{CO}_3)_3^{3-} + 3\text{H}^+ + \text{e}^-$	-19.77
$\text{HCO}_3^- + \text{H}_2\text{O} + \text{Fe}^{2+} \leftrightarrow \text{FeOHCO}_3 + 2\text{H}^+ + \text{e}^-$	-12.59

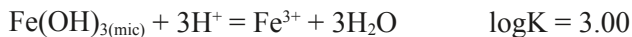
### **Equilibrium with pure mineral phases and solid solutions**

Mineralogical composition of the till shows the existence of calcite, quartz and illite as major minerals (> 5 wt%) /SKB 2005b/. In the reactive transport calculations, calcite is considered to contain trace amounts of Sr forming a solid solution /Grandia et al. 2007, section 3.2.1/.

Illite dissolution kinetics are very slow under the environmental conditions modelled in this study. /Köhler et al. 2003/ found very slow dissolution rates in circumneutral pH's, from  $10^{-14}$  to  $10^{-15}$  mol·m<sup>-2</sup>·s<sup>-1</sup>. Consequently, dissolution of illite is not considered in the numerical simulations, and only participates as a charged surface for cation exchange.

As discussed in /Grandia et al. 2007, section 2.5/, it is very likely that other phases exist at minor and trace concentrations, some of which can play a very important role in the control of the redox conditions and radionuclide retention. Among these, Fe(III)-hydroxide (ferrihydrite) is thought to be the controlling phase for the redox of the till porewater and to be the main uranium sorbent. In the reactive transport, it has been arbitrarily (due to the lack of field data) but reasonably considered an initial concentration of 0.1 wt% in the till.

The log K of the reaction involving this mineral has been long discussed and a wide range of values has been reported in literature. The disparity in the log K values is mainly caused by the variable crystallinity of the samples used in the laboratory experiments. For the numerical simulations in the present study, we have selected the following constant:



which corresponds to microcrystalline ferrihydrite /Grivé 2005/. The thermodynamic constant used in this report differs approximately two orders of magnitude from the one used in /Grandia et al. 2007/ (log K=5.00). The reason for this modification is that the thermodynamic constant considered in /Grandia et al. 2007/ was calculated through 0.45 µm filtration, which accounted for small solid particles, like colloids. Instead, the thermodynamic constant used now was determined through a 0.02 µm filtration, which avoids the influence of colloids /Grivé 2005/.

Another mineral that is not cited in the mineralogical inspections of the till samples is siderite (FeCO<sub>3</sub>). This mineral is redox sensitive and can precipitate in the till domain after the deep inflow. Therefore, in the reactive transport model it is allowed to precipitate if oversaturation in water in this mineral is reached. It is worth mentioning that this mineral rarely precipitates as a pure FeCO<sub>3</sub> but it forms solid solutions with calcium carbonate [ankerite, (Ca,Fe)CO<sub>3</sub>]. The thermodynamics of this solid solution series is still not well known, and therefore, the pure phase is selected for the current model calculations.

According to /Seaman et al. 2001, Fuller et al. 2002, Krestou et al. 2004/, apatite [Ca<sub>5</sub>(OH)(PO<sub>4</sub>)<sub>3</sub>] is a good sorbent for uranium, so that it is interesting to include it in the reactive transport calculations. There is no evidence of apatite in the till, but deep groundwater intrusion could lead to precipitation of this phase and becoming potential uranium sorbent. For this reason, the predicted evolution of the saturation index of this mineral has been monitored in the preliminary simulations. The phosphate concentration is low enough to keep the porewater undersaturated in apatite. However, apatite precipitation is allowed in the model if oversaturation is reached.

A set of minerals has been selected as possible solubility-limiting phases of aqueous uranium. For U(IV), a hydrated, amorphous phase (UO<sub>2</sub>·2H<sub>2</sub>O) has been preferred instead of a crystalline phase (e.g. uraninite, UO<sub>2</sub>). Moreover, coffinite (USiO<sub>4</sub>·nH<sub>2</sub>O) formation is not allowed since it is considered that its precipitation is not kinetically favoured /Grandia et al. 2007, section 3.1/. For U(VI) schoepite [UO<sub>2</sub>(OH)<sub>2</sub>], soddyite [(UO<sub>2</sub>)<sub>2</sub>SiO<sub>4</sub>(H<sub>2</sub>O)<sub>2</sub>], uranophane [Ca(UO<sub>2</sub>)(SiO<sub>3</sub>OH)<sub>2</sub>(H<sub>2</sub>O)<sub>5</sub>] and becquerelite [Ca(UO<sub>2</sub>)<sub>6</sub>O<sub>4</sub>(OH)<sub>6</sub>·8H<sub>2</sub>O] are allowed to precipitate if the solution becomes oversaturated in any of these phases.

In Table 3-3, the dissolution reactions of all minerals considered in the numerical simulations with the corresponding thermodynamic constants have been listed. All reactions are simulated under local equilibrium approach.

**Table 3-3. Dissolution reaction of the reactive solid phases in the numerical simulations. Thermodynamic equilibrium constants and references are also listed.**

Reaction	LogK (25°C)	Reference
Mineral solubility		
Calcite: $\text{CaCO}_3 + \text{H}^+ \leftrightarrow \text{Ca}^{2+} + \text{HCO}_3^-$ <sup>(I)</sup>	+1.85	(1)
Strontianite: $\text{SrCO}_3 + \text{H}^+ \leftrightarrow \text{Sr}^{2+} + \text{HCO}_3^-$ <sup>(I)</sup>	+1.05	(1)
Barite: $\text{BaSO}_4 \leftrightarrow \text{Ba}^{2+} + \text{SO}_4^{2-}$ <sup>(II)</sup>	-9.97	(2)
$\text{RaSO}_{4(\text{cr})} \leftrightarrow \text{Ra}^{2+} + \text{SO}_4^{2-}$ <sup>(II)</sup>	-10.26	(3)
Siderite: $\text{FeCO}_3 + \text{H}^+ \leftrightarrow \text{Fe}^{2+} + \text{HCO}_3^-$	-0.47	(4)
Gypsum: $\text{CaSO}_4 \cdot 2\text{H}_2\text{O} \leftrightarrow \text{Ca}^{2+} + \text{SO}_4^{2-} + 2\text{H}_2\text{O}$	-4.85	(4)
Quartz: $\text{SiO}_2 + \text{H}_2\text{O} \leftrightarrow \text{Si}(\text{OH})_4$	-3.75	(5)
Pyrite: $\text{FeS}_2 + 2\text{H}^+ + 2\text{e}^- \leftrightarrow \text{Fe}^{2+} + 2\text{HS}^-$	-18.5	(6)
Hydroxylapatite: $\text{Ca}_5(\text{OH})(\text{PO}_4)_3 + 4\text{H}^+ \leftrightarrow \text{H}_2\text{O} + 3\text{HPO}_4^{2-} + 5\text{Ca}^{2+}$	-3.07	(7)
$\text{UO}_2 \cdot 2\text{H}_2\text{O}_{(\text{am})} + 4\text{H}^+ \leftrightarrow \text{U}^{4+} + 4\text{H}_2\text{O}$	+1.50	(8)
Ferrihydrite: $\text{Fe}(\text{OH})_3_{(\text{am})} + 3\text{H}^+ \leftrightarrow \text{Fe}^{3+} + 3\text{H}_2\text{O}$	+5.00	(9)
Uranophane: $\text{Ca}(\text{UO}_2)_2(\text{SiO}_3\text{OH})_2 \cdot 5\text{H}_2\text{O} + 6\text{H}^+ \leftrightarrow \text{Ca}^{2+} + 2\text{UO}_2^{2+} + 2\text{Si}(\text{OH})_4 + 5\text{H}_2\text{O}$	+9.42	(10)
Becquerelite: $\text{Ca}(\text{UO}_2)_6\text{O}_4(\text{OH})_6 \cdot 8\text{H}_2\text{O} + 14\text{H}^+ \leftrightarrow \text{Ca}^{2+} + 6\text{UO}_2^{2+} + 18\text{H}_2\text{O}$	+29.00	(11)
Soddyite: $(\text{UO}_2)_2\text{SiO}_4 \cdot 2\text{H}_2\text{O} + 4\text{H}^+ \leftrightarrow 2\text{UO}_2^{2+} + \text{Si}(\text{OH})_4 + 2\text{H}_2\text{O}$	+5.00	(12)
Schoepite: $\text{UO}_3 \cdot 2\text{H}_2\text{O} + 2\text{H}^+ \leftrightarrow \text{UO}_2^{2+} + 3\text{H}_2\text{O}$	+5.96	(13)

(I) Minerals involved in the  $\text{Ca}_{1-x}\text{Sr}_x\text{CO}_3$  solid solutions.

(II) Minerals involved in the  $\text{Ba}_{1-x}\text{Ra}_x\text{SO}_4$  solid solutions.

(1) /Plummer and Busenberg 1982/. (2) /Blount 1977/. (3) /Langmuir and Riese 1985/. (4) /Nordstrom et al. 1990/. (5) /Cox et al. 1989/. (6) /Robbie and Waldbaum 1968/. (7) /Johnson 2005/. (8) /Guillamont et al. 2003/. (9) /Hummel et al. 2002/. (10) /Nguyen et al. 1992/. (11) /Casas et al. 1997/. (12) /Pérez et al. 1997/. (13) /Bruno and Sandino 1989/.

Pure mineral phases are rarely found in natural environments. Instead, many solid phases are “mixtures” of two or more end-members at variable proportions forming solid solutions. A well-known example of solid solution is the uptake of strontium in calcite, forming  $\text{Ca}_{1-x}\text{Sr}_x\text{CO}_3$ , where  $x$  is the molar fraction of strontium. At Forsmark, strontium concentration in shallow groundwaters is thought to be influenced by the equilibrium with host rock.

The till contains carbonate particles derived from the erosion of Cambro-Ordovician marine carbonate rocks, and contains significant amounts of strontium /Grandia et al. 2007, section 2.5/. The Sr/Ca molar ratio observed in these rocks in the Forsmark area is fairly constant, around  $4 \times 10^{-4}$  /Grandia et al. 2007, section 2.5/. On the other hand, two distinct Sr/Ca molar ratios in shallow groundwaters can be defined /Grandia et al. 2007, section 2.5/: the first one is around  $7 \times 10^{-4}$  and it is found in samples from soil pipes SFM0002, -32 and -57 in the Lake Bolundsfjärden area. The second ratio is lower, and seems to reflect the mixing between shallow dilute groundwaters and more saline waters.

The incorporation of strontium in the calcium carbonate lattice has widely been studied, since it was suggested that  $(\text{Ca},\text{Sr})\text{CO}_3$  solid solutions could control the strontium concentrations in seawater /Stumm and Morgan 1996/. This solid solution series is highly non-ideal, i.e. the activity coefficients of the end-members are not equal to 1 (for more details see /Grandia et al. 2007, section 5.3.1/).

In /Grandia et al. 2007/ the initial composition of the solid solution present in the till considered in the reactive transport calculations was set  $\text{Ca}_{0.9996}\text{Sr}_{0.0004}\text{CO}_3$ , which is in agreement with the elemental composition measured in the till at Forsmark /Grandia et al. 2007, cf Figure 2-13/. From the results attained in /Grandia et al. 2007/ it was seen that the reference groundwater

is not strictly in equilibrium with a solid solution of this composition, but it does with a more Sr-depleted solid solution. Therefore, and since the initial strontium molar fraction considered the reactive transport calculations has a major influence in strontium mobility, the present models are set with a strontium molar fraction that is in equilibrium with the selected reference groundwaters of the till and glacial clay domains. This subject will be explained in detail in section 4.1.

The very low concentration of aqueous radium measured (from  $10^{-14}$  to  $10^{-11}$  M) in both natural and anthropogenic environments indicates that the solubility of radium is not controlled by pure phases (mainly  $\text{RaSO}_4$ ). Instead, the formation of solid solutions of Ba-Ca-Sr sulphates and carbonates is considered to be the solubility-limiting process (see review in /Grandia et al. 2008/). In many aqueous systems, radium is strongly co-precipitated with barium sulphate (barite,  $\text{BaSO}_4$ ) due to the chemical similarity between radium and barium.  $(\text{Ba,Ra})\text{SO}_4$  solid solutions are commonly found in scales in facilities of oil extraction, in geothermal systems and in uranium mining areas.

This solid solution series can be considered as ideal; nevertheless, only very small fractions of  $\text{RaSO}_4$  are typically measured due to the low radium concentration in water compared with barium. Initially, till groundwater in the Forsmark area is very close to barite saturation, and the precipitation of this mineral (and radium co-precipitation) is expected due to the intrusion of deep groundwater because of the relative high sulphate concentration in this water.

### ***Cation exchange in illite-bearing till***

Like other clay minerals, illite balances its electric charge deficit through adsorption of cations in the interlayers. The composition of these interlayers is conditioned by the equilibrium with the porewater and the selectivity coefficients of each cation involved. According to available studies dealing with the adsorption of caesium on illite, it is known that cation exchange in this mineral takes place in different surface sites /Poinssot et al. 1999, and references therein/. /Bradbury and Baeyens 2000/ proposed a model of cation exchange in illite considering three types of sites (Table 3-4). The most abundant sites (~80% of the total CEC, which is  $0.2 \text{ eq}\cdot\text{kg}^{-1}$ ) are the so-called “Planar sites”, which can adsorb either divalent cations such as  $\text{Ca}^{2+}$ ,  $\text{Mg}^{2+}$  and  $\text{Sr}^{2+}$  or monovalent ( $\text{Na}^+$ ,  $\text{K}^+$  and  $\text{Cs}^+$ ); these sites are considered of “low affinity”, and are usually associated with the fixed negative charge on the surface of illite arising from isomorphous substitution (e.g.  $\text{Al}^{3+}$  for  $\text{Si}^{4+}$  in tetrahedral sites; /Poinssot et al. 1999/).

Due to steric reasons, divalent cations are only involved in this type of sites /Poinssot et al. 1999/. The second and the third types of sites, called “Type II” and “Frayed Edge Sites” (FES), are considered of “high affinity” and involve monovalent cations such as  $\text{Na}^+$ ,  $\text{K}^+$ ,  $\text{Cs}^+$  and  $\text{NH}_4^+$ . The site density is much lower (20% and 0.25% of the total sites, respectively), but the uptake of some cations such as  $\text{Cs}^+$  on these sites (especially on FES) is particularly efficient and dominant. Interestingly, these sites are not generally associated to other clay minerals, such as smectite, chlorite or kaolinite /Bradbury and Baeyens 2000/.

Under oxidizing conditions, uranium (as U(VI)) transport in aquifers is mainly limited by the adsorption on mineral surfaces, and, at higher concentrations by the precipitation of mineral phases. U(VI) can be adsorbed in a number of mineral surfaces, especially onto clays and iron oxyhydroxides. In the reactive transport simulations, uranium is assumed to be adsorbed only on ferrihydrite [ $\text{Fe}(\text{OH})_3(\text{mic})$ ]. The surface complexation model followed is that of /Waite et al. 1994/. This model considers two types of adsorption sites (of strong and weak binding, respectively). The adsorbable species and corresponding constants are listed in Table 3-5. Note that adsorbing carbonate species have also been included in the simulations. This is because the amount of aqueous carbonate is expected to be high due to the equilibrium with the (Ca,Sr)  $\text{CO}_3$  solid solution present in the till, and, under these conditions, carbonate adsorption on ferrihydrite surface can be significant /Bruno et al. 1992, Van Geen et al. 1994/. Two types of uranium complexes are included:  $\equiv(\text{HFO\_O})\text{UO}_2$  and  $\equiv(\text{HFO\_O})\text{UO}_2\text{CO}_3^{2-}$  which are capable of being adsorbed in both weak and strong sites. The total concentration of sites is  $0.875 \text{ mol/mol Fe}$  /Waite et al. 1994/. Most of these sites are of low affinity (weak binding) and only  $0.0018 \text{ mol/mol Fe}$  correspond to high-affinity (strong binding) sites.



**Table 3-4. Cation exchange reactions and thermodynamic constants in the illite interlayer.**

Reaction	LogK (25°C)	Reference
Total exchange capacity (CEC) = 200 meq/kg		
Planar sites (0.8 × CEC)		
$X^- + Na^+ \leftrightarrow NaX$	0.0	(1)
$X^- + K^+ \leftrightarrow KX$	1.1	(1)
$X^- + Cs^+ \leftrightarrow CsX$	1.6	(1)
$2X^- + Sr^{2+} \leftrightarrow SrX_2$	1.5	(2)
$2X^- + Ca^{2+} \leftrightarrow CaX_2$	1.3	(3)
$2X^- + Mg^{2+} \leftrightarrow MgX_2$	1.5	(3)
Type II sites (0.2 × CEC)		
$X^{II-} + Na^+ \leftrightarrow NaX^{II}$	0.0	(1)
$X^{II-} + K^+ \leftrightarrow KX^{II}$	2.1	(1)
$X^{II-} + Cs^+ \leftrightarrow CsX^{II}$	3.6	(1)
Frayed edge sites (FES) (0.0025 × CEC)		
$X^{FES-} + Na^+ \leftrightarrow NaX^{FES}$	0.0	(1)
$X^{FES-} + K^+ \leftrightarrow KX^{FES}$	2.4	(1)
$X^{FES-} + Cs^+ \leftrightarrow CsX^{FES}$	7	(1)
$X^{FES-} + NH_4^+ \leftrightarrow NH_4X^{FES}$	3.5	(1)

(1) /Bradbury and Baeyens 2000/. (2) /Cole et al. 2000/. (3) /Tournassat et al. 2007/.

**Table 3-5. Complexation reactions on ferrihydrite surface and corresponding thermodynamic constants (from /Waite et al. 1994/).**

Reaction	LogK (25°C)
Strong sites ( $1.8 \times 10^{-3} \text{ mol}_{\text{site}} \cdot \text{mol}_{\text{Fe}(\text{OH})_3}^{-1}$ )	
$\equiv\text{HFO}^{\text{s}}\text{OH} + \text{H}^+ \leftrightarrow \equiv\text{HFO}^{\text{s}}\text{OH}_2^+$	6.51
$\equiv\text{HFO}^{\text{s}}\text{OH} \leftrightarrow \equiv\text{HFO}^{\text{s}}\text{O}^- + \text{H}^+$	-9.13
$\equiv\text{HFO}^{\text{s}}\text{OH} + \text{UO}_2^{2+} \leftrightarrow \equiv(\text{HFO}^{\text{s}}\text{O})_2\text{UO}_2 + 2\text{H}^+$	-2.57
$\equiv\text{HFO}^{\text{s}}\text{OH} + \text{UO}_2^{2+} + \text{CO}_3^{2-} \leftrightarrow \equiv(\text{HFO}^{\text{s}}\text{O})_2\text{UO}_2\text{CO}_3^{2-} + 2\text{H}^+$	3.67
$\equiv\text{HFO}^{\text{s}}\text{OH} + \text{CO}_3^{2-} + 2\text{H}^+ \leftrightarrow \equiv\text{HFO}^{\text{s}}\text{CO}_3\text{H} + \text{H}_2\text{O}$	19.50
$\equiv\text{HFO}^{\text{s}}\text{OH} + \text{CO}_3^{2-} + \text{H}^+ \leftrightarrow \equiv\text{HFO}^{\text{s}}\text{CO}_3^- + \text{H}_2\text{O}$	11.51
Weak sites ( $0.875 \text{ mol}_{\text{site}} \cdot \text{mol}_{\text{Fe}(\text{OH})_3}^{-1}$ )	
$\equiv\text{HFO}^{\text{w}}\text{OH} + \text{H}^+ \leftrightarrow \equiv\text{HFO}^{\text{w}}\text{OH}_2^+$	6.51
$\equiv\text{HFO}^{\text{w}}\text{OH} \leftrightarrow \equiv\text{HFO}^{\text{w}}\text{O}^- + \text{H}^+$	-9.13
$\equiv\text{HFO}^{\text{w}}\text{OH} + \text{UO}_2^{2+} \leftrightarrow \equiv(\text{HFO}^{\text{w}}\text{O})_2\text{UO}_2 + 2\text{H}^+$	-6.28
$\equiv\text{HFO}^{\text{w}}\text{OH} + \text{UO}_2^{2+} + \text{CO}_3^{2-} \leftrightarrow \equiv(\text{HFO}^{\text{w}}\text{O})_2\text{UO}_2\text{CO}_3^{2-} + 2\text{H}^+$	-0.42
$\equiv\text{HFO}^{\text{w}}\text{OH} + \text{CO}_3^{2-} + 2\text{H}^+ \leftrightarrow \equiv\text{HFO}^{\text{w}}\text{CO}_3\text{H} + \text{H}_2\text{O}$	19.50
$\equiv\text{HFO}^{\text{w}}\text{OH} + \text{CO}_3^{2-} + \text{H}^+ \leftrightarrow \equiv\text{HFO}^{\text{w}}\text{CO}_3^- + \text{H}_2\text{O}$	11.51

Unlike illite surface, ferrihydrite is a reactive mineral very sensitive to changes in the redox state of the system. Intrusion of deep groundwaters into the till domain may lead to dissolution or precipitation of ferrihydrite. For this reason, in the reactive transport simulations the total amount of sites available for adsorption depends on the remaining moles of ferrihydrite in each time step.

## 3.2.2 Reference case #2: The clay system

### *Aqueous speciation*

The aqueous species selected and the thermodynamic database are the same as for the reference case #1 (section 3.2.1). Moreover, organic species have been included as humic acids to simulate the metal complexation in waters with high concentration of organic compounds. The metals considered for complexation with humic acids are calcium and uranium. Six different organic species have been considered: Humate<sup>-</sup>, CaHumate<sup>+</sup>, UHumate<sup>3+</sup>, U(Humate)<sub>2</sub><sup>2+</sup>, UO<sub>2</sub>Humate<sup>+</sup> and UO<sub>2</sub>(Humate)<sub>2</sub>. The first two complexes of uranium are for U(IV), and the last two are for U(VI). The reactions and thermodynamic constants for these species are listed in Table 3-6.

### *Equilibrium with pure mineral phases and solid solutions*

According to /Hedenström 2004/, the glacial clays present in the lake sediments and the Baltic Sea of Forsmark show considerable amounts of illite, quartz and calcite. As in the previous reference case, it was considered that calcite present in the glacial clays has trace amounts of Sr forming a solid solution, which can be a sink for the incoming Sr from deep fluids. The set of the initial amount of Sr-bearing calcite and respective strontium molar fraction in the modelled glacial clay is shown in section 4.1.

As explained for the reference case #1 (section 3.2.1), no reactivity is given to illite in the numerical simulations, and therefore illite only participates as a charged surface for cation exchange. It is very likely that other phases exist at minor and trace concentrations, some of which can play a very important role in the control of the redox conditions and radionuclide retention. Among these, pyrite is considered to significantly affect the redox of the glacial clay porewater. Since no data on pyrite content in glacial clay sediments is available for Forsmark, an initial concentration of 1 mol·L<sup>-1</sup> of pyrite (which corresponds to approximately 1.5 wt% of pyrite, considering a clay bulk density of 2 kg/L and a total porosity of 20%) has been considered in the model in order to ensure the relatively reducing conditions in the glacial clays.

The uranium mineral phases allowed to precipitate in the reactive transport simulations are the same as in the previous till system. Nevertheless, due to the prevailing reducing conditions of the glacial clays, it is expected that the U(IV) mineral phases will be favoured.

### *Cation exchange in illite*

The configuration of the illite interlayer applied to the clay system is the same as in the till system (Table 3-4), except for the percentage of illite in the modelled domain. This will be shown in section 4.1.

**Table 3-6. Complexation reactions of organic compounds and the corresponding thermodynamic constants.**

Reaction	LogK (25°C)
Ca <sup>2+</sup> + Humate <sup>-</sup> ↔ CaHumate <sup>+</sup>	4.7 <sup>(1)</sup>
U <sup>4+</sup> + Humate <sup>-</sup> = UHumate <sup>3+</sup>	7.0 <sup>(2)</sup>
2U <sup>4+</sup> + Humate <sup>-</sup> = U(Humate) <sub>2</sub> <sup>2+</sup>	11.5 <sup>(2)</sup>
UO <sub>2</sub> <sup>2+</sup> + Humate <sup>-</sup> = UO <sub>2</sub> Humate <sup>+</sup>	7.64 <sup>(3)</sup>
2UO <sub>2</sub> <sup>2+</sup> + Humate <sup>-</sup> + H <sub>2</sub> O = UO <sub>2</sub> (Humate) <sub>2</sub>	11.54 <sup>(3)</sup>

<sup>(1)</sup> /Choppin and Shanbhag 1981/, <sup>(2)</sup> /Li et al. 1980/, <sup>(3)</sup> /Shanbhag and Choppin 1981/.

### 3.3 Numerical tool and thermodynamic database

The reactive transport simulations have been performed using the code PHAST version 1.4.2 /Parkhurst et al. 2004/. This code is the result of coupling a transport code, HST3D /Kipp 1997/ and a geochemical code, PHREEQC /Parkhurst and Appelo 1999/. It is able to simulate multi-component, reactive solute transport in three-dimensional saturated groundwater flow systems. A number of boundary conditions are available (specified-head, flux and leakage conditions), and chemical reactions include homogeneous equilibria using an ion-association thermodynamic model, heterogeneous equilibria between the aqueous solution and minerals, gases, surface complexation sites, ion exchange sites, solid solutions, and kinetic reactions.

The reaction transport equations are solved by sequential iteration approach in which solute transport and chemical reaction are decoupled into separate calculations for each time step. First, the primary species are transported and, then, the outcome of the geochemical reactions occurring in the cell is calculated. The transport and geochemical calculations are evaluated by an iterative approach until prescribed convergence criteria are fulfilled. PHAST uses porous media properties and boundary conditions defined by zones for a point-distributed-finite-difference grid.

The database used in the present study is an extension of the NAGRA-PSI database, compiled by /Hummel et al. 2002/. The extension was made in the frame of the SKB's project SKB-TDB /Duro et al. 2006a/. This database contains a large set of complexation reactions as well as pure mineral equilibrium reactions for many radionuclides and trace elements. Additional Fe(III) carbonate complexes have been added to the database due to the high bicarbonate content of the till groundwaters (see section 3.2.1).

Data for humic complexes are not initially included in the database. As explained in section 3.2.2, thermodynamic data for complexation with humic acids was selected from /Choppin and Shanbhag 1981, Li et al. 1980, Shanbhag and Choppin 1981/.

## 4 Numerical models setup

### 4.1 Refinement of geochemical initial and boundary conditions

In order to improve the reliability of the numerical models developed in /Grandia et al. 2007/ with respect to site specific features of the till and glacial clay deposits of Forsmark, the geochemical initial and boundary conditions of these numerical models have been refined in the present work.

The results from numerical simulations in /Grandia et al. 2007/ reveal that the deep groundwater discharge into Quaternary deposits causes relatively long transient states of reactive transport. Deep groundwaters, which would be the radionuclide carrier from the repository, have been discharging into Quaternary deposits for long periods, leading to the establishment of the natural hydrochemical steady state that occurs nowadays. In order to simulate more realistic scenarios and reproduce the initial geochemical conditions prior to the release of radionuclides from the repository, the reference cases have been simulated during 2700 years (which is approximately the time needed to reach stable hydrogeochemical conditions in the numerical simulations) before the release of radionuclides.

From available geochemical data of Forsmark it is seen that calcium carbonate is present in both till and glacial clays /SKB 2005a/. In the reactive transport simulations, the initial till and clay systems are assumed to contain calcium carbonate with trace amounts of strontium, forming a  $(Ca,Sr)CO_3$  non-ideal solid solution that is assumed to be in equilibrium with the reference waters. This solid solution may re-precipitate in a new phase with higher strontium content as a response to the inflow of a strontium-enriched deep groundwater. Consequently strontium may be retained in the solid phase, or it may be released by dissolution of the  $(Ca,Sr)CO_3$  solid solution as a response to changes in the pH conditions and/or carbonate equilibrium.

The dissolution of the carbonate mineral has additional implications in the clay system, since the release of  $Ca^{2+}$  into solution will increase the competition for the complexation with humic acids. Consequently, the concentration of free aqueous uranium increases favouring the precipitation of uranium pure phases. However, the dissolution of carbonate minerals also releases  $CO_3^{2-}$  into solution that may form aqueous uranium carbonate complexes that prevent the precipitation of uranium pure phases.

For all these reasons it is important to have a good estimation of the reactive carbonate mineral pool in both numerical models. As it is shown in the next sections, it was possible to estimate the carbonate content of the till and clay systems based on the available geochemical data from Forsmark /SKB 2005a, SKB 2005b/.

#### 4.1.1 Reference case #1: The till system

The  $CaCO_3$  content of the till system considered in the reactive transport calculations was set as follows:

Input data /SKB 2005a/: mean  $CaCO_3$  content is 24 wt%.

/SKB 2005a/: 43.2% of till is composed of 2 mm sized grains (sand grain size).

/Johansson et al. 2005/: Total porosity = 25%.

Till bulk density: 1.95 kg/L ((1-Total porosity)×2.6 kg/L, attributed value, not reported in the literature).

Assuming that all  $\text{CaCO}_3$  grains are 2 mm in size, and that in each grain only the outer 0.05 mm rim is reactive (Figure 4-1), we obtain the reactive  $\text{CaCO}_3$  volume per grain ( $V_{\text{reactive}}$ ) of:

$$V_{\text{reactive}} = \frac{4}{3}\pi \cdot (1 \text{ mm})^3 - \frac{4}{3}\pi \cdot (0.95 \text{ mm})^3 = 0.6 \text{ mm}^3$$

Knowing that the volume of each 2 mm grain is 4.2  $\text{mm}^3$ , the reactive volume of  $\text{CaCO}_3$  in the till deposit ( $\%V_{\text{reactive}}$ ) corresponds to:

$$\%V_{\text{reactive}} = \frac{0.6 \text{ mm}^3 \times 43.2\%}{4.2 \text{ mm}^3} = 6.2\%$$

According to the data listed above, the concentration (in mol/L) of total  $\text{CaCO}_3$  in the till system is:

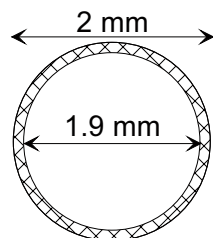
$$\begin{aligned} \text{CaCO}_3(\text{total}) &= \frac{24 \text{ kg CaCO}_3}{100 \text{ kg Till}} \times \frac{1.95 \text{ kg Till}}{1 \text{ L}} \times \frac{1}{0.25} = 1.872 \text{ kg / L} = 1.872 \times 10^3 \text{ g / L} = \\ &= \frac{1.872 \times 10^3 \text{ g / L}}{100.06 \text{ g / mol}} = 18.71 \text{ mol / L} \end{aligned}$$


Considering both the percentage of reactive  $\text{CaCO}_3$  volume and the concentration of total  $\text{CaCO}_3$  present in the till deposit, the reactive  $\text{CaCO}_3$  expressed in mol/L is:

$$\text{CaCO}_3(\text{reactive}) = 18.71 \text{ mol / L} \times 6.2\% \approx 1 \text{ mol / L}$$

The cation exchange capacity (CEC) is a parameter quantifying properties with significant influence on the geochemistry of groundwaters that flow through clay-rich sediments. The CEC of a sediment does not only depend on the clay content but also on the mineralogy of the clay fraction. Among the radionuclides selected in the present study, either strontium or caesium are prone to be exchanged in the illite interlayer. Since there are no reported CEC values for the surface sediments in the Forsmark area, data from the Laxemar area /Sohlenius et al. 2006/ was used. There, the CEC of till deposit varies from 17.6 meq/kg to 202 meq/kg /Appendix 10b of Sohlenius et al. 2006/.

The cation exchange model built for the present reactive transport models is based on the cation exchange equilibrium constants of the clay mineral illite according to /Bradbury and Baeyens 2000/, and the CEC values reported in /Sohlenius et al. 2006/ correspond to the bulk till deposit. In order to account for the illite fraction in the till deposit, a reducing coefficient (10%) was applied. This is an arbitrary value, since there are no reported values for the illite content in the till deposits of Forsmark and Laxemar areas.



 Reactive rim

**Figure 4-1.** Scheme of a 2 mm  $\text{CaCO}_3$  grain with an external reactive rim of 0.05 mm.

The CEC value reported for illite in /Bradbury and Baeyens 2000/ is 200 meq/L (which is very similar to maximum CEC value reported for till /Sohlenius et al. 2006/). Therefore it was decided to set this value for the reference case.

According to the adopted CEC value the concentration of available cation exchange sites for the reference case of the till deposit was set as follows:

Input data    CEC = 200 meq/kg = 0.200 eq/kg = 0.200 mol/kg (exchange species is a monovalent X<sup>-</sup>).  
                   /SKB 2005a/: Total porosity = 25%.  
                   Illite content: 10 wt% (estimated value, not reported in the literature).  
                   Till bulk density: 1.95 kg/L ((1-Total porosity)×2.6 kg/L, estimated value, not reported in the literature).

Considering a CEC of 200 meq/kg, the concentration of cation exchange sites [CES] in the till deposit is:

$$[CES] = \frac{0.200 \text{ mol}}{1 \text{ kg}} \times \frac{10 \text{ kg Illite}}{100 \text{ kg Till}} \times \frac{1.95 \text{ kg Till}}{1 \text{ L}} \times \frac{1}{0.25} = 0.16 \text{ mol / L}$$

#### 4.1.2 Reference case #2: The clay system

The CaCO<sub>3</sub> content of the clay system was calculated as follows:

Input data    /SKB 2005a/: mean CaCO<sub>3</sub> content is 26 wt%.  
                   /SKB 2005a/: 55.48% of clay is composed of 0.002 mm (clay grain size).  
                   /Johansson et al. 2005/: Total porosity = 20%.  
                   Clay bulk density: 2 kg/L ((1-Total porosity)×2.5 kg/L, estimated value, not reported in the literature).

If we take into account the next considerations: (1) only 5% of the 0.002 mm grains is composed of CaCO<sub>3</sub>, and (2) the whole volume of these grains is reactive, since their volume is very small, we obtain a reactive CaCO<sub>3</sub> volume for the clay sediment of 5%.

The concentration (in mol/L) of total CaCO<sub>3</sub> in the clay system is:

$$\begin{aligned} CaCO_3(\text{total}) &= \frac{26 \text{ kg CaCO}_3}{100 \text{ kg Clay}} \times \frac{2 \text{ kg Clay}}{1 \text{ L}} \times \frac{1}{0.2} = 2.6 \text{ kg / L} = 2.6 \times 10^3 \text{ g / L} = \\ &= \frac{2.6 \times 10^3 \text{ g / L}}{100.06 \text{ g / mol}} = 26.0 \text{ mol / L} \end{aligned}$$

Considering the percentage of reactive CaCO<sub>3</sub> volume calculated above and the concentration of total CaCO<sub>3</sub> in the clay deposit, the reactive CaCO<sub>3</sub> expressed in mol/L is:

$$CaCO_3(\text{reactive}) = 26.0 \text{ mol / L} \times 5\% \approx 1 \text{ mol / L}$$

/Sohlenius et al. 2006/ reported a CEC for the glacial clay ranging from 15.2 meq/kg to 194 meq/kg. The latter value is again very close to the CEC for illite /Bradbury and Baeyens 2000/, and therefore this value was selected for the reference case of the clay system.

Considering that 50% of the clay sediment is composed of illite, the concentration of available cation exchange sites in the modelled clay deposit was set as follows:

Input data CEC = 200 meq/kg = 0.200 eq/kg = 0.200 mol/kg (exchange species is a monovalent X<sup>-</sup>).

/Johansson et al. 2005/: Total porosity = 20%.

Illite content: 50 wt% (estimated value, not reported in the literature).

Clay bulk density: 2 kg/L ((1-Total porosity)×2.5 kg/L estimated value, not reported in the literature).

Assuming a CEC of 200 meq/kg, the concentration of cation exchange sites [CES] in the clay deposit is:

$$[CES] = \frac{0.200 \text{ mol}}{1 \text{ kg}} \times \frac{50 \text{ kg Illite}}{100 \text{ kg Clay}} \times \frac{2 \text{ kg Clay}}{1 \text{ L}} \times \frac{1}{0.20} = 1.0 \text{ mol / L}$$

## 4.2 Spatial and time discretisation

The spatial and time discretisation are the same as described in /Grandia et al. 2007/. A summary of the spatial and time discretisation is presented here, and for further details see section 5.4 in /Grandia et al. 2007/.

### 4.2.1 Reference case #1: The till system

The modelled domain of reference case #1 is a 2D vertical cross-section of the till deposit. Following /Johansson et al. 2005/, the thickness is 3 m, and, based on the dimensions of the subcatchments in the Forsmark area, the horizontal length is set to 100 m. The modelled till deposit was divided into three layers following the simplified till profile proposed by /Johansson et al. 2005/ (Figure 3-1). These three layers show different hydraulic properties derived from the different clay contents (Table 3-1).

Since the till deposit hosts phreatic aquifers that may be locally confined, and that may discharge to distinct surface water bodies /Johansson et al. 2005/, it was decided to simulate a confined aquifer that discharges into a surface water body located at the top-right corner of the modelled domain. The spatial discretisation of the modelled domain was adapted according to the main features of the boundary conditions, which will influence the groundwater flow directions and the groundwater chemistry of the modelled domain, namely the position of the deep groundwater inflow and the position of the discharge area (outflow boundary).

In the reference case #1, the spatial discretisation along the X-axis is refined in the till directly overlying the area where the deep groundwater accesses into the till domain. Similarly, the discretisation is also refined under the discharge area. The spatial discretisation along the Y-axis is also finer in the discharge area due to the large upward vertical component of the shallow groundwater flow (Figure 4-2).

There are two important time stages regarding the chemical conditions of the system: the first stage occurs at the beginning of the simulation period, when the deep groundwater flows into the modelled domain and triggers major geochemical changes, and the second stage occurs when the increased concentration of radionuclides in the deep groundwater disturbs the previous geochemical state.

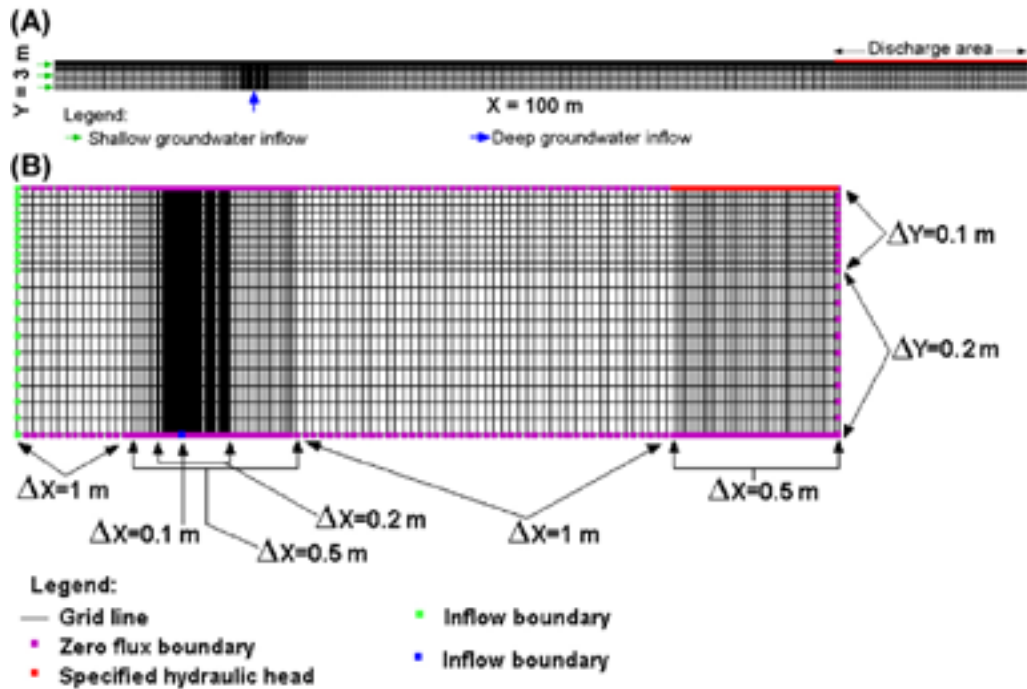


**Figure 4-2.** Numerical grid showing the distinct spatial discretisations along the X- and Y-axis, and the boundary conditions assigned to the till system (reference case #1). Grid A shows the length of each axis, whereas grid B explains where the finer discretisations occur and the boundary conditions (Y-axis is magnified 10 times).

Therefore, time discretisation was refined at the beginning of the simulation period, then set progressively coarser until approximately 2,700 years, and then refined again when the increment of radionuclides takes place. Finally time discretisation becomes coarser again, until the end of the simulation period. According to these criteria, the time discretisation for both modelled domains (till and clay systems) was set as shown in Figure 4-3.

#### 4.2.2 Reference case #2: The clay system

The modelled domain considered for the reference case #2 is a 2D symmetric vertical cross section of a clay layer that can be present at the bottom of discharge areas of Forsmark. Based on the characterization of the lake sediments reported in /Johansson et al. 2005/, the thickness of the clay layer in the model was set to 1 m, and taking into account the present-day extent of the lakes at Forsmark, the length of the X-axis was set to 10 m. The hydrodynamic parameters of the clay deposit to be used in the numerical simulations were set according to /Johansson et al. 2005/, and are shown in Table 4-1.

In this case, the shallow groundwater flowing in the underlying till aquifer enters in the clay domain through the left and bottom boundaries. The deep groundwater inflow for the reference case #2 will occur at the bottom right corner of the domain that represents a higher permeability area of the underlying till deposit. The water flowing in this domain will flow out through the whole top boundary. Since the modelled domain in the reference case #2 is relatively small (1 m x 10 m), it was set a fine spatial discretisation of 0.1 m along both axes for the whole domain (Figure 4-4).



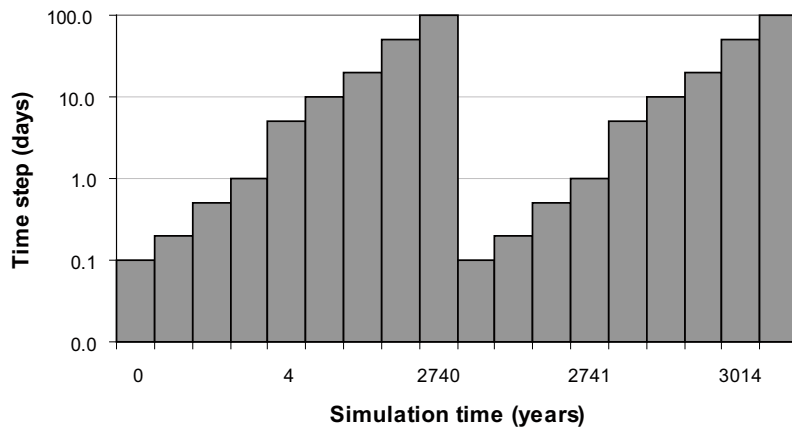


Figure 4-3. Time discretisation for reference case #1 and reference case #2.

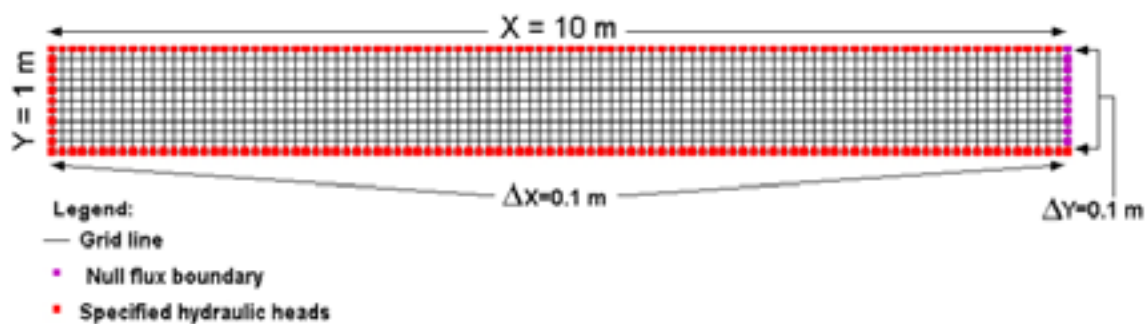


Figure 4-4. Numerical grid showing the spatial discretisation of the modelled domain and the boundary conditions assigned to the clay system (reference case #2).

The time discretisation is the same as in reference case #1 (Figure 4-3), since it is expected that major chemical changes will occur at the same time, i.e. at the beginning of the simulation time and after the input of radionuclides derived from the repository. To ensure stability in the numerical calculations, the Péclet criterion ( $Pe \leq 2$ ) is met for the maximum  $\Delta X$  (maximum  $\Delta X = 1$  m, and longitudinal dispersivity = 0.5 m) in both numerical models.

## 4.3 Initial and boundary conditions

### 4.3.1 Reference case #1: The till system

#### Hydrogeological initial and boundary conditions

According to the water balance calculations developed with the MIKE SHE model for the Forsmark site /Johansson et al. 2005/, the shallow aquifers hosted by till deposits discharge 66 mm/year to the surface water bodies. Therefore, for the present numerical model, a flow of 66 mm/year has been prescribed in the top boundary of the modelled domain.

Of the total length of the top boundary, only 80 m correspond to the recharge area, and the remaining 20 m correspond to the discharge area. Considering a surface of  $80 \text{ m} \times 1 \text{ m}$ , the net recharge flow entering the system would be:

$$\frac{6.6 \times 10^{-2} \text{ m}^3}{\text{m}^2 \cdot \text{year}} \times 80 \text{ m} \times 1 \text{ m} = 5.28 \text{ m}^3/\text{year} = 14.5 \text{ L/day}$$

The net recharge flow of 14.5 L/day is applied to the left boundary to simulate a locally confined aquifer with a predominantly horizontal flow direction, before reaching the discharge area (Figure 4-5).

The discharge area of the modelled domain is located in the last 20 m of the top right boundary, where a constant head of 3 m is set.

At the bottom boundary of the modelled domain, between X=20 m and X=20.2 m, the deep groundwater flows into the domain. The remaining bottom boundary (from X=0 m to X=19.9 m, and from X=20.3 to X=100 m) is considered impervious. The flux of deep groundwater entering through the 0.2 m of the bottom boundary was calculated from the 2 mm/year of inflow across bottom boundary obtained in the water balance from the MIKE SHE model applied to the Forsmark area /Johansson et al. 2005/.

The 2 mm/year were multiplied by the total bottom area of 100 m × 1 m, and applied to the discrete deep inflow boundary of 0.2 m. Therefore, the total deep inflow passing through the 0.2 m is:

$$\frac{2 \times 10^{-3} \text{ m}^3}{\text{m}^2 \cdot \text{year}} \times 100 \text{ m} \times 1 \text{ m} = 0.2 \text{ m}^3 / \text{year} = 0.5 \text{ L/day}$$

It is assumed that the simulated catchment has a deep groundwater inflow concentrated at a single point which would correspond to a hypothetical fracture zone (Figure 4-5).

### Hydrogeochemical initial and boundary conditions

#### Initial groundwater composition in the till

The chemistry of the groundwater in equilibrium with the till deposit has been obtained after equilibration of the sample taken in soil pipe SFM0002 with (Ca,Sr)CO<sub>3</sub> solid solution, siderite and ferrihydrite (Table 4-2). As this groundwater is close to the equilibrium with these minerals, the resulting composition does not differ much from the sampled water. Iron concentration is slightly modified by the equilibrium with ferrihydrite, and strontium by the equilibrium with the solid solution.

The redox state of the solution is controlled by the Fe<sup>2+</sup>/ferrihydrite pair, and the pH is slightly lower than the original pH (shown in Table 2-1) due to equilibrium with the (Ca,Sr)CO<sub>3</sub> solid solution and siderite. Initially, uranium is found as U(VI) and the dominant aqueous species are carbonate complexes, mainly UO<sub>2</sub>(CO<sub>3</sub>)<sub>3</sub><sup>4-</sup>. All uranium solid phases are far from saturation.

Strontium is found almost completely as Sr<sup>2+</sup> cation. The most abundant solid phases in nature, celestite (SrSO<sub>4</sub>) and strontianite (SrCO<sub>3</sub>) are clearly undersaturated, with saturation indexes (SI) of -3.16 and -2.29, respectively. The relatively low chloride content prevents a significant complexation of Cs, and, therefore, the free species Cs<sup>+</sup> is dominant in the till groundwater.

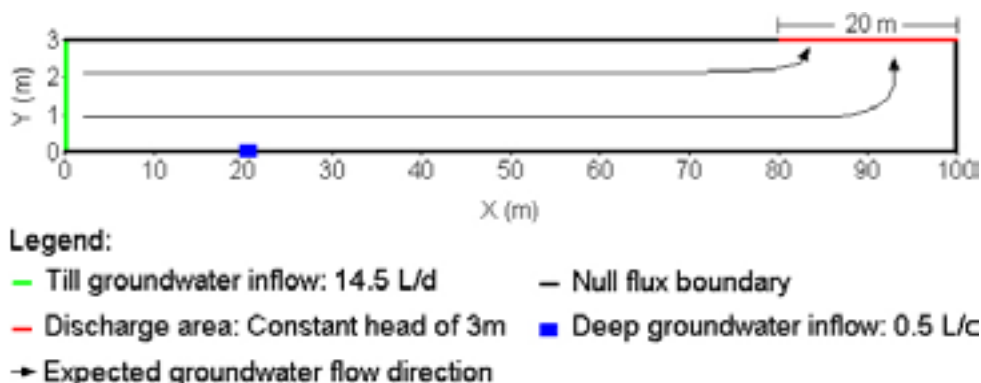


Figure 4-5. Boundary conditions for the numerical model applied to the reference case #1.

**Table 4-1. Initial composition of till groundwater and deep groundwater in reference case #1. Concentrations of <sup>RD</sup>Cs, <sup>RD</sup>U, <sup>RD</sup>Sr and Ra in the deep groundwater (affected by repository release) represent the increment of these radionuclides due to repository release. Further explanation of these modified values is given in the following section.**

	Till GW	Deep GW (before repository release)	Deep GW (after repository release)
pH	7.12	7.16	7.16
Eh(mV)	3	-145	-145
Na	$1.22 \times 10^{-3}$	$6.93 \times 10^{-2}$	$6.93 \times 10^{-2}$
K	$1.22 \times 10^{-4}$	$1.67 \times 10^{-3}$	$1.67 \times 10^{-3}$
Ca	$2.79 \times 10^{-3}$	$1.35 \times 10^{-2}$	$1.35 \times 10^{-2}$
Mg	$3.54 \times 10^{-4}$	$7.18 \times 10^{-3}$	$7.18 \times 10^{-3}$
C(IV)	$5.57 \times 10^{-3}$	$2.46 \times 10^{-3}$	$2.46 \times 10^{-3}$
Cl	$1.90 \times 10^{-3}$	$1.07 \times 10^{-1}$	$1.07 \times 10^{-1}$
SO <sub>4</sub> <sup>2-</sup>	$2.41 \times 10^{-4}$	$3.73 \times 10^{-3}$	$3.73 \times 10^{-3}$
Si	$9.74 \times 10^{-5}$	$7.56 \times 10^{-5}$	$7.56 \times 10^{-5}$
Fe <sub>total</sub>	$1.50 \times 10^{-5}$	$4.91 \times 10^{-4}$	$4.91 \times 10^{-4}$
Sr	$2.10 \times 10^{-6}$	$4.13 \times 10^{-5}$	$4.13 \times 10^{-5}$
U	$2.23 \times 10^{-8}$	$4.62 \times 10^{-10}$	$4.62 \times 10^{-10}$
Cs	$6.48 \times 10^{-11}$	$1.62 \times 10^{-8}$ (*)	$1.62 \times 10^{-8}$ (*)
NH <sub>4</sub> <sup>+</sup>	$6.62 \times 10^{-6}$	$1.95 \times 10^{-4}$	$1.95 \times 10^{-4}$
<sup>RD</sup> Cs	–	–	$3.48 \times 10^{-7}$
<sup>RD</sup> U	–	–	$1.73 \times 10^{-8}$
<sup>RD</sup> Sr	–	–	$8.37 \times 10^{-4}$
Ra	–	–	$9.15 \times 10^{-11}$

Concentrations in mol/L

(\*) Taken from maximum Cs concentration in KFM01A.

### Deep groundwater before repository release

The composition of the reference water that represents the deep groundwater prior to repository release results from the equilibrium of the water sampled in soil pipe SFM0023 with pyrite and calcite. The composition of the deep groundwater before repository release is slightly modified from reference water taken from SFM0023, due to equilibrium with calcite and pyrite which are the pure phases expected to control pH and pe, respectively. This equilibrium produces a slight change not only in the pH of the water, but also on the concentration of Ca and C(IV).

### Deep groundwater after repository release

The increment of radionuclide concentration in the deep groundwater, due to repository release, is set according to a very pessimistic scenario. In this scenario the geosphere does not have any retention capacity for radionuclides, and the transport between the repository and the near-surface systems is assumed to be instantaneous. In this context, radionuclide concentrations calculated for the near-field (i.e. the canister containing the spent fuel and the engineered barrier system surrounding it) in case of dissolution of the spent nuclear fuel, are applied as the input concentrations in the simulations.

The groundwater composition in this case is the same as before repository release, except for the radionuclide concentrations. The radionuclide concentrations have been calculated to be in equilibrium with their respective solubility limiting phases in the near-field, according to the methodology described in /Duro et al. 2006b/.

The concentrations of  $^{RD}Sr$  and  $^{RD}U$  in the deep groundwater after repository release are calculated by assuming the equilibrium of the reference deep groundwater with their solubility limiting phases (i.e. only the concentrations of the radionuclides are modified), which correspond to  $SrSO_4$  (celestite) and  $UO_2 \cdot 2H_2O(am)$ , respectively /Duro et al. 2006b/. The concentrations of  $^{RD}Sr$  and  $^{RD}U$  in the deep groundwater influenced by repository release that result from this equilibrium, are  $8.4 \times 10^{-4}$  mol/L of  $^{RD}Sr$ , and  $1.7 \times 10^{-8}$  mol/L of  $^{RD}U$ .

Since the solubility limiting phases for Ra and  $^{RD}Cs$  in the near-field are difficult to define, it was decided to calculate the corresponding concentration from the radioactive release doses estimated for both radionuclides in the near-field /SKB 2006/. The concentration of the radionuclides in the deep groundwater depends on the type of repository release considered (growing pinhole failure, advection/corrosion failure, and the shear movement failure /SKB 2006/) and on the migration path of the radionuclides in the geosphere (fracture intersecting the deposition hole (Q1), the excavation damaged zone (Q2), fracture intersecting the deposition tunnel (Q3)) /SKB 2006/.

The scenario Q1 (growing pinhole failure combined with the fracture intersecting the deposition hole) was selected for the calculation of the  $^{RD}Cs$  and Ra concentrations, since it is considered the worst scenario. This is because Q1 leads to higher groundwater flow velocities from the spent nuclear fuel to the geosphere and, consequently, higher radionuclide release.

In /SKB 2006, Figure 10-14/ the radioactive dose in the near-field, at time of repository release, of  $^{135}Cs$  is 450 Bq/yr, while for  $^{226}Ra$  is 170 Bq/yr. By dividing the radioactive doses expressed in Bq/yr by the Q1 flow ( $2.25 \times 10^{-4}$  m<sup>3</sup>/yr, /SKB 2006, Table 10-5/) we obtain the radionuclide concentration expressed in Bq/L, which is converted to mol/L, for the numerical simulations developed in the present work:

$$[^{226}Ra] = \frac{170 Bq / yr}{2.25 \times 10^{-4} m^3 / yr} = 7.55 \times 10^2 Bq / L$$

Knowing that the radioactive decay constant of  $^{226}Ra$  is  $1.37 \times 10^{-11} s^{-1}$  and using the Avogadro constant, we obtain the following concentration in mol/L:

$$[^{226}Ra] = \frac{7.55 \times 10^2 Bq / L}{1.37 \times 10^{-11} s^{-1}} \times \frac{1 atoms / L}{6.023 \times 10^{23} atoms / mol} = 9.15 \times 10^{-11} mol / L$$

For  $^{135}Cs$  (radioactive decay constant of  $^{135}Cs$  is  $9.54 \times 10^{-15} s^{-1}$ ) the concentration of  $^{135}Cs$  in the near field is  $3.48 \times 10^{-7}$  mol/L.

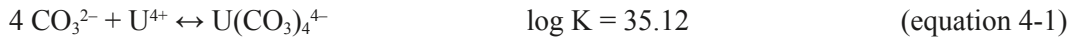
These radionuclide concentrations are very high, taking into consideration that the engineered barriers and geosphere would be able to retain much of these radionuclides, preventing them from accessing the near-surface systems. Nevertheless, since the objective of the simulations is to evaluate the retention capacity of the Quaternary sediments, an extreme scenario has been assumed in this work.

### Repository derived radionuclides

In order to trace radionuclides released from repository and distinguish them from naturally occurring isotopes, each repository derived radionuclide was labelled as follows:  $^{RD}Sr$ ,  $^{RD}Cs$  and  $^{RD}U$ . Ra has not been labelled since it is considered to be below the detection limit in the porewater of the studied Quaternary deposits before repository release.

The labelling of repository derived radionuclides involved the addition of the labelled species as primary species to the thermodynamic database used in the numerical reactive transport simulations. Also the secondary aqueous species and the reactions involving solid phases for labelled radionuclides have been added by duplicating the reactions for non-labelled isotopes and replacing the isotope with the labelled radionuclide, as in the following example:

The following speciation reaction for non-labelled uranium,



has been duplicated for the labelled uranium as follows,

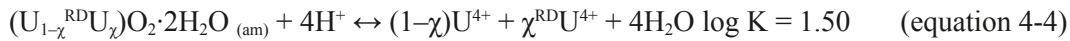


In the numerical simulations of the period after repository release, the total concentration of a selected radionuclide at any given time and any given node of the modelled domain can be calculated by simply adding repository derived species to naturally occurring species. In order to involve repository-derived radionuclides and the naturally occurring isotopes in the same solid phase, without causing isotopic fractionation, new solid solutions that involve both species have been added to the thermodynamic database. The modifications applied for the case of U and amorphous uraninite, and Sr and the calcite-strontianite solid solution are shown in the next paragraphs.

The dissolution reaction of amorphous uraninite applied in the present simulations is defined as:

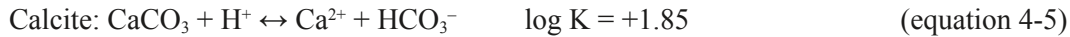


In order to trace the incorporation of repository derived U and natural U in amorphous uraninite, the following ideal solid solution has been introduced in the reactive transport simulations, replacing the pre-existing equation 4-3:



where  $\chi$  is the molar fraction of  ${}^{\text{RD}}\text{U}$  in amorphous uraninite.

As already mentioned, Sr forms a non-ideal solid solution with calcite. In order to trace the incorporation of  ${}^{\text{RD}}\text{Sr}$  and natural Sr in this solid solution, a new solid solution with three end-members (Sr,  ${}^{\text{RD}}\text{Sr}$ , and Ca) has been defined in the numerical simulations. The binary non-ideal solid solution between strontianite and calcite is defined by the solubility constant of each end-member, as follows:



The new solid solution that involves the three end-members Sr,  ${}^{\text{RD}}\text{Sr}$ , and Ca, has been implemented by defining a conditional solubility constant for the strontianite end-members. This approach is necessary since ternary non-ideal solid solutions cannot be considered in PHAST. Only ideal multicomponent solid solutions and binary non-ideal solid solutions can be treated. The non-ideal behaviour implies that the activity of the solid phase end-members depends not only on its molar fraction in the solid solution, but also on an activity coefficient.

In order to take this non-ideality into account, conditional solubility constants have been considered for the strontianite end-members. Therefore, by taking this approach the solid solution can be treated as ideal. This approach is valid only when the molar fractions of the trace end-members do not change much through time and if they are always within the natural miscibility range. The values for the conditional solubility constants are calculated as follows:

$$K^*_{\text{SrCO}_3} = K_{\text{SrCO}_3} \times \chi_{\text{SrCO}_3} \times \lambda_1 \quad (\text{equation 4-7})$$

$$K^*{}^{\text{RD}}_{\text{SrCO}_3} = K^{\text{RD}}_{\text{SrCO}_3} \times \chi^{\text{RD}}_{\text{SrCO}_3} \times \lambda_2 \quad (\text{equation 4-8})$$

$$K^*_{\text{CaCO}_3} = K_{\text{CaCO}_3} \times \chi_{\text{CaCO}_3} \times \lambda_3 \quad (\text{equation 4-9})$$

where  $K^*$  is the conditional solubility constant,  $K$  is the solubility constant,  $\chi$  is the molar fraction and  $\lambda$  is the activity coefficient that is proportional to the interaction parameter (the nondimensional Guggenheim parameter)  $a_0$ . In the case of the non-ideal  $(\text{Ca}_{(1-\gamma)}\text{Sr}_{\gamma})\text{CO}_3$  solid solution  $a_0 = 5.7$  /Tesoriero and Pankow 1996/. According to the aqueous concentration of

Sr and <sup>RD</sup>Sr, it can be assumed that both SrCO<sub>3</sub> and <sup>RD</sup>SrCO<sub>3</sub> will have a molar fraction close to 1×10<sup>-4</sup> during the simulation time. This value is below the miscibility gap defined for the (Ca<sub>(1-γ)</sub>Sr<sub>γ</sub>)CO<sub>3</sub>/Tesoriero and Pankow 1996/. Also, the consideration of these trace molar fractions for Sr and <sup>RD</sup>Sr implies that  $\chi_{\text{CaCO}_3} \approx 1$ , and then,  $K^*_{\text{CaCO}_3} \approx K_{\text{CaCO}_3}$ .

Between natural and repository-derived strontium end-members (SrCO<sub>3</sub> and <sup>RD</sup>SrCO<sub>3</sub>) the solid solution is considered ideal, and therefore  $\lambda_1 = \lambda_2$ . Consequently, the conditional solubility constants of SrCO<sub>3</sub> and <sup>RD</sup>SrCO<sub>3</sub> are the same. The calculated conditional solubility constants for both SrCO<sub>3</sub> and <sup>RD</sup>SrCO<sub>3</sub> are:



### Initial composition of the exchanger

The clay content in the till is usually more than 5 wt%, with illite being the most abundant clay mineral. For modelling purposes and after refinement of the geochemical initial conditions (see section 4.1) the content of illite is set 10 wt%, which represents a site density of 1.2 mol/L.

The total concentration of sites in illite is kept constant during the reactive transport simulations since it is assumed that this mineral does not dissolve (nor precipitate) in the environmental conditions considered in the model. Exchange constants have been implemented following the Gaines-Thomas convention and are shown in Table 3-4.

The composition of the exchangeable sites in the illite in the till at Forsmark is unknown. For this reason, the initial exchanger composition has been considered to be in equilibrium with the reference groundwater. This calculation has been conducted using the PHREEQC code /Parkhurst and Appelo 1999/ and the resulting initial composition is shown in Table 4-2. From this calculation, the interlayer in the illite in equilibrium with the reference water is rich in calcium, which is the dominant cation in the illite exchanger, occupying approximately 86% of the total number of exchangeable sites.

**Table 4-2. Calculated initial composition of the illite interlayer in reference case #1.**

Site	mol·L <sub>water</sub> <sup>-1</sup>
Planar sites	
NaX	5.67 × 10 <sup>-3</sup>
KX	7.12 × 10 <sup>-3</sup>
CsX	1.20 × 10 <sup>-8</sup>
SrX <sub>2</sub>	4.35 × 10 <sup>-4</sup>
CaX <sub>2</sub>	5.48 × 10 <sup>-1</sup>
MgX <sub>2</sub>	3.53 × 10 <sup>-2</sup>
Type II sites	
NaX <sup>II</sup>	2.36 × 10 <sup>-3</sup>
KX <sup>II</sup>	2.96 × 10 <sup>-2</sup>
CsX <sup>II</sup>	4.97 × 10 <sup>-7</sup>
Frayed edge sites (FES)	
NaX <sup>FES</sup>	9.13 × 10 <sup>-6</sup>
KX <sup>FES</sup>	2.29 × 10 <sup>-4</sup>
CsX <sup>FES</sup>	4.84 × 10 <sup>-6</sup>
NH4X <sup>FES</sup>	1.57 × 10 <sup>-4</sup>

Considering only the planar sites, calcium covers approximately 91% of these type of sites, with a concentration of  $5.48 \times 10^{-1} \text{ mol} \cdot \text{L}_{\text{water}}^{-1}$ . Magnesium is the second most important cation in these sites (occupying approximately 7% of the planar sites, one order of magnitude lower than calcium). The concentrations of sodium and potassium are two orders lower than the concentration of calcium. Caesium is weakly retained in this type of sites (with a concentration of  $1.20 \times 10^{-8} \text{ mol} \cdot \text{L}_{\text{water}}^{-1}$ ). In contrast, in the frayed edge sites (“FES”) and “Type II” sites, caesium is strongly retained (up to  $4.84 \times 10^{-6} \text{ mol} \cdot \text{L}_{\text{water}}^{-1}$  in FES) despite the relative low site density.

In the Type II and FES, potassium is the most abundant cation. Interestingly, ammonium is also abundant in the FES (up to  $1.57 \times 10^{-4} \text{ mol} \cdot \text{L}_{\text{water}}^{-1}$ ).

### Initial composition of ferrihydrite surface

The initial composition of the ferrihydrite surface in equilibrium with the till system is shown in Table 4-3. The most abundant surface complex is the neutral  $\equiv\text{HFO}^{\circ}\text{OH}$ , although the concentration of surface carbonate complexes is also significant. Uranium is mainly sorbed as the carbonate complex  $\equiv(\text{HFO}^{\circ}\text{O})_2\text{UO}_2\text{CO}_3^{2-}$  in the high-affinity sites. The initial concentration of total uranium sorbed is  $1.89 \times 10^{-5} \text{ mol} \cdot \text{L}_{\text{water}}^{-1}$ , corresponding to uranium concentration in the till of  $3.23 \times 10^{-6} \text{ mol} \cdot \text{kg}^{-1}_{\text{till}}$  (considering a total porosity of 25% and a bulk density of 1.95 kg/L) if all immobilised uranium in the system is considered to be sorbed onto ferrihydrite. The U/Fe molar ratios in the till range from  $1.5 \times 10^{-5}$  to  $1.5 \times 10^{-4}$  /Grandia et al. 2007, Figure 2-15/. In the numerical model, an initial ferrihydrite concentration of 0.1 wt% in the till has been considered, which corresponds to  $1.1 \times 10^{-2} \text{ mol} \cdot \text{kg}^{-1}_{\text{till}}$ . Assuming that most Fe and U are linked to iron oxyhydroxides, which is a realistic approach, the resulting U/Fe molar ratio in the numerical model is  $2.94 \times 10^{-4}$ , which is within the range of U/Fe actually measured in the till.

**Table 4-3. Initial concentration of the species adsorbed on ferrihydrite surfaces in reference case #1.**

Sites	$\text{mol} \cdot \text{L}_{\text{water}}^{-1}$
Strong sites	
$\equiv\text{HFO}^{\circ}\text{OH}$	$9.91 \times 10^{-5}$
$\equiv\text{HFO}^{\circ}\text{OH}_2^+$	$1.24 \times 10^{-5}$
$\equiv\text{HFO}^{\circ}\text{O}^-$	$1.90 \times 10^{-6}$
$\equiv(\text{HFO}^{\circ}\text{O})_2\text{UO}_2$	$1.26 \times 10^{-6}$
$\equiv(\text{HFO}^{\circ}\text{O})_2\text{UO}_2\text{CO}_3^{2-}$	$1.77 \times 10^{-5}$
$\equiv\text{HFO}^{\circ}\text{CO}_3\text{H}$	$3.77 \times 10^{-5}$
$\equiv\text{HFO}^{\circ}\text{CO}_3^-$	$1.00 \times 10^{-5}$
Weak sites	
$\equiv\text{HFO}^{\text{w}}\text{OH}$	$5.37 \times 10^{-2}$
$\equiv\text{HFO}^{\text{w}}\text{OH}_2^+$	$6.71 \times 10^{-3}$
$\equiv\text{HFO}^{\text{w}}\text{O}^-$	$1.03 \times 10^{-3}$
$\equiv(\text{HFO}^{\text{w}}\text{O})_2\text{UO}_2$	$6.68 \times 10^{-7}$
$\equiv(\text{HFO}^{\text{w}}\text{O})_2\text{UO}_2\text{CO}_3^{2-}$	$1.33 \times 10^{-7}$
$\equiv\text{HFO}^{\text{w}}\text{CO}_3\text{H}$	$2.05 \times 10^{-2}$
$\equiv\text{HFO}^{\text{w}}\text{CO}_3^-$	$5.42 \times 10^{-3}$

### 4.3.2 Reference case #2: The clay system

#### **Hydrogeological initial and boundary conditions**

As already mentioned, the reference case #2 simulates the water flow and geochemical processes that occur in a clay layer located immediately underneath a surface water body that constitutes a discharge area of the till aquifer. The flow conditions prescribed for the clay system depend on the flow conditions of the surrounding till aquifer. After analysing the flow conditions in a complex model with a layer of clay in the top right corner of a till aquifer, the prescribed boundary conditions were set as shown in Figure 4-6 (for more details see /Grandia et al. 2007, section 5.5.2/).

#### **Hydrogeochemical initial and boundary conditions**

##### **Initial groundwater composition**

The redox state of clay porewaters is expected to be controlled by microbial activity. In some lakes similar to those at Forsmark, reducing conditions are evidenced by the presence of biogenic pyrite /Percival et al. 2001, Outridge et al. 2005/. Given that a relatively reducing environment in the lake bottom sediments is expected, and that these sediments are relatively rich in calcite /Hedenström 2004/, the porewater in the clay layer has been considered in equilibrium with pyrite, siderite and calcite.

Consequently, the composition of the initial porewater in the reference case #2 results from the equilibration of the water sample collected at the sampling point PFM117 with these minerals (Table 4-4). This water was also equilibrated with amorphous uraninite since this phase represents the solubility limiting phase in this system, and the precipitation of this uranium phase is expected to be the only process able to retain uranium in the clay system. The composition of the deep groundwater before and after repository release is the same as in reference case #1.

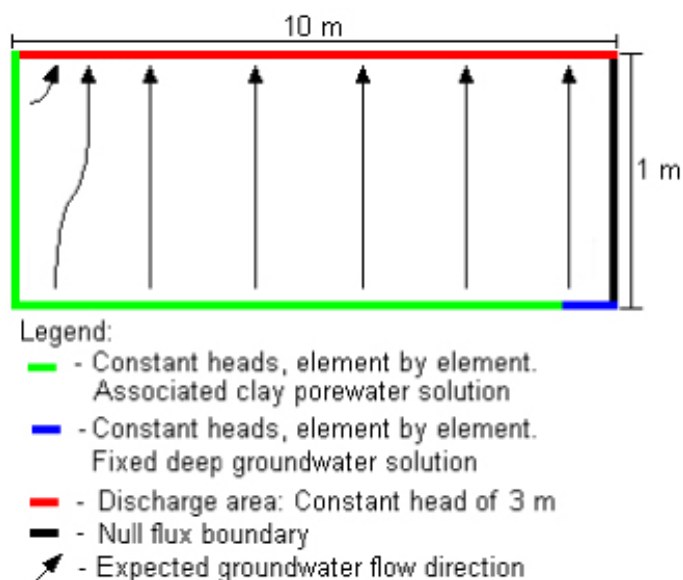


Figure 4-6. Boundary conditions for reference case #2.



**Table 4-4. Initial composition of glacial clay porewater. Deep groundwater before and after repository release has the same composition as in reference case #1 (Table 4-1).**

Glacial clay porewater	
pH	7.75
Eh(mV)	-204
Na	$2.65 \times 10^{-4}$
K	$5.19 \times 10^{-5}$
Ca	$1.18 \times 10^{-3}$
Mg	$1.16 \times 10^{-4}$
C(IV)	$2.50 \times 10^{-3}$
Cl	$1.53 \times 10^{-4}$
SO <sub>4</sub> <sup>2-</sup>	$6.39 \times 10^{-5}$
Si	$4.63 \times 10^{-4}$
Fe <sub>total</sub>	$8.34 \times 10^{-7}$
Sr	$6.23 \times 10^{-7}$
U	$1.979 \times 10^{-9}$
Cs	$4.50 \times 10^{-11}$ <sup>(1)</sup>
NH <sub>4</sub> <sup>+</sup>	$1.81 \times 10^{-5}$
Humic acid	$1.00 \times 10^{-4}$ <sup>(1)</sup>

Concentrations in mol·L<sup>-1</sup>.

<sup>(1)</sup> Taken from maximum [Cs] in water sample from KFM01A, <sup>(1)</sup> assuming that humic acid is approximately 10% of DOC.

The presence of organic acids dissolved in the porewater is represented by  $1.0 \times 10^{-4}$  mol·L<sup>-1</sup> of humic acid. This value corresponds to 10% of the total DOC in the bottom lake porewater. Under the pH and redox conditions of the clay porewater the U(VI) dominant species are uranium carbonate complexes, namely UO<sub>2</sub>(CO<sub>3</sub>)<sub>3</sub><sup>4-</sup> and UO<sub>2</sub>(CO<sub>3</sub>)<sub>2</sub><sup>2-</sup>. The main humate is the complex formed with calcium (CaHumate<sup>+</sup>) representing a 97.5% of the dissolved humics.

### Initial composition of the exchanger

The modelled domain of the clay system is composed of glacial clays that are rich in illite /Hedenström 2004/. In the simulations, an illite content of 50 wt% has been considered in the model, which leads to an exchange site density of 0.8 mol/L, as shown in section 4.1. As in the reference case #1, the total concentration of sites in illite is kept constant during the reactive transport simulations, and the implemented exchange constants follow the Gaines-Thomas convention (Table 3-4).

The initial composition of the exchangeable sites in the illite present in the glacial clays has been calculated by equilibrating these exchangeable sites with the glacial clay porewater, using the PHREEQC code /Parkhurst and Appelo 1999/. The resulting initial exchanger composition is shown in Table 4-5.

The illite exchanger composition after the equilibration of the illite exchangeable sites with the glacial clay porewater may be summarised as follows: (1) the most abundant cation in the illite interlayer is calcium, which occupies 93% of the planar sites, with a concentration of  $2.97 \times 10^{-1}$  mol·L<sub>water</sub><sup>-1</sup>, followed by magnesium which is the second most abundant cation in the planar sites, with a concentration one order of magnitude lower than that of calcium; (2) in the planar sites, caesium is the less abundant cation, while potassium, sodium and strontium show intermediate concentrations in this type of sites; (3) potassium is the most abundant cation in the type II sites, while in the FES ammonium is the most abundant cation (Table 4-5). As shown in Table 4-5, caesium is most effectively retained in the FES, followed by the type II sites, as expected by the exchange constants given in Table 3-4.

**Table 4-5. Initial composition of the illite interlayer in reference case #2.**

Site	mol·L <sub>water</sub> <sup>-1</sup>
Planar sites	
NaX	$1.19 \times 10^{-3}$
KX	$2.94 \times 10^{-3}$
CsX	$8.08 \times 10^{-9}$
SrX <sub>2</sub>	$2.14 \times 10^{-4}$
CaX <sub>2</sub>	$3.71 \times 10^{-1}$
MgX <sub>2</sub>	$2.54 \times 10^{-2}$
Type II sites	
NaX <sup>II</sup>	$7.79 \times 10^{-3}$
KX <sup>II</sup>	$1.93 \times 10^{-1}$
CsX <sup>II</sup>	$5.28 \times 10^{-6}$
Frayed edge sites (FES)	
NaX <sup>FES</sup>	$9.29 \times 10^{-6}$
KX <sup>FES</sup>	$4.58 \times 10^{-4}$
CsX <sup>FES</sup>	$1.59 \times 10^{-5}$
NH4X <sup>FES</sup>	$2.01 \times 10^{-3}$

## 4.4 Set-up of the sensitivity analysis

The sensitivity analysis is developed in order to estimate the impact of considering distinct values for the most important geochemical parameters on model results. Since the purpose of this sensitivity analysis is to investigate site specific conditions, in order to have a realistic approach to the natural geochemical variability at Forsmark and its impact on model results, the ranges for the parameters selected for sensitivity analysis were set according to site specific features of the till and the clay deposits.

### 4.4.1 Reference case #1: The till system

The sensitivity analysis developed for the till system focuses on two main geochemical features: the (Ca,Sr)CO<sub>3</sub> solid solution and the cation exchange capacity (CEC). As mentioned above, the calcium carbonate present in the till and clay deposits is considered to have trace amounts of strontium and, therefore, the CaCO<sub>3</sub> contents calculated for each system actually correspond to the contents of a (Ca,Sr)CO<sub>3</sub> solid solution.

The sensitivity analysis for (Ca,Sr)CO<sub>3</sub> solid solution is based in three cases. The first case, being the reference case #1, is set with 1 mol/L of Sr-bearing calcium carbonate that forms a non-ideal solid solution between both end-members (CaCO<sub>3</sub> and SrCO<sub>3</sub>) and the equilibrium with siderite. The second case is as the reference case #1, but without considering the equilibrium with siderite. The third case is set without solid solution nor calcite, in order to evaluate the role of the (Ca,Sr)CO<sub>3</sub> solid solution in strontium mobility, and the relative importance of cation exchange and (Ca,Sr)CO<sub>3</sub> solid solution for the retention of Sr.

In reference case #1, the strontium molar fraction of the solid solution initially present in the modelled domain was set adjusting the strontium molar fraction in the solid solution to a value that is in equilibrium with the natural aqueous strontium concentration. The resulting strontium molar fraction is  $1.73 \times 10^{-5}$ .

In order to study the impact of variable CEC values of the till deposit, that lead to distinct concentrations of available cation exchange sites, it was decided to evaluate the results in two scenarios. One scenario corresponds to the reference case with a CEC of 200 meq/L ( $1.6 \times 10^{-1}$  mol/L of cation exchange sites), and an alternative scenario with a CEC of 20 meq/L, which corresponds to  $1.6 \times 10^{-2}$  mol/L of cation exchange sites in the till deposit. Table 4-6 shows the summary of the sensitivity analysis set for the till system.

#### 4.4.2 Reference case #2: The clay system

In the clay system, the sensitivity analysis developed focuses on three main features: the (Ca,Sr) CO<sub>3</sub> solid solution, the cation exchange capacity (CEC) and the humic acids. In a similar way as in the till system, the sensitivity analysis for Sr deals with the variation of the concentration of (Ca,Sr)CO<sub>3</sub> solid solution and the CEC. The reference case #2 is set with 1 mol/L of (Ca,Sr) CO<sub>3</sub>, with a strontium molar fraction of  $1.4 \times 10^{-5}$ , which is in equilibrium with the reference water selected for the clay system. As in the till system, the effect of not considering siderite will be evaluated. An alternative scenario will be simulated without (Ca,Sr)CO<sub>3</sub> solid solution.

The reference case #2 considers a CEC of 200 meq/L, which corresponds to 1 mol/L of exchange sites). As an alternative scenario, a CEC of 20 meq/L which corresponds to 0.1 mol/L of cation exchange sites, has been simulated. The sensitivity analysis for the humic acids concentration is based on the changes in uranium speciation caused by the increment of the concentration of these organic acids in the clay porewater (Figure 4-7).

**Table 4-6. Summary of the sensitivity analysis set for the till system. RC refers to reference case #1.**

Radionuclide	Initial geochemical conditions	
Sr	With (Ca,Sr)CO <sub>3</sub> solid solution (Sr molar fraction = $1.73 \times 10^{-5}$ ) Without (Ca,Sr)CO <sub>3</sub> solid solution	With siderite (RC) Without siderite
Sr, Cs	CEC = 200 meq/L (RC) CEC = 20 meq/L	

$[\text{CO}_3^{2-}]_{\text{tot}} = 2.47 \text{ mM}$     $[\text{UO}_2^{2+}]_{\text{tot}} = 1.98 \text{ nM}$     $[\text{Ca}^{2+}]_{\text{tot}} = 1.15 \text{ mM}$     $[\text{Cl}]_{\text{tot}} = 0.15 \text{ mM}$   
 $\text{pe} = -3.65$     $[\text{SO}_4^{2-}]_{\text{tot}} = 63.90 \text{ }\mu\text{M}$     $\text{pH} = 7.65$     $[\text{Si}(\text{OH})_4]_{\text{tot}} = 46.30 \text{ }\mu\text{M}$

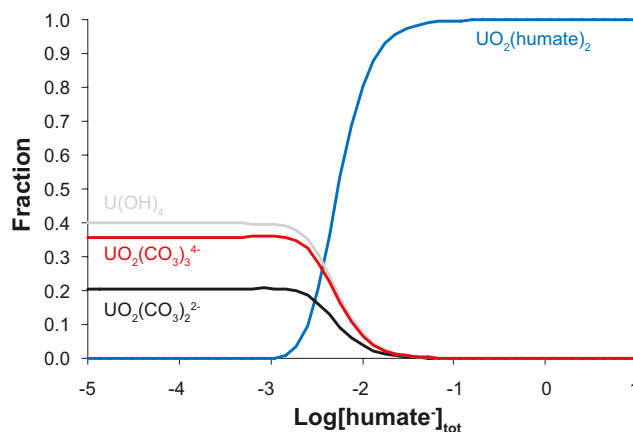


**Figure 4-7. Evolution of the uranium speciation in a solution with a variable humic acid concentration, under the hydrochemical conditions of the clay porewater.**

In reference case #2, the clay porewater has a humic acid concentration of  $1 \times 10^{-4}$  M (which corresponds approximately to 10% of the DOC in the reference water, collected in sampling point PFM117). Under this conditions the uranium complexation with humic acids is not very important, since the concentration of these aqueous complexes is extremely low, being  $U(OH)_4$  the dominant aqueous species (Figure 4-7).

When the concentration of humic acids increases, the aqueous complex  $UO_2(\text{humate})_2$  becomes progressively more abundant (see reactions in Table 3-6), which may prevent the precipitation of amorphous uraninite. Since the precipitation of this uranium solid phase is the only process able to retain uranium in the clay system it was decided to evaluate three alternative scenarios: (1) with a humic acid concentration of  $3 \times 10^{-3}$  M and (2) of 0.1 M and (3) without humic acids.

Table 4-7 shows the summary of the sensitivity analysis set for the clay system.

**Table 4-7. Summary of the sensitivity analysis set for the clay system. RC refers to reference case #2.**

Radionuclide	Initial geochemical conditions	
Sr	With (Ca,Sr)CO <sub>3</sub> solid solution (Sr molar fraction = $1.4 \times 10^{-5}$ )	With siderite (RC)
	With CaCO <sub>3</sub> solid solution	Without siderite
Sr, Cs	CEC = 200 meq/L (RC)	
	CEC = 20 meq/L	
U	With humic acids	$1 \times 10^{-4}$ mol/L (RC)
		$3 \times 10^{-3}$ mol/L
		$1 \times 10^{-1}$ mol/L
	Without humic acids	
	Without siderite	

## 5 Numerical model results

### 5.1 Reference case #1: The till system

#### 5.1.1 Conservative transport

The transport of solutes is affected by geochemical processes and by the hydraulic gradient and groundwater flow generated from the prescribed boundary conditions. Figure 5-1 shows the groundwater flow directions and hydraulic gradient calculated by the numerical tool. In this figure it is possible to see that the groundwater entering through the left boundary, moves horizontally along most of the domain, and flows out through the last 20 m of the top boundary, where a significant upward flow is generated.

The conservative transport in the reference case #1 has been studied using chloride as a tracer, given that no retention processes have been implemented for this element. Initial chloride concentration in the till groundwater is  $1.9 \times 10^{-3}$  mol/L, whereas in the deep groundwater  $[Cl^-]$  is  $1.07 \times 10^{-1}$  mol/L.

The tracer reaches the discharge area ( $X=80-100$  m,  $Y=3$  m) approximately 5 years after the intrusion of the deep groundwater (Figure 5-2). This means that after this time, a steady-state is reached for the conservative transport. The dilution of the deep groundwater in the till domain has been calculated by using the following equation:

$$[Cl_{mix}] = (1 - X)[Cl_{deep}] + X[Cl_{till}] \quad (\text{equation 5-1})$$

where  $[Cl_{mix}]$  is the chloride concentration in a given node of the modelled domain after the steady-state for conservative transport has been reached,  $[Cl_{deep}]$  is the concentration of chloride in the reference deep groundwater ( $1.07 \times 10^{-1}$  mol/L),  $[Cl_{till}]$  is the concentration of chloride in the till reference water ( $1.9 \times 10^{-3}$  mol/L), and  $X$  is the relative volume of the till reference water in a given node of the modelled domain after the conservative transport steady-state has been reached, i.e. it is the dilution factor.

Equation 5-1 has been applied to the till system using the value of  $[Cl_{mix}]$  that is obtained in the node located in the discharge area of the domain ( $5.55 \times 10^{-3}$  mol/L), at  $X=80$  m and  $Y=3$  m. A dilution factor of 96% has been estimated for the discharge area of the till system.

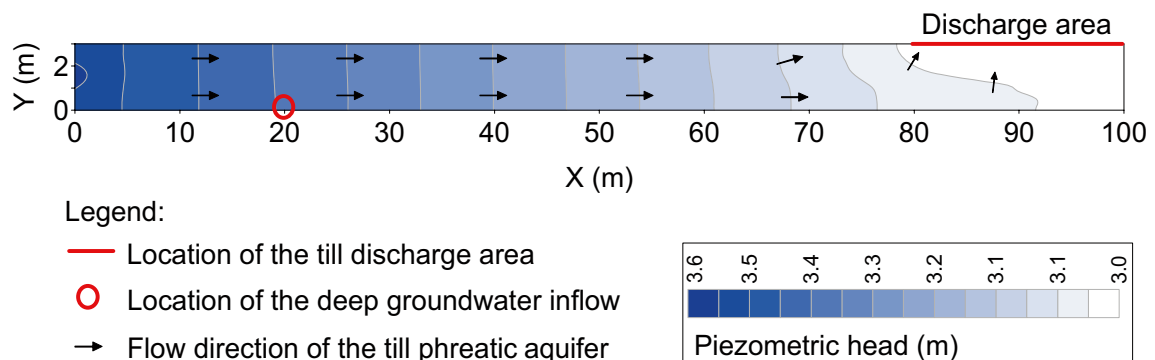
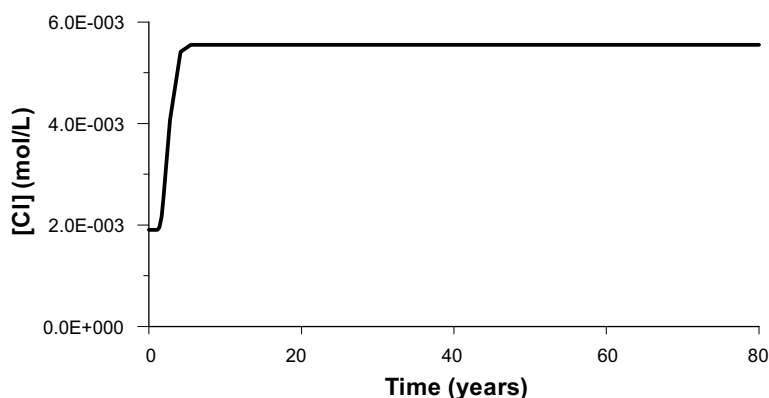


**Figure 5-1.** Groundwater flow directions and hydraulic gradient obtained from the numerical transport simulation after setting the prescribed boundary conditions.

(A)



(B)

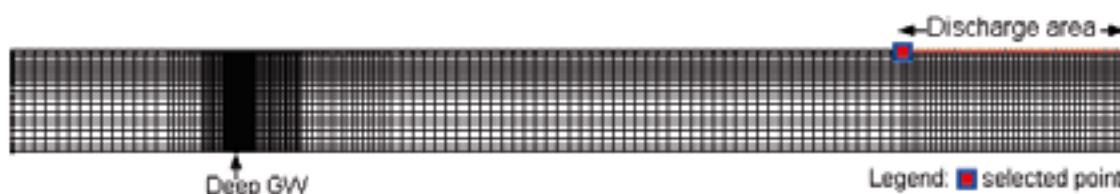


**Figure 5-2.** (A) Breakthrough curve of [Cl] in the node  $X=80$  m,  $Y=3$  m. The time needed to reach the stationary state of solute transport is approximately 5 years. (B) Location of selected point for the study of the evolution of the outflowing solution.

### 5.1.2 Reactive transport prior to repository release

While chloride is considered to behave conservatively other ions, including the selected radionuclides, are expected to react with the host rock. Strontium, uranium and caesium are naturally present in trace amounts in the three water compositions selected for the numerical simulations (Table 2-1). Since radium is below detection limit (or in the range of  $1 \times 10^{-14}$  mol/L) in the referred water samples (Forsmark data freeze v. 1.2), the presence of this radionuclide in the modelled domains, is exclusively related to repository release.

This section deals with the study of the system prior to the arrival of radionuclides released from repository. The study of this stage is necessary to establish a geochemical stationary state in the domain, since the intrusion of the deep groundwater causes changes in the chemical equilibrium between the host rock and the till porewater.

The evolution of the concentration of the naturally occurring radionuclides during this initial period is shown in Figure 5-3. The most important changes in the geochemical state of the system occur from 0 to 80 years. After 2,700 years it is assumed that the system has approached a geochemical stationary state.

The aqueous strontium concentration in the deep groundwater is 1.5 orders of magnitude higher than in the till groundwater (see Table 4-1); therefore, initially (0–5 years), a notable increment of the aqueous strontium concentration is observed in the monitoring point (Figure 5-4). After this period, and until approximately 40 years of simulation, a steep decrease of the aqueous strontium concentration is predicted. This reflects the relatively fast retention of strontium in illite and  $(\text{Ca,Sr})\text{CO}_3$  solid solution, as a response to the deep groundwater inflow. From 30 until 200 years of simulation the system is relatively stable, followed by an increment of the aqueous strontium concentration at the discharge area that stabilizes at  $3.45 \times 10^{-6}$  mol/L.

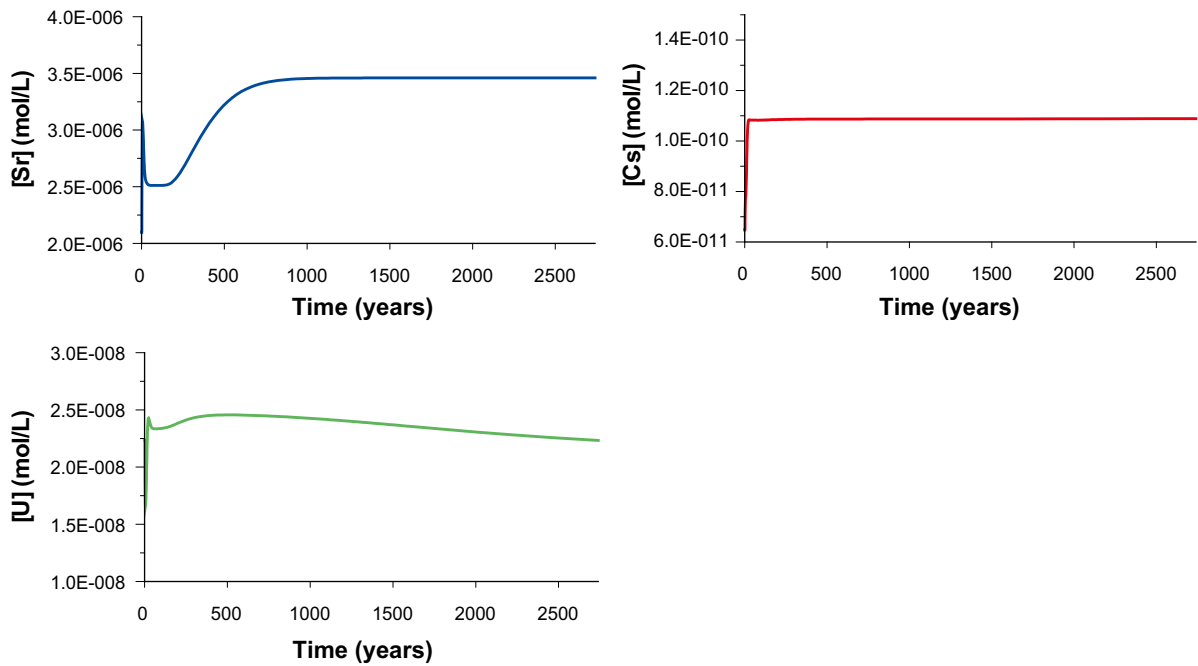


**Figure 5-3.** Predicted evolution of strontium, uranium, and caesium aqueous concentrations during the first 2,700 years of reactive transport model, at the discharge area, prior to repository release. The distinct behaviours of these elements reflect the geochemical processes that affect each one of them. Monitoring point located at  $X=80$  m,  $Y=3$  m.

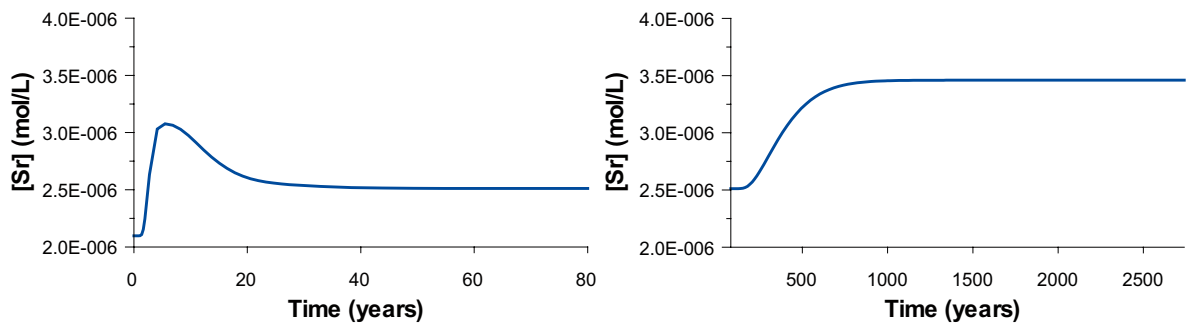


**Figure 5-4.** Predicted evolution of strontium aqueous concentration during the first 80 years, and from 80 to 2,700 years of reactive transport simulation, at the discharge area, prior to repository release. Monitoring point located at  $X=80$  m,  $Y=3$  m.

The aqueous caesium concentration in the deep groundwater is approximately two orders of magnitude higher than in the till groundwater (see Table 4-1), and therefore, up to 5 years of simulation time, it is seen an increment of the aqueous caesium concentration at the discharge area (Figure 5-5). After this advective travel time, and until approximately 25 years of simulation, the aqueous caesium concentration keeps increasing at the monitoring point, and then reaches a more or less stable concentration that reflects the approach to the geochemical steady state.

Retention of caesium in illite induces a progressively lower increase of the aqueous concentration of Cs in the discharge area. After 100 years, the concentration of aqueous Cs at the discharge area, keeps increasing, but at a much slower rate than during the first 100 years. The behaviour of aqueous Cs at the discharge area of the till deposit reflects the fact that, until the end of the simulation, illite has still sites able to accommodate Cs entering into the system from deep source.

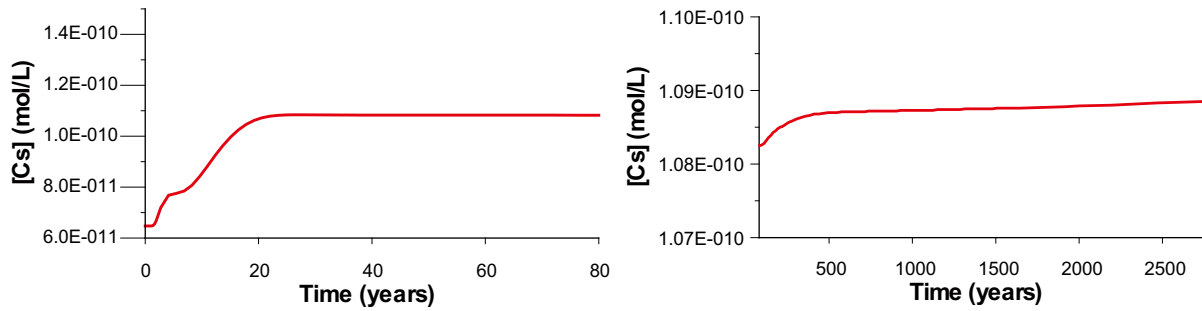


**Figure 5-5.** Predicted evolution of caesium aqueous concentration during the first 80 years, and from 80 to 2,700 years of reactive transport simulation, at the discharge area, prior to repository release. Note that vertical scales are different for each plot. Monitoring point located at  $X=80$  m,  $Y=3$  m.

The concentration of aqueous uranium in the deep groundwater is approximately 1.5 orders of magnitude lower than in the till groundwater (see Table 4-1). Consequently, a decrease of the aqueous uranium concentration at the discharge area is predicted for the initial 5 years of simulation (Figure 5-6). In the next 25–30 years, the aqueous uranium concentration increases up to values slightly higher than the initial till groundwater composition. This increment is caused by ferrihydrite dissolution during the whole simulation period, as a response to the deep groundwater inflow. Since uranium is adsorbed to this phase, ferrihydrite dissolution leads to a release of uranium into solution (Figure 5-7).

After this first disturbance, uranium aqueous concentration at the discharge area evolves with smaller oscillations, but showing a decreasing tendency during the last 1,700 years of simulation (Figure 5-6). Although ferrihydrite keeps dissolving during this last 1,700 years, the adsorption on the remaining moles of ferrihydrite is sufficiently efficient to lead the system towards a decrease of the uranium aqueous concentration. In addition, the continued inflow of deep groundwater with a slightly lower U concentration than that of the till porewater also contributes to the progressive decrease of U concentration observed at the end of the simulation.

The disturbance of the geochemical system of the till deposit due to the inflow of the deep groundwater is also reflected by the evolution of pH and pe, which are initially controlled by the equilibrium of  $(Ca,Sr)CO_3$  solid solution, siderite and ferrihydrite with the till groundwater. Figure 5-8 shows the evolution of pH and pe at the discharge area, during the 2,700 years of reactive transport simulation, prior to radionuclide release from repository.

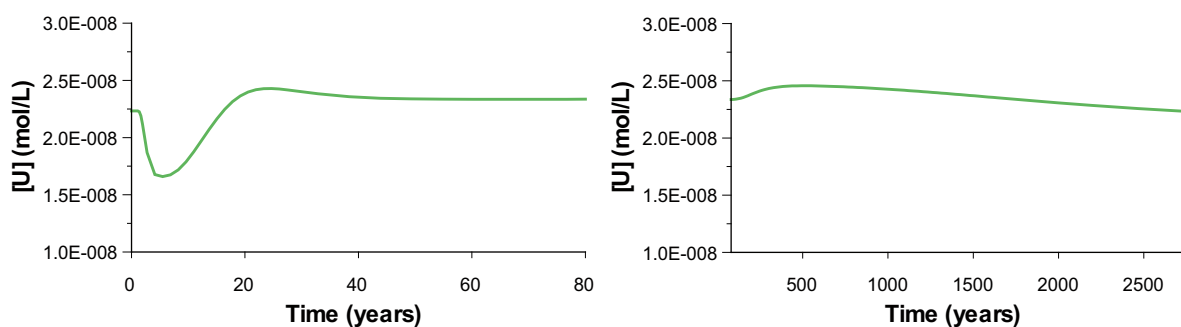


**Figure 5-6.** Predicted evolution of uranium aqueous concentration during the first 80 years, and from 80 to 2,700 years of reactive transport simulation, at the discharge area, prior to repository release. Monitoring point located at  $X=80$  m,  $Y=3$  m.





**Figure 5-7.** Predicted evolution of aqueous uranium in the modelled domain prior to repository release. At the initial 5 years, a transient plume of lower uranium concentration (light blue area) is predicted since deep groundwater has a lower uranium concentration than till porewater. Then, uranium is released into solution due to dissolution of  $\text{Fe}(\text{OH})_3$ , leading to the higher concentration plume (yellow area). And finally, a balance between release of uranium into solution and adsorption of uranium on  $\text{Fe}(\text{OH})_3$  is reached.

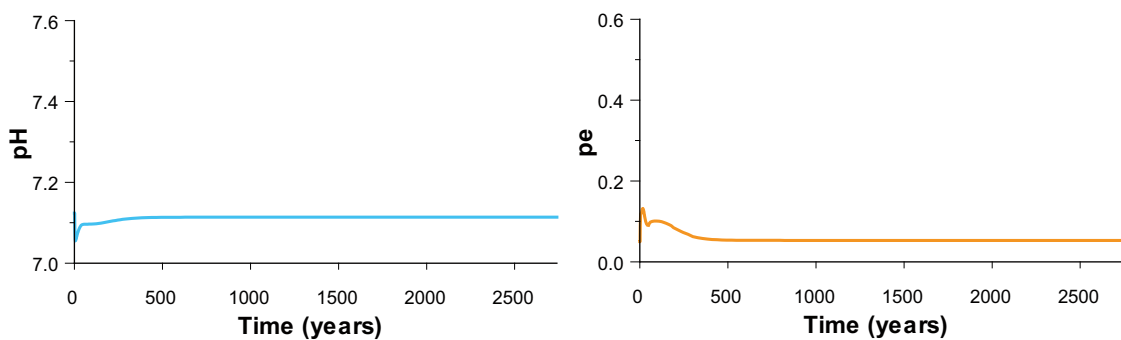


**Figure 5-8.** Predicted evolution of pH and pe. In the initial 500 years, small oscillations of pH and pe occur; due to the inflow of deep groundwater. During the remaining simulation period (until 2,700 years) these parameters are quite stable. Monitoring point located at  $X=80$  m,  $Y=3$  m.

### 5.1.3 Reactive transport after repository release

In the present numerical models, the simulation of repository release consists of an increment of Sr, Cs, U and Ra concentrations in the deep groundwater that enters in the till deposit through a fracture located at the bottom of the modelled domain. As already stated, the radionuclides derived from repository release were labelled in order to distinguish natural and repository-derived species. Exception is made for Ra, since this radionuclide is considered to be present below detection limit before repository release.

Figure 5-9 shows the evolution of natural and repository-derived strontium concentration at the discharge area of the till deposit. Deep groundwater affected by repository release, has a  $^{87}\text{Sr}$  concentration of  $8.37 \times 10^{-4}$  mol/L, which is approximately 1.5 orders of magnitude higher than the natural deep groundwater Sr concentration, and almost 2 orders of magnitude higher than the till groundwater Sr concentration.

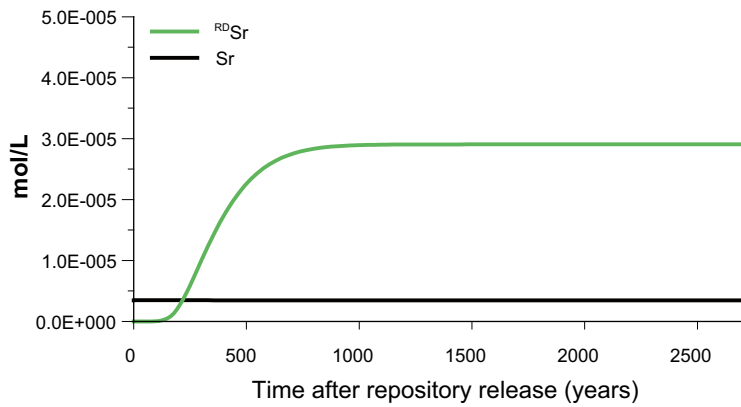


**Figure 5-9.** Predicted evolution of natural ( $Sr$ ) and repository-derived ( $^{RD}Sr$ ) strontium after repository release, at the discharge area. Monitoring point  $X=80$  m;  $Y=3$  m.

Approximately 1,000 years after repository release, the  $^{RD}Sr$  concentration in the discharge area reaches a stationary concentration of  $2.9 \times 10^{-5}$  mol/L, which is less than 5% of the concentration of  $^{RD}Sr$  achieved in the calculations for the deep groundwater after repository release. The retention capacity exerted by the sediments is dominated by illite sorption, as around 95% of the  $^{RD}Sr$  retained in the sediments occurs in the illite fraction (Figure 5-10).

The predicted evolution of natural and repository-derived caesium concentration at the discharge area of the till deposit is shown in Figure 5-11. Deep groundwater after repository release, has a  $^{RDCs}$  concentration of  $3.48 \times 10^{-7}$  mol/L, which is approximately 1.5 orders of magnitude higher than the natural deep groundwater caesium concentration, and 3.5 orders of magnitude higher than the till groundwater caesium concentration.

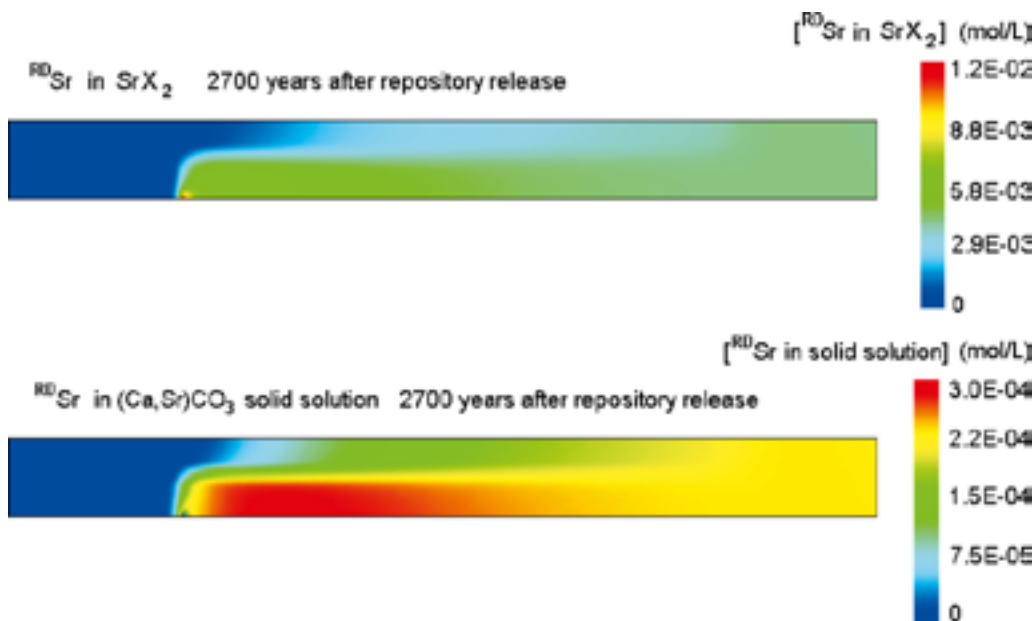


**Figure 5-10.**  $^{RD}Sr$  retained in the planar sites of illite and the  $(Ca,Sr)CO_3$  solid solution, at the end of the simulation period (2,700 years after repository release). It is seen that  $^{RD}Sr$  is incorporated preferentially in the illite fraction (note the different scales for both graphics) through the whole modelled domain.

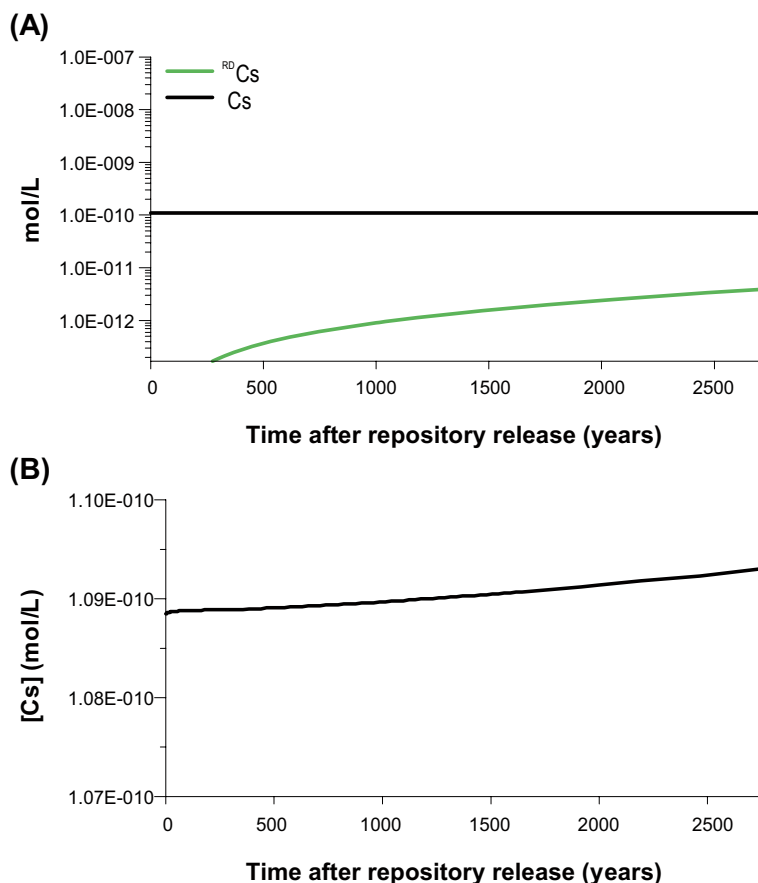


**Figure 5-11.** (A) Predicted evolution of natural (Cs) and repository-derived ( ${}^{\text{RD}}\text{Cs}$ ) caesium after repository release, at the discharge area. (B) Predicted evolution of natural Cs after repository release, plotted with a linear scale in order to observe the small increase of [Cs] during this period. Monitoring point  $X=80$  m;  $Y=3$  m.

In Figure 5-11A it seems that the aqueous concentration of natural Cs, at the discharge area, is stable. Nevertheless, after detailed observation (Figure 5-11B), it is seen that the concentration of natural Cs keeps increasing. Moreover, the corresponding rate of increment becomes slightly higher after repository release when compared with the tendency observed before repository release (Figure 5-5). The observed increase of natural Cs after repository release is due to the inflow of  ${}^{\text{RD}}\text{Cs}$  that competes with natural Cs for adsorption on illite.

After 2,500 years, only 3.5% of caesium flowing out of the till deposit is derived from repository release. The remarkable decrease of caesium concentration from the deep groundwater inflow point to the till discharge area is due to the high affinity of caesium for the FES of illite that readily retain caesium via cation exchange (Figure 5-12) and the replacement of Cs by  ${}^{\text{RD}}\text{Cs}$  in these sites in order to reach equilibrium.

Figure 5-13 shows the evolution of natural and repository-derived uranium concentration at the till discharge area. Deep groundwater after repository release, has a  ${}^{\text{RD}}\text{U}$  concentration of  $1.73 \times 10^{-8}$  mol/L, which is approximately 1.5 orders of magnitude higher than the natural deep groundwater uranium concentration, but 25% lower than the till groundwater uranium concentration. After 2,500 years, only 1.8% of uranium flowing out of the till deposit is derived from repository release.  ${}^{\text{RD}}\text{U}$  is retained in the till deposit due to the adsorption on  $\text{Fe}(\text{OH})_3$  surface (Figure 5-14).

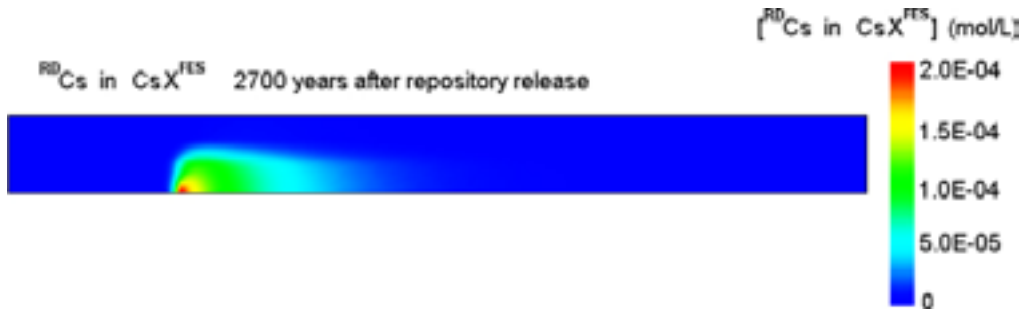


**Figure 5-12.** Predicted concentration of  $^{RD}Cs$  retained in FES of illite, at the end of the simulation period (2,700 years after repository release). Since caesium has a relatively high affinity for the FES,  $^{RD}Cs$  is readily retained in the vicinity of the deep groundwater inflow point.

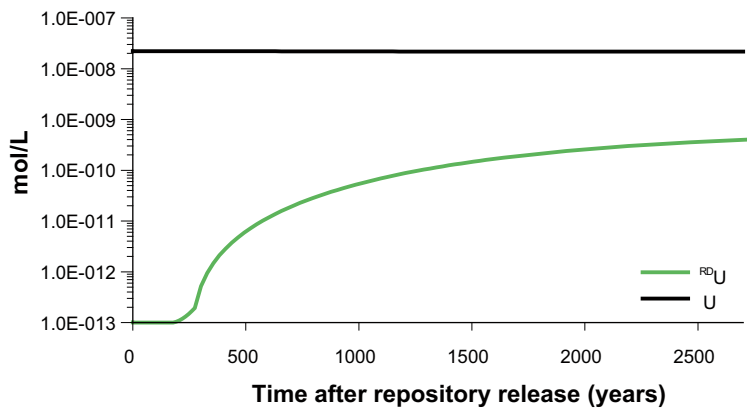


**Figure 5-13.** Predicted evolution of natural ( $U$ ) and repository-derived ( $^{RD}U$ ) uranium after repository release, at the discharge area. Monitoring point  $X=80$  m;  $Y=3$  m.

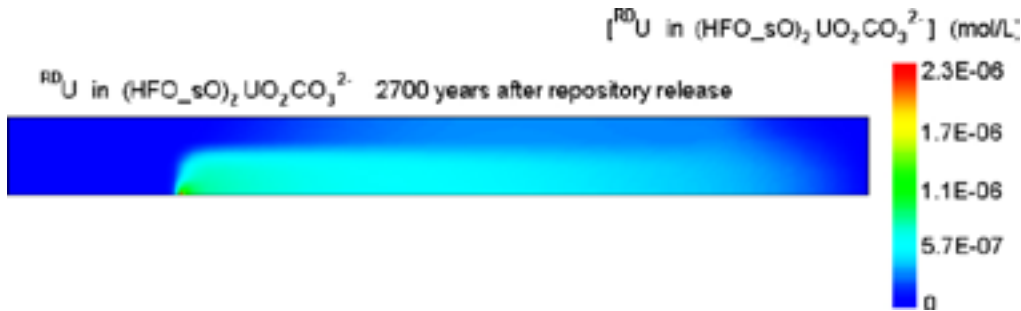


**Figure 5-14.** Predicted concentration of  $^{RD}U$  retained in the strong sites of  $Fe(OH)_3$  surface as  $UO_2CO_3^{2-}$ , at the end of simulation period (2,700 years after repository release).  $^{RD}U$  adsorbed on this surface site reaches a relatively wide area of the modelled domain.

Although it seems that after repository release the concentration of natural  $U$  is stable (Figure 5-13), in fact it is decreasing (Figure 5-15), as previously observed for the simulation performed before repository release (Figure 5-6). The addition of  $^{RD}U$  to the till system induces the inversion of a decreasing tendency of the total concentration of  $U$  ( $U + ^{RD}U$ ) to an increasing tendency, approximately at 1,300 years after repository release (Figure 5-15), despite that the natural uranium concentration is still decreasing.

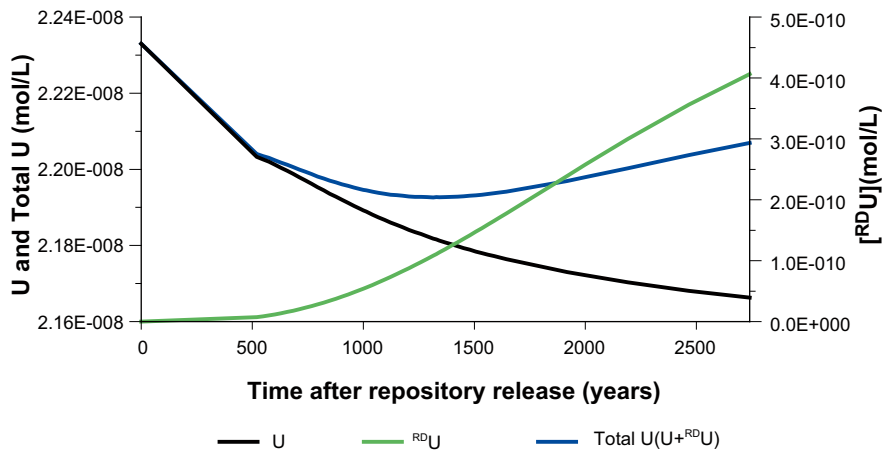


**Figure 5-15.** Predicted evolution of the concentration of natural U, <sup>RD</sup>U and total U (U + <sup>RD</sup>U) after repository release, at the discharge area. Monitoring point X=80 m; Y=3 m. It is seen that the concentration of natural U is decreasing, the concentration of <sup>RD</sup>U is increasing and the sum of both is increasing.

Figure 5-16 shows the evolution of repository-derived radium concentration at the till discharge area. Deep groundwater affected by repository release, has a Ra concentration of  $9.15 \times 10^{-11}$  mol/L. After 2,500 years Ra concentration at the discharge area of the till deposit is  $2 \times 10^{-12}$  mol/L. Ra is retained, in the vicinity of the deep groundwater inflow point via precipitation of (Ba,Ra)SO<sub>4</sub> (Figure 5-17).

#### 5.1.4 Conservative transport versus reactive transport

The reactive transport simulations predict that Sr, Cs, U and Ra derived from repository release would be retained in the till deposit. It is worth mentioning that in addition to geochemical reactions, dilution also plays an important role for the concentration of Cs and Ra in the till domain, as the considered concentrations of these radionuclides in deep groundwater after repository release compared to the concentrations of their natural counterparts are very different (around 3 orders of magnitude), whereas for Sr and U the difference in concentrations is less significant (around one order of magnitude for Sr and in the same order of magnitude for U). For a better quantification of the retention capacity of the Quaternary deposits, reactive and conservative numerical simulations are compared.

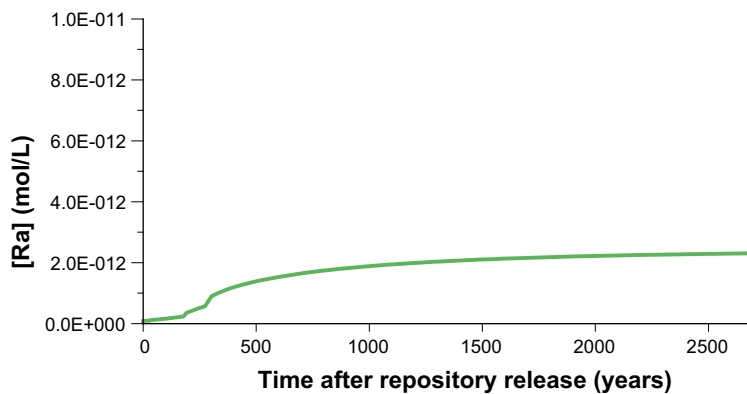


**Figure 5-16.** Predicted evolution of repository-derived (Ra) radium after repository release, at the discharge area. Monitoring point X=80 m; Y=3 m.



**Figure 5-17.** Predicted absolute concentration of Ra retained in  $(Ba,Ra)SO_4$  solid solution, at the end of the simulation time (2,700 years after repository release). Ra is readily retained in the vicinity of the deep groundwater inflow point due to precipitation of  $(Ba,Ra)SO_4$  solid solution.

The evolution of  $^{RD}Sr$  concentration considering the reactive transport shows that the maximum strontium concentration at the discharge area is retarded 1,000 years with respect to the conservative transport (Figure 5-18). The retention of strontium in the till deposit is limited since the maximum strontium concentration reached in the conservative transport is also reached in the reactive transport. Retention of strontium in the till deposit does not reduce the maximum strontium concentration reached when no reactions are considered, only delays the strontium breakthrough curve approximately 400 years.

Since a steady-state is reached for the reactive transport of  $^{RD}Sr$ , its concentration after this steady-state is mainly controlled by dilution (see section 5.1.1). After reaching the reactive transport steady-state, the retention capacity of the till system for  $^{RD}Sr$  is very little because the geochemical system has reached equilibrium, and therefore exchange of  $^{RD}Sr$  between the aqueous and solid phases is very small.

For caesium, the maximum  $^{RDCs}$  concentration predicted in the reactive transport simulation, at the discharge area of the till deposit, is approximately 3.5 orders of magnitude lower than the maximum  $^{RDCs}$  concentration reached in the conservative transport (Figure 5-19). This reflects the efficient retention of caesium in the till deposit.

Contrary to what was observed for  $^{RD}Sr$ , the reactive transport of  $^{RDCs}$  does not reach a steady-state during the time period simulated here. Therefore, the role of dilution on the concentration of  $^{RDCs}$  at the discharge area of the modelled domain does not have the same importance as for  $^{RD}Sr$ . At the end of the simulation period, the geochemical processes that retain  $^{RDCs}$  in the solid phase still play a major role on the concentration of  $^{RDCs}$  observed at the discharge area.

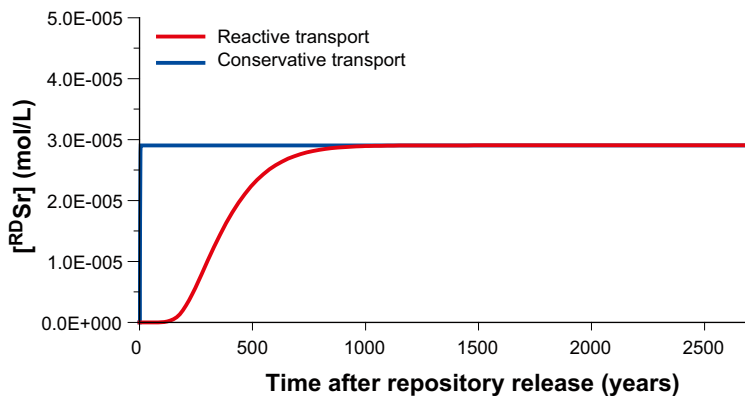


**Figure 5-18.** Breakthrough curves for  $^{RD}Sr$ , considering reactive and conservative transport. Monitoring point  $X=80$  m,  $Y=3$  m (discharge area).

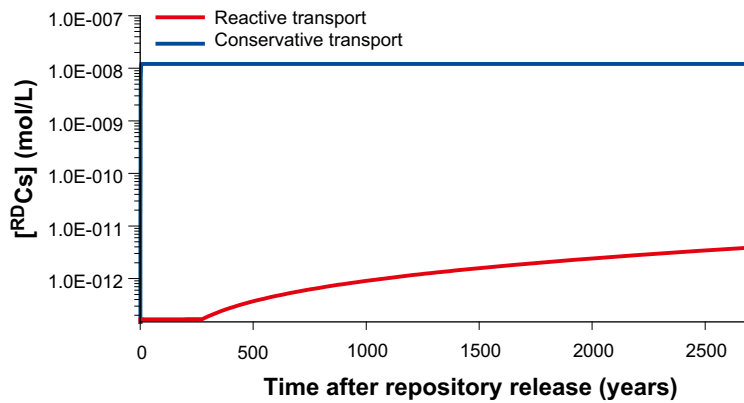


**Figure 5-19.** Breakthrough curves for  $^{RD}Cs$ , considering reactive and conservative transport. Monitoring point  $X= 80\text{ m}$ ,  $Y= 3\text{ m}$  (discharge area).

The evolution of  $^{RD}U$  concentration considering both reactive and conservative transport is shown in Figure 5-19. In the reactive transport, the maximum concentration of  $^{RD}U$  at the discharge area is approximately 67% of the maximum concentration of  $^{RD}U$  reached in the conservative transport.

As observed for  $^{RD}Cs$ , the reactive transport of  $^{RD}U$  does not reach a steady-state during the time period simulated here. Therefore, at the end of the simulation, adsorption of  $^{RD}U$  on ferrihydrite still plays a major role on the concentration of  $^{RD}U$  at the discharge area of the modelled domain, when compared to the effect of dilution.

Finally, for radium, the maximum concentration reached in the reactive transport is 30% lower than the maximum Ra concentration reached when no reactions with the solid phase are considered, i.e. in the conservative transport (Figure 5-21). Further, as observed for  $^{RD}Cs$  and  $^{RD}U$ , the reactive transport of Ra does not reach a steady-state during the time period simulated here.

### 5.1.5 Quantitative assessment of the retention efficiency

The efficiency of the near-surface Quaternary system for radionuclide retention can be quantitatively evaluated by comparison of the conservative versus reactive transport computed results. This evaluation is done in the observation point shown in Figure 5-2, which corresponds to the point where the most rapid arrival of deep contaminants to the surface can be expected.

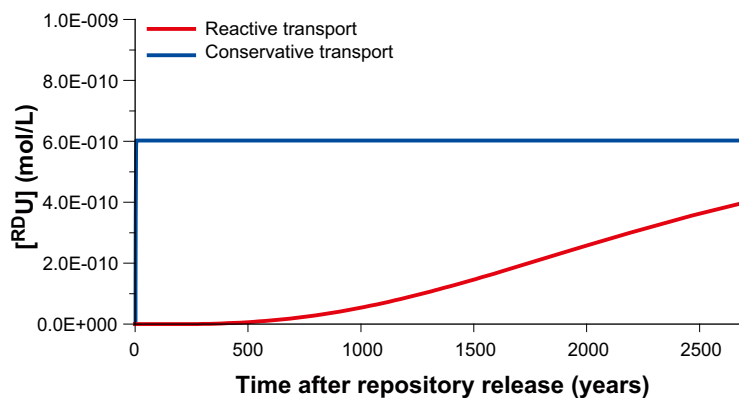


**Figure 5-20.** Breakthrough curves for  $^{RD}U$ , considering reactive and conservative transport. Monitoring point  $X= 80\text{ m}$ ,  $Y= 3\text{ m}$  (discharge area).

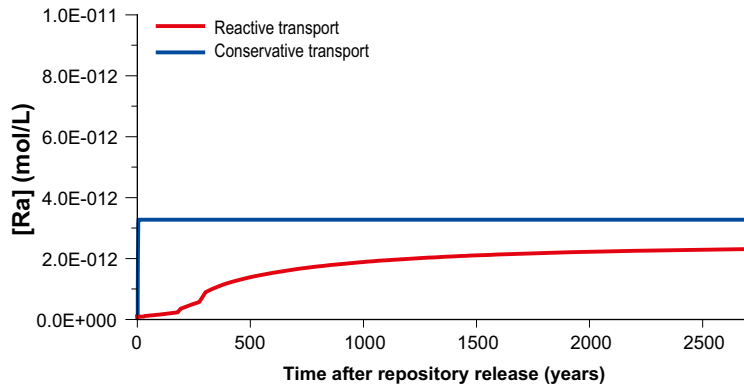


**Figure 5-21.** Breakthrough curves for Ra, considering reactive and conservative transport. Monitoring point  $X= 80 \text{ m}$ ,  $Y= 3 \text{ m}$  (discharge area).

The radionuclide retention efficiency ( $E$ ) of the system at a given time ( $\tau$ ) can be quantitatively evaluated according to:

$$E^{\tau} = 100 \times \left( 1 - \frac{R^{\tau}}{C^{\tau}} \right) \quad (\text{equation 5-2})$$

where  $R^{\tau}$  stands for the concentration of a solute at a given time ( $\tau$ ), observed in the modelled domain, when reactive transport is considered, and  $C^{\tau}$  stands for the concentration of a solute at a given time ( $\tau$ ), when conservative transport is considered.

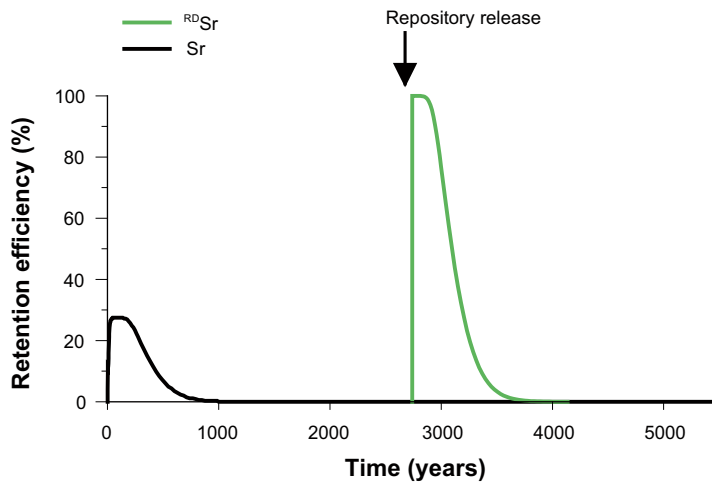
According to this expression, a null reactive concentration ( $R$ ) at a given time ( $\tau$ ) means that no mass of radionuclide is leaving the system at such time, resulting in a retention efficiency of 100%. A reactive concentration ( $R$ ) equal to the conservative concentration means that no retention is occurring at all so that the corresponding retention efficiency would be 0%. Negative efficiency means that in the reactive transport, the solid phase is releasing the radionuclide into solution, and therefore reactive concentration is higher than conservative concentration.

Figure 5-22 shows the time evolution of computed retention efficiencies of natural and repository-derived strontium. The maximum retention efficiency of natural strontium (30%) is reached at the beginning of the simulation time, when the system is evolving towards a geochemical steady state. This stage of favourable retention lasts approximately 125 years. Thereafter, retention efficiency of natural strontium drops to 0% until the end of the simulation period. This means that the till capacity to retain strontium is limited, i.e. illite and  $(\text{Ca,Sr})\text{CO}_3$  become progressively unable to incorporate more strontium.

When repository release is simulated, repository-derived strontium is retained in the modelled domain, although the system efficiency to retain natural strontium has reached a zero value. Immediately after repository release, the system reaches a retention efficiency for  $^{\text{RD}}\text{Sr}$  of 100%, which lasts again c. 125 years. After this period, retention efficiency for repository-derived strontium drops to zero. This behaviour of the till system reflects the tendency of the solid phase to establish a thermodynamic equilibrium with the “new” solution that results from deep groundwater intrusion, and therefore, when an increment of solute concentration in the aqueous phase occurs (like the one that simulates repository release), the solid phase reacts, retaining the excess of solute, until a new geochemical steady state is reached.

The maximum retention efficiency of natural caesium (82%) is reached at the beginning of the simulation time (Figure 5-23), when the system is evolving towards a geochemical steady state, and lasts approximately until the end of the simulation. The maximum retention of repository-derived caesium (100%) is reached 400 years after repository release, and it is maintained at 100% until the end of the simulation period.





**Figure 5-22.** Computed retention efficiency for natural (*Sr*) and repository-derived ( $^{RD}Sr$ ) strontium along the simulation time. Monitoring point  $X=80\text{ m}$ ,  $Y=3\text{ m}$  (discharge area).

The behaviour of the till system with respect to caesium reflects the high affinity of caesium for the FES of illite and the influence of concentration gradient on the retention capacity of the system. This means that the retention capacity of illite for caesium increases when the difference between the till porewater and the deep groundwater caesium concentration is higher.

The maximum retention efficiency of natural uranium is 22%, which is reached immediately after the advective travel time of 5 years (Figure 5-24). Thereafter, the retention efficiency drops to a negative value of -14%, due to the dissolution of  $Fe(OH)_3$ , induced by the deep groundwater inflow, prior to repository release (see section 5.1.2). After this initial transient state of the geochemical system, the retention efficiency for natural uranium increases towards a null retention efficiency, meaning that a balance between  $Fe(OH)_3$  dissolution and adsorption of uranium in the remaining solid amount is reached.

The till system reaches a 99% retention efficiency for repository-derived uranium, during the first 500 years. After the reaction of the system to the increment of radionuclide concentration due to repository release, the retention efficiency for repository-derived uranium progressively decreases.

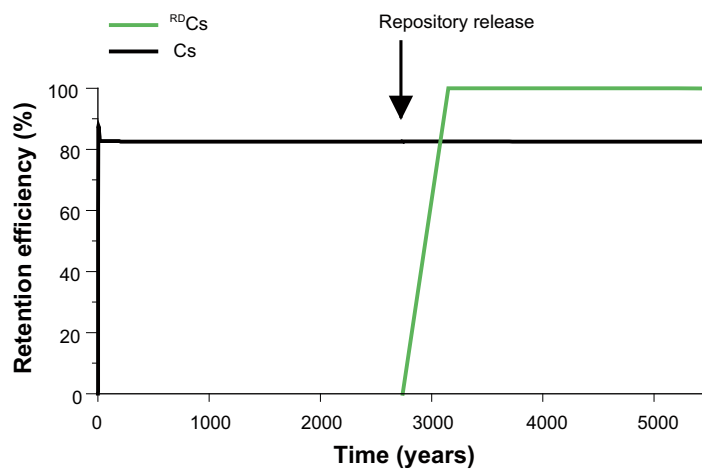


**Figure 5-23.** Computed retention efficiency for natural (*Cs*) and repository-derived ( $^{RD}Cs$ ) caesium along the simulation time. Monitoring point  $X=80\text{ m}$ ,  $Y=3\text{ m}$  (discharge area).

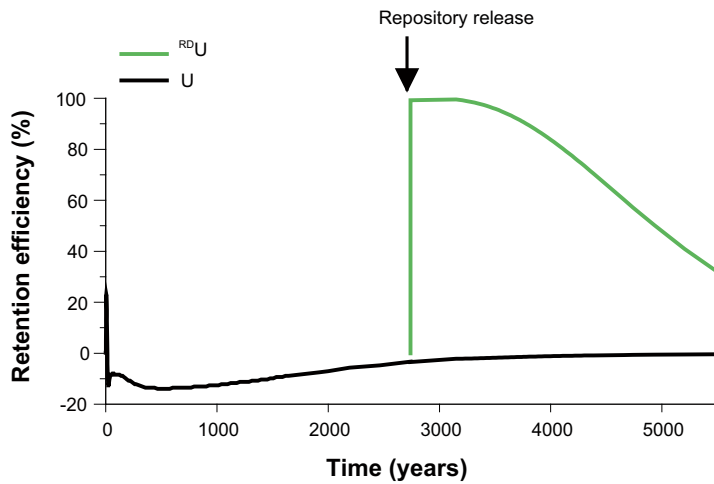


Figure 5-24. Computed retention efficiency for natural (U) and repository-derived ( $^{RD}U$ ) uranium along the simulation time. Monitoring point  $X= 80$  m,  $Y= 3$  m (discharge area).

The retention of radium in the till system is closely linked to the precipitation of barium sulphate (barite). Initially the till deposit is in equilibrium with barite, but no moles of this mineral are considered in the beginning of the simulation. After 2 days of reactive transport (prior to repository release), barite starts to precipitate in the vicinity of the deep groundwater inflow point. This precipitation is triggered by the increment of  $SO_4^{2-}$  in the till porewater, since the concentration of  $SO_4^{2-}$  in the deep groundwater is considerably higher than in the till porewater.

The precipitation of barite occurs during the whole simulation, and when Ra is introduced in the till system, due to repository release, a solid solution between Ba and Ra starts to precipitate, retaining Ra in the solid phase. This retention is higher immediately after repository release (retention efficiency of 97%), and gradually decreases towards a stable value of 30% retention efficiency. Ra is the only radionuclide that is not assumed to be involved in sorption reactions in the till system, and therefore, the evolution of its retention efficiency reflects the evolution towards a thermodynamic equilibrium between the aqueous phase and the precipitation of a mineral phase (Figure 5-25). The computed retention efficiencies of the till system for the 4 radionuclides derived from repository release are plotted all together in Figure 5-25.

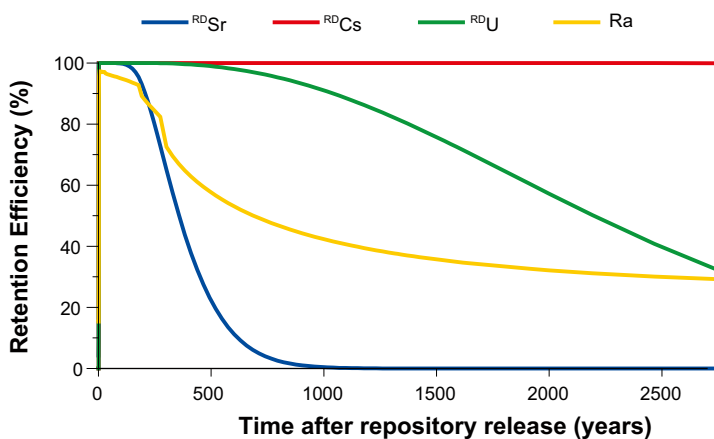


Figure 5-25. Computed retention efficiencies for strontium, caesium, uranium and radium, derived from repository release. Monitoring point  $X= 80$  m,  $Y= 3$  m (discharge area).

### 5.1.6 Sensitivity analysis

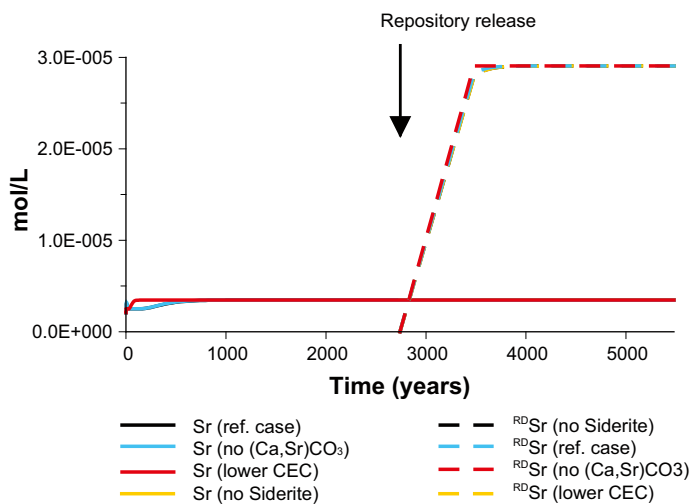
A sensitivity analysis has been developed for the till system in order to estimate the impact of considering distinct values for the most important geochemical parameters. The purpose of the sensitivity analysis is to illustrate the implications of the natural geochemical variability considered to prevail at Forsmark. The variability of the parameters selected for sensitivity analysis is in accordance to site specific features of the till and the clay deposits (as shown in section 4.4).

Figure 5-26 shows the evolution of strontium concentration at the discharge area for the reference case and three alternative scenarios developed for sensitivity analysis. From these results, none of the three alternative scenarios influences significantly the strontium concentration at the discharge area.

The reduction of the CEC (from 200 meq/L to 20 meq/L) in the till system greatly affects caesium retention (Figure 5-27). With a lower CEC, caesium concentration increases along the simulation time, meaning that the capacity of illite to adsorb more caesium is becoming progressively limited, while in the reference case illite still shows a relatively high capacity to adsorb caesium.

The impact of considering a lower CEC value is much more evident in the evolution of repository-derived caesium than in the natural caesium. This difference reflects not only the impact of a lower CEC, i.e. a lower density of exchangeable sites, but also the influence of concentration gradients for both Cs and <sup>RD</sup>Cs between deep groundwater and till porewater.

In the lower CEC case, since there is a lower density of exchangeable sites, these sites approach quicker the equilibrium with natural Cs. Therefore, when <sup>RD</sup>Cs is introduced in the till system, there are less available sites (compared with the reference case) for adsorption. In addition, since the concentration of <sup>RD</sup>Cs is higher than the concentration of natural Cs, the concentration of <sup>RD</sup>Cs at the discharge area of the till system reaches a higher value than that of Cs, in the lower CEC case.



**Figure 5-26.** Evolution of natural (Sr) and repository-derived (<sup>RD</sup>Sr) strontium concentration along the simulation time, at the discharge area (Monitoring point: X= 80 m, Y= 3 m). None of the alternative scenarios to the reference case shows significant changes in strontium concentration at the discharge area.

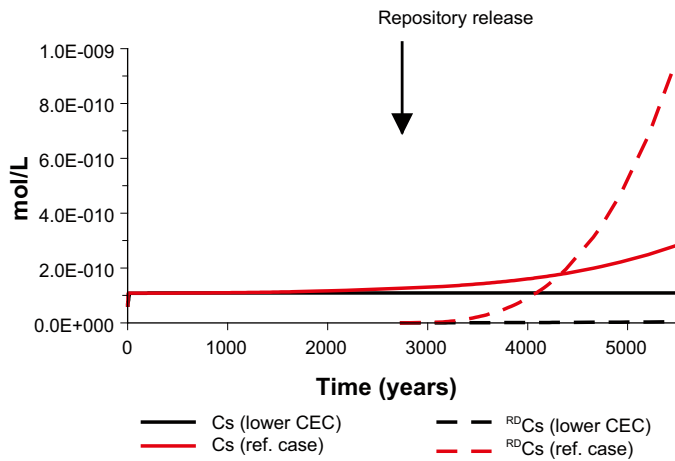


**Figure 5-27.** Evolution of natural (Cs) and repository-derived (<sup>RD</sup>Cs) caesium concentration along the simulation time, at the discharge area (Monitoring point: X= 80m, Y= 3 m). When a lower CEC (one order of magnitude lower than the reference case) is considered the concentrations of natural and repository-derived caesium increase along the simulation time, meaning that the illite interlayer is progressively becoming unable to retain this cation.

In the reference case, when repository release is simulated there is still a considerable amount of available sites in illite (compared to the lower CEC case), and therefore as <sup>RD</sup>Cs is transported through the till domain, it is efficiently retained, in contrast to the lower CEC case.

## 5.2 Reference case #2: The clay system

### 5.2.1 Conservative transport

The groundwater flow directions and hydraulic gradient computed with the numerical model will constitute the physical driving force for the migration of radionuclides within the clay layer. Figure 5-28 shows the flow field computed with the boundary conditions prescribed for the clay system (for more details see /Grandia et al. 2007, sections 5.5 and 6.2/). In this figure it is possible to see that the flow directions are mainly vertical and upward. This flow conditions were applied to the reactive transport simulation for the reference case #2.

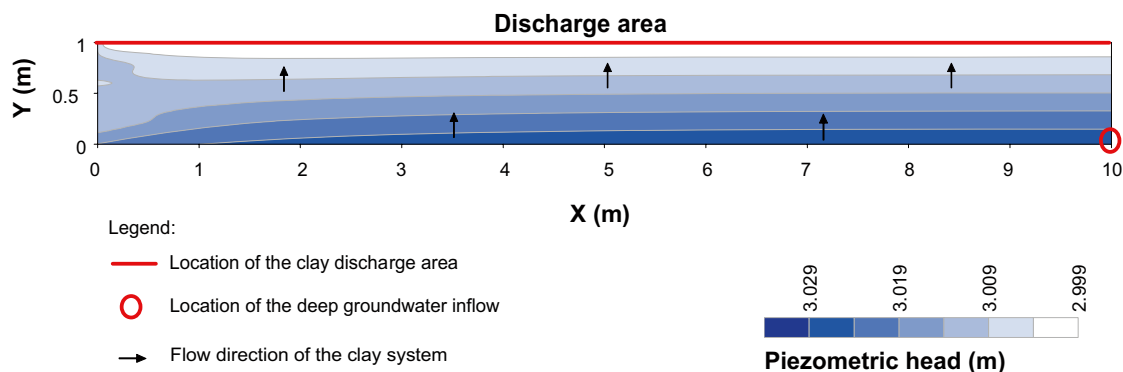


**Figure 5-28.** Groundwater flow directions and hydraulic gradient obtained from the numerical tool transport simulation after setting the prescribed boundary conditions of the clay system.

The conservative transport for reference case #2 has also been studied using chloride as a tracer, since no retention processes have been implemented for this ion. The initial chloride concentration in the clay porewater is  $1.5 \times 10^{-4} \text{ mol}\cdot\text{L}^{-1}$ , whereas in the deep groundwater  $[\text{Cl}^-]$  is  $1.07 \times 10^{-1} \text{ mol}\cdot\text{L}^{-1}$ .

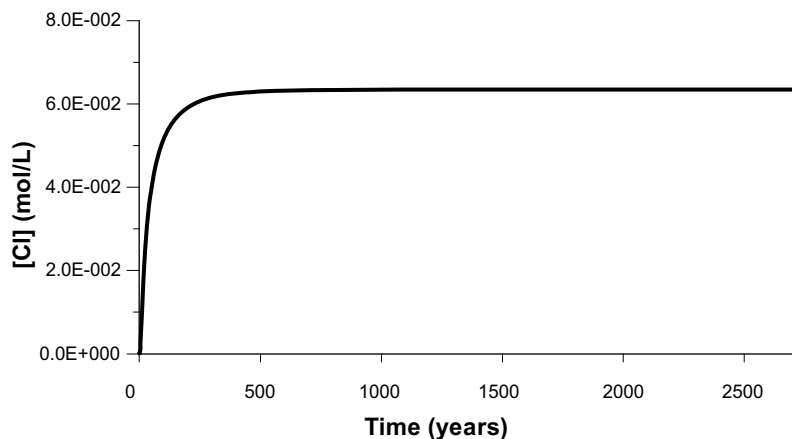
The model predicts that a conservative transport pseudo-steady state is reached approximately after 500 years (Figure 5-29). It is worth noting that the time needed to reach the transport steady state is much longer than in the previous reference case #1. This reflects the contrasting hydrogeological properties of the media in both reference cases. The first model simulates a relatively high permeable medium (the till aquifer), with average porewater velocities on the order of  $10^{-2} \text{ m}\cdot\text{d}^{-1}$ , while the second model simulates a low permeability medium (clay) with average porewater velocities of about  $10^{-5} \text{ m}\cdot\text{d}^{-1}$ . These hydrogeological conditions imply that diffusion plays a more relevant role in the transport of solutes in the clay system in comparison with the till system, where advection and dispersion are dominant.

The dilution of the deep groundwater in the clay domain has been assessed by using the following equation:

$$[Cl_{mix}] = (1 - X)[Cl_{deep}] + X[Cl_{clay}] \quad (\text{equation 5-3})$$

where  $[Cl_{mix}]$  is the chloride concentration in a given node of the modelled domain after the steady-state for conservative transport has been reached,  $[Cl_{deep}]$  is the concentration of chloride

(A)



(B)

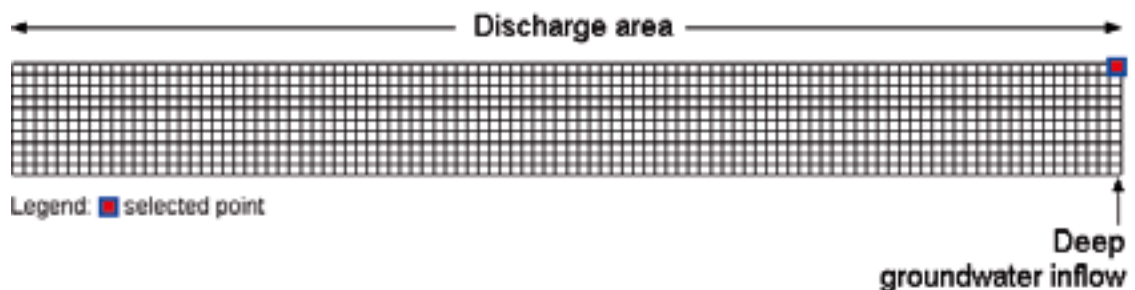


**Figure 5-29.** (A) Breakthrough curve of chloride concentration in an observation point located at the discharge area. The time needed to reach the stationary state of solute transport (advective travel time) is approximately 500 years. (B) Location of monitoring point ( $X= 10 \text{ m}$ ,  $Y= 1 \text{ m}$ ).

in the reference deep groundwater ( $1.07 \times 10^{-1}$  mol/L),  $[Cl_{clay}]$  is the concentration of chloride in the clay reference water ( $1.53 \times 10^{-4}$ ), and  $X$  is the relative volume of the clay reference water in a given node of the modelled domain after the conservative transport steady-state has been reached, i.e. it is the dilution factor.

Equation 5-3 has been applied to the clay system using the value of  $[Cl_{mix}]$  that is obtained in the node located in the discharge area of the domain ( $6.34 \times 10^{-2}$  mol/L), at  $X = 10$  m and  $Y = 1$  m. A dilution factor of 41% has been estimated for the discharge area of the clay system.

## 5.2.2 Reactive transport prior to repository release

As above mentioned for the till system, the behaviour of strontium, uranium and caesium in the clay system, will be studied during 2,700 years, before the release of radionuclides from repository. The calculated breakthrough curves of aqueous strontium, caesium and uranium at the monitoring point located at  $X = 10$  m,  $Y = 1$  m, until 2,700 years of reactive transport simulation are shown in Figure 5-29.

The aqueous strontium concentration in the deep groundwater is approximately one order of magnitude higher than in the clay porewater (see Table 4-4). Therefore, the aqueous strontium concentration gradually increases through time, with a faster increase at the beginning, and a slower increase at the end of the simulation, reflecting the retention of strontium in the solid phase (Figure 5-30). The continuous increase of the strontium aqueous concentration at the discharge area reflects the decreasing capacity of illite and  $(Ca,Sr)CO_3$  to incorporate more strontium along time.

The uranium aqueous concentration in the deep groundwater is approximately 0.5 orders of magnitude lower than in the clay porewater (Table 4-4). Consequently, uranium concentration sharply decreases during the initial 500 years; thereafter, it keeps stable until the end of the simulation time (2,700 years; Figure 5-30). Interestingly, the saturation of amorphous uraninite is reached only after repository release, so that uranium behaves in a conservative way until that time.

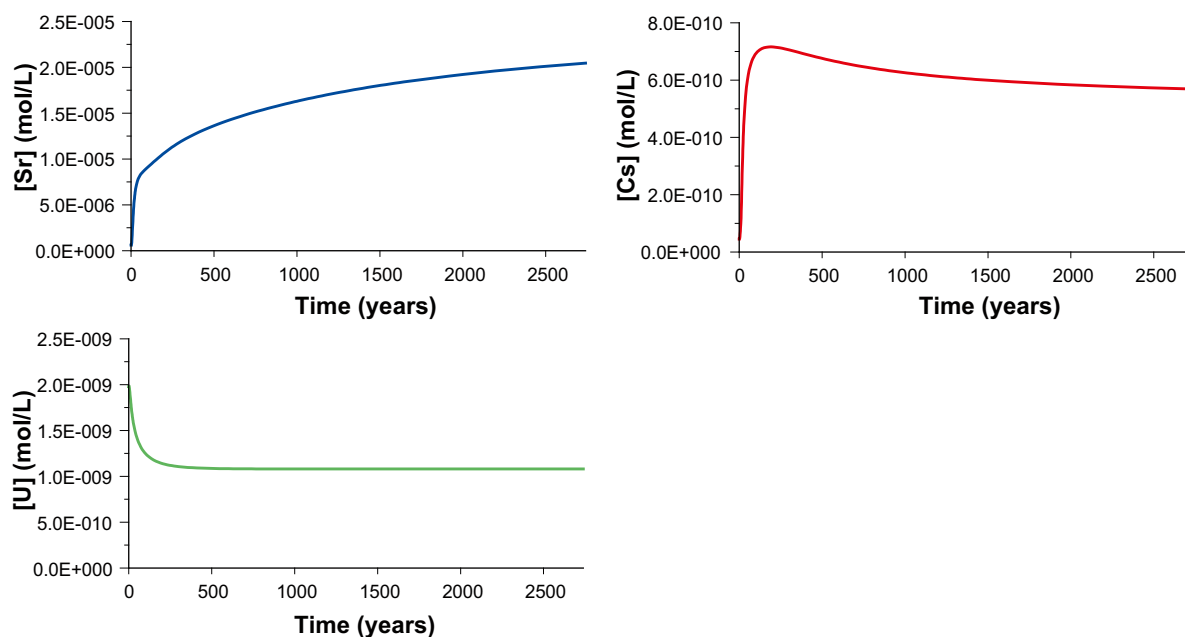


**Figure 5-30.** Breakthrough curves of strontium, caesium and uranium aqueous concentration during the first 2,700, prior to repository release. Monitoring point located at  $X = 10$  m,  $Y = 1$  m.

The aqueous caesium concentration in the deep groundwater is approximately 2.5 orders of magnitude higher than in the clay porewater. The simulation predicts an increase of caesium concentration in the outflowing water in the first 250 years. After this period, a progressive decrease is observed, mainly due to cation exchange in the illite interlayer (Figure 5-30).

The pH and pe evolution show similar but opposite evolution during the initial 2,700 years (Figure 5-31). In the first 120 years, fast changes in these parameters are predicted. Afterwards, siderite precipitation helps to stabilize them by releasing protons into solution and involves a redox sensitive species like  $\text{Fe}^{2+}$ .

### 5.2.3 Reactive transport after repository release

Deep groundwater affected by repository release has a  ${}^{\text{RD}}\text{Sr}$  concentration of  $8.37 \times 10^{-4}$  mol/L, which is approximately 1.5 orders of magnitude higher than the natural deep groundwater Sr concentration, and 3 orders of magnitude higher than the clay porewater Sr concentration. At the end of the simulation,  $\sim 94\%$  of strontium flowing out of the clay deposit is derived from repository release (Figure 5-32).

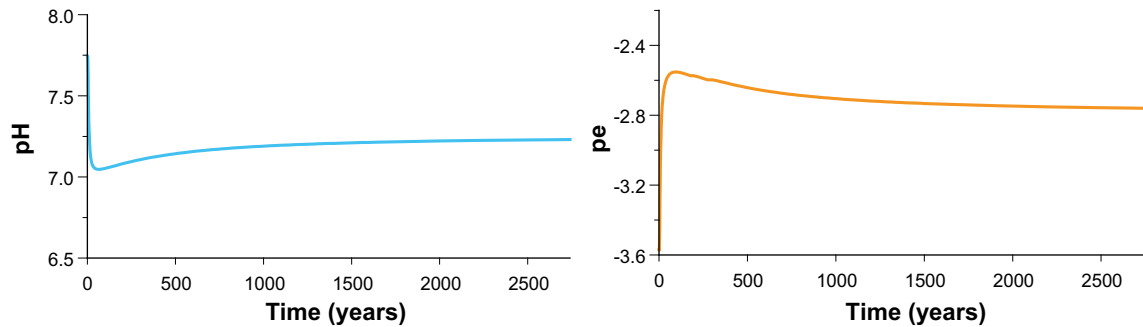


**Figure 5-31.** Evolution of pH and pe during 2,700 years of reactive transport simulation. A rapid change of both pH and pe values in the first 120 years of simulation is predicted, followed by a progressive evolution towards a geochemical steady state. Monitoring point located at  $X=10$  m,  $Y=1$  m.

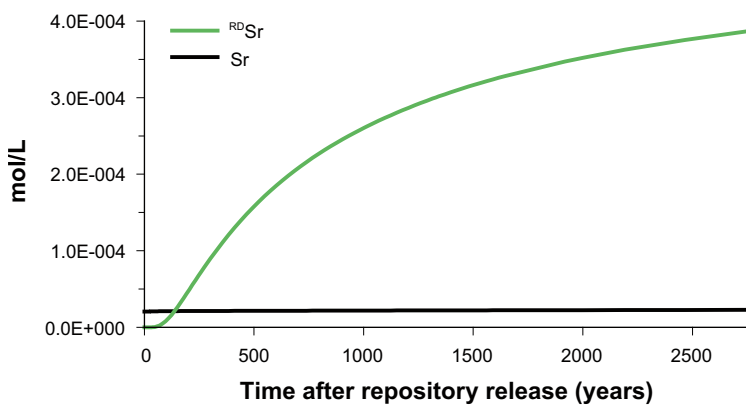


**Figure 5-32.** Predicted evolution of natural (Sr) and repository-derived ( ${}^{\text{RD}}\text{Sr}$ ) strontium after repository release, at the discharge area. Monitoring point  $X=10$  m;  $Y=1$  m.

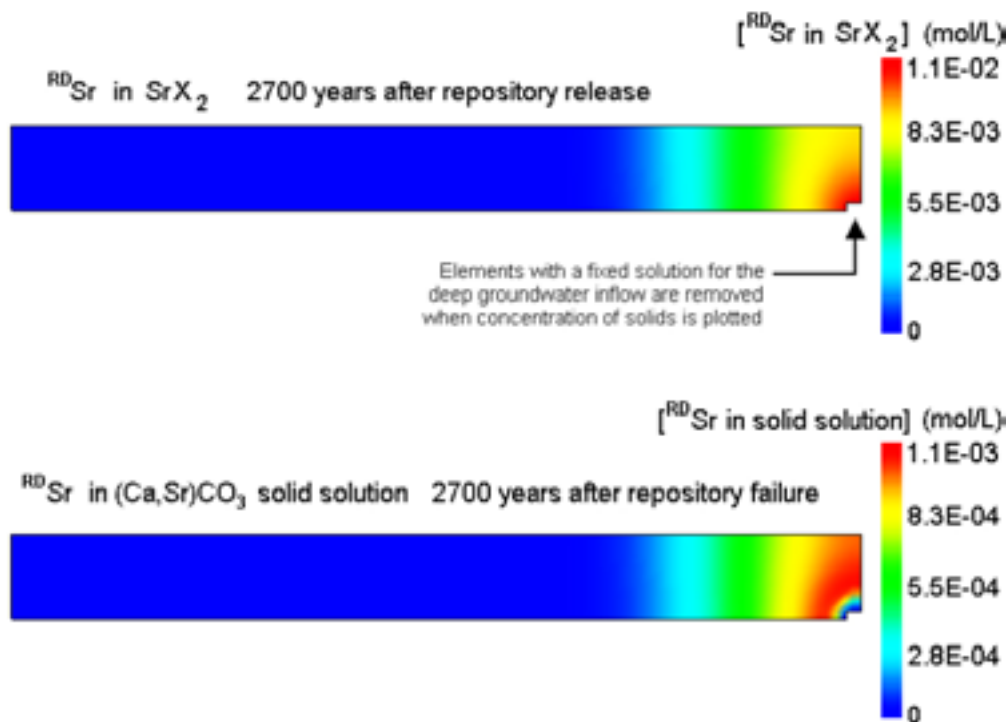


**Figure 5-33.** Concentration of  $^{RD}Sr$  retained in illite and the  $(Ca,Sr)CO_3$  solid solution, at the end of the simulation period (2,700 years after repository release). It  $^{RD}Sr$  is incorporated in both solid phases, but preferentially in the illite phase (note the different scale for both graphics) through a large area of the modelled domain.

The maximum concentration at the discharge area is slightly above 30% that of the simulated deep groundwater entering in the system, indicating that the system has a limited capacity to buffer the strontium increment derived from repository release. Only part of the repository-derived strontium is retained preferentially via cation exchange in illite in front of precipitation of  $(Ca,Sr)CO_3$  (Figure 5-33).

The concentration of  $^{RD}Cs$  in the deep groundwater after repository release is  $3.48 \times 10^{-7}$  mol/L, which is approximately 1.5 orders of magnitude higher than the natural deep groundwater

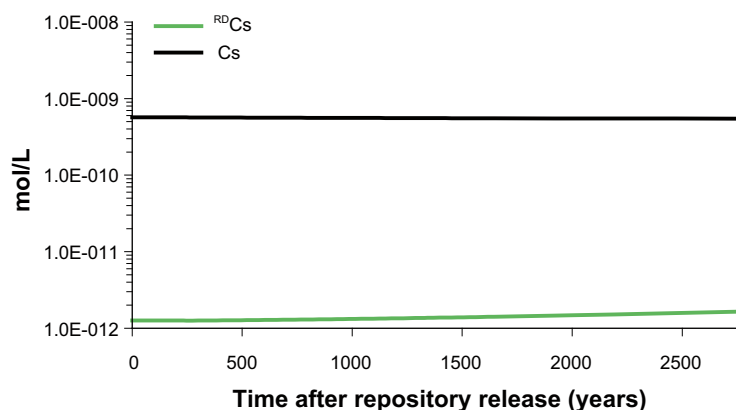


**Figure 5-34.** Predicted evolution of natural ( $Cs$ ) and repository-derived ( $^{RD}Cs$ ) caesium after repository release, at the discharge area. Monitoring point  $X=10$  m;  $Y=1$  m.





**Figure 5-35.** Concentration of  $^{RD}Cs$  retained in FES of illite, at the end of the simulation period (2,700 years after repository release). Since caesium has a relatively high affinity for the FES,  $^{RD}Cs$  is readily retained in the vicinity of the deep groundwater inflow point.

caesium concentration, and 4 orders of magnitude higher than the clay porewater. Approximately 2,500 years after repository release, only 0.3% of caesium flowing out of the clay deposit is derived from repository release (Figure 5-34). The remarkable decrease of caesium concentration, from the deep groundwater inflow point to the clay discharge area is due to the high affinity of Cs for the FES of illite which readily retain caesium via cation exchange (Figure 5-35).

Figure 5-36 shows the evolution of natural and repository-derived uranium concentration at the discharge area of the clay deposit. The concentration of  $^{RD}U$  in the deep groundwater affected by repository release is  $1.73 \times 10^{-8}$  mol/L. This concentration is approximately 1.5 orders of magnitude higher than the natural deep groundwater uranium concentration, and 30% higher than the clay porewater.

After 2,500 years, 87% of uranium flowing out of the clay deposit is derived from repository release (Figure 5-36), which reflects the limited capacity of amorphous uraninite to retain uranium (Figure 5-37). During the first 500 years after repository release, natural uranium concentration drops slightly due to precipitation of amorphous uraninite.

The numerical simulations predict that radium is not retained in the clay system since saturation with barite is not reached along the simulation time. The initial Ra concentration due to

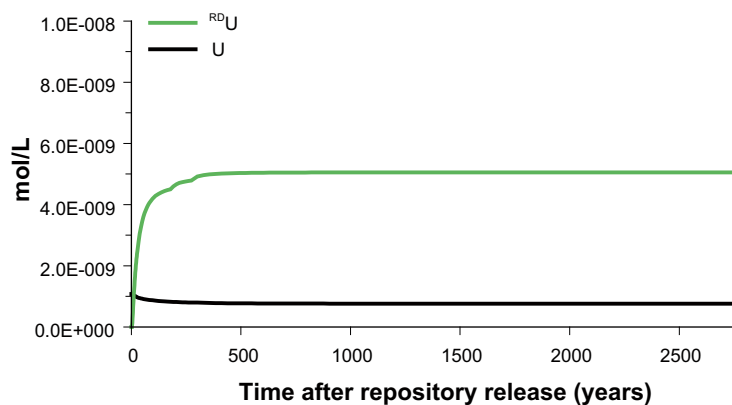


**Figure 5-36.** Predicted evolution of natural ( $U$ ) and repository-derived ( $^{RD}U$ ) uranium after repository release, at the discharge area. Monitoring point  $X=10$  m;  $Y=1$  m.

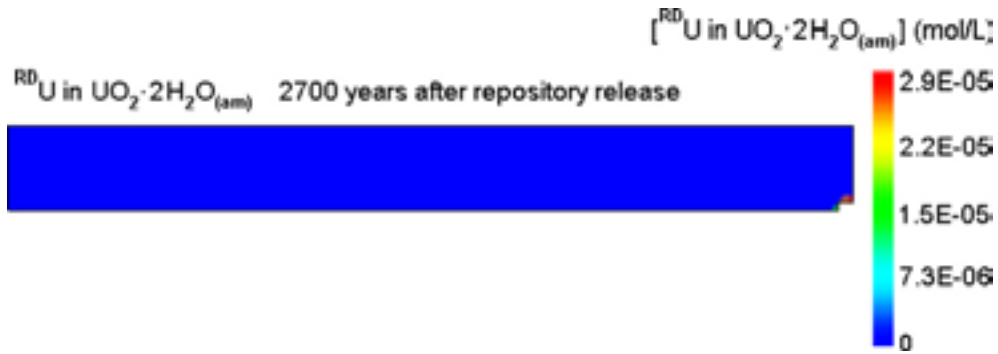


**Figure 5-37.** Concentration of <sup>RD</sup>U retained in amorphous uraninite, at the end of the simulation period (2,700 years after repository release). The precipitation of this solid phase occurs in the immediate vicinity of the deep groundwater inflow point.

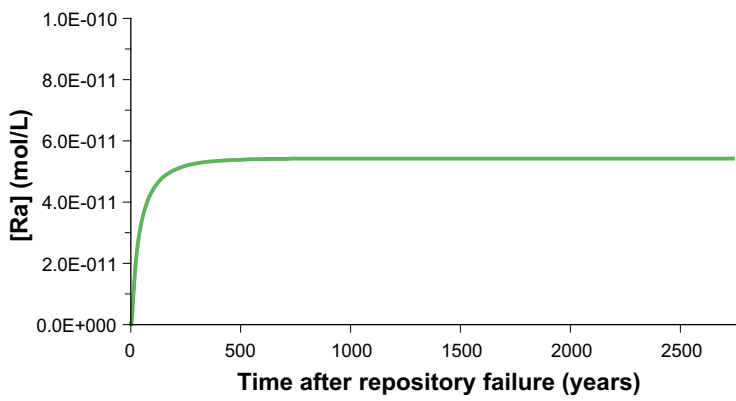


**Figure 5-38.** Predicted evolution of repository-derived (Ra) radium after repository release, at the discharge area.

repository release in the deep groundwater is  $9.15 \times 10^{-11}$  mol/L. At the discharge area of the clay deposit, the radium concentration is  $5.4 \times 10^{-11}$  mol/L (Figure 5-38). The decrease of Ra concentration from the deep groundwater inflow point to the discharge area of the clay deposit is exclusively due to diffusion into the clay system, which leads to dilution of radium concentration.

#### 5.2.4 Conservative transport versus reactive transport

Following the same methodology as in reference case #1, the quantification of the retention capacity of the surface systems at Forsmark is evaluated comparing the results yielded by the reactive and conservative transport models. In the reactive transport simulation, at the end of the simulation period the maximum <sup>RD</sup>Sr concentration at the discharge area is 22% lower than the maximum <sup>RD</sup>Sr concentration reached in the conservative transport model (Figure 5-39). This means that the clay system is moderately efficient to retain <sup>RD</sup>Sr in the solid phase.

At the end of the simulation period, <sup>RD</sup>Cs concentration in the reactive transport simulation is much lower (5 orders of magnitude) than in the conservative transport simulation (Figure 5-40).

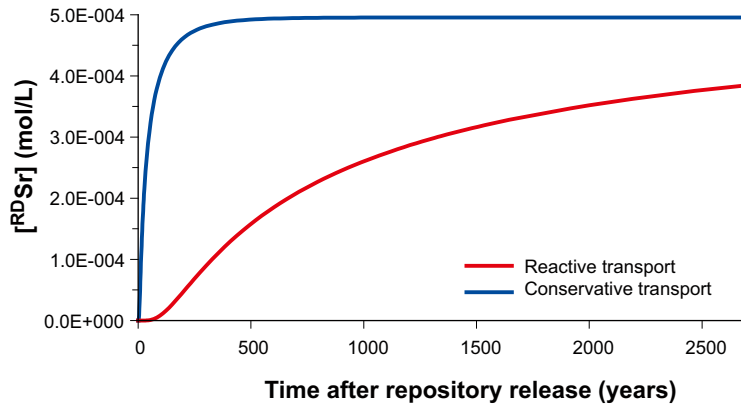


**Figure 5-39.** Breakthrough curves for <sup>RD</sup>Sr in the reactive and conservative transport simulations. Monitoring point X= 10 m, Y= 1 m (discharge area).

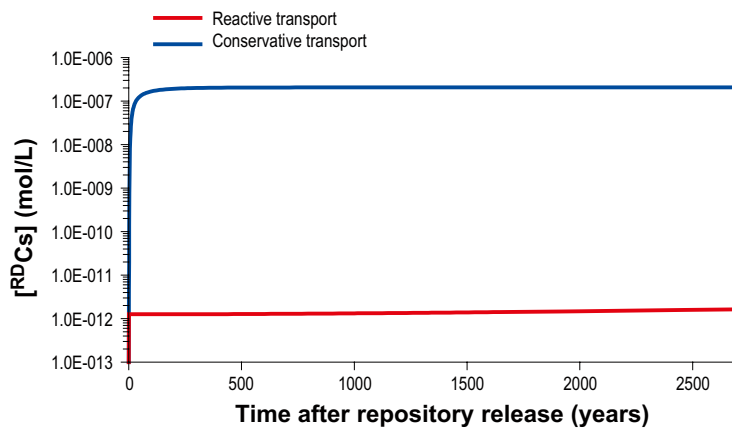


**Figure 5-40.** Breakthrough curves for <sup>RD</sup>Cs in the reactive and conservative transport simulations. Monitoring point X= 10 m, Y= 1 m (discharge area).

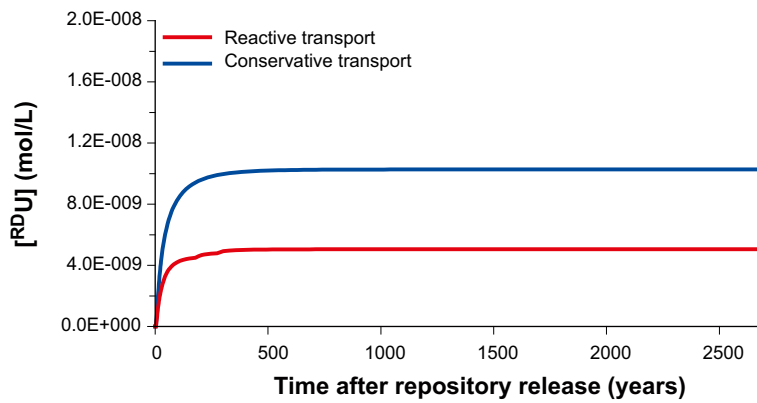


**Figure 5-41.** Breakthrough curves for <sup>RD</sup>U in the reactive and conservative transport simulations. Monitoring point X= 10 m, Y= 1 m (discharge area).

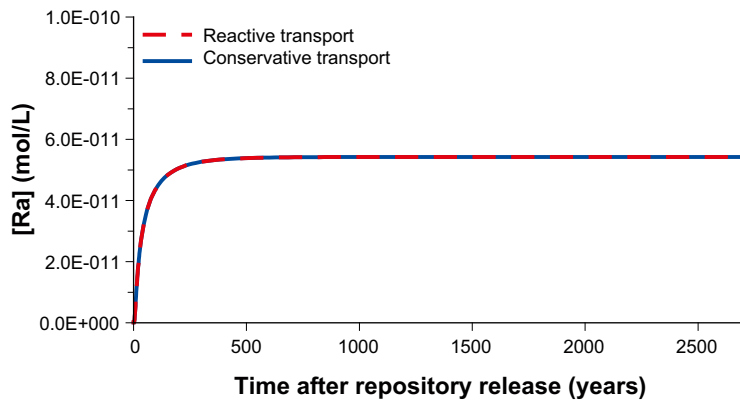


**Figure 5-42.** Breakthrough curves for Ra in the reactive and conservative transport simulations. Monitoring point  $X= 10\text{ m}$ ,  $Y= 1\text{ m}$  (discharge area). Since Ra is not retained in the solid phase of the clay system, its concentration at the discharge area is the same in the reactive and conservative transport simulations.

For  $^{235}\text{U}$ , its concentration in the reactive transport simulation is controlled by precipitation of amorphous uraninite. At the end of the simulation time, this concentration is half of the  $^{235}\text{U}$  concentration calculated in the conservative transport model (Figure 5-41).

As already mentioned, radium is not retained in any solid phase of the clay system so that its concentration evolves in the same way in the reactive and conservative transport simulations (Figure 5-42).

### 5.2.5 Quantitative assessment of the retention efficiency

As explained in section 5.1.4, the retention capacity is evaluated using the retention efficiency parameter. For strontium, the maximum retention efficiency of natural strontium (55%) is reached at the beginning of the simulation time, when the system is evolving towards a geochemical steady state. Thereafter, the retention efficiency of natural strontium drops to 7% until the end of the simulation period (Figure 5-43).

When repository release is simulated, repository-derived strontium is predicted to be retained in the clay deposit, although the system efficiency to retain natural strontium has reached a very

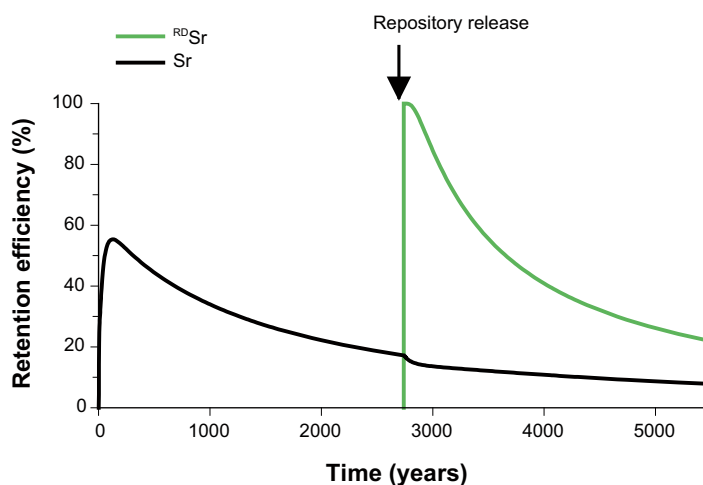


**Figure 5-43.** Computed retention efficiency for natural (Sr) and repository-derived ( $^{RD}\text{Sr}$ ) strontium along the simulation time. Monitoring point  $X= 10\text{ m}$ ,  $Y= 1\text{ m}$  (discharge area).

low value. Immediately after repository release, the system reaches a retention efficiency (for  $^{RD}Sr$ ) of 100%. After this period, retention efficiency for repository-derived strontium drops to 20%. The behaviour of the clay system is similar to the behaviour of the till system, but delayed by the higher transport time of the clay system due to its low hydraulic conductivity. If the clay system is evolving towards an equivalent state of retention efficiency for strontium as in the till deposit, it is expected that the clay retention efficiency for strontium will be null at longer times.

The retention efficiency for natural caesium reaches 90% at the beginning of the simulation time, and gradually increases to 94%, until the end of the simulation time (Figure 5-44). Repository-derived caesium is also readily retained in the clay system, and its retention efficiency quickly reaches a maximum value of 100%, that is maintained until the end of the simulation.

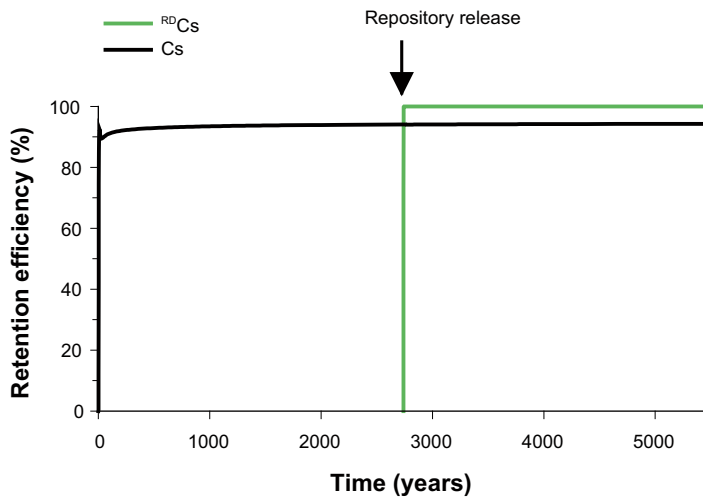


**Figure 5-44.** Computed retention efficiency for natural ( $Cs$ ) and repository-derived ( $^{RD}Cs$ ) caesium along the simulation time. Monitoring point  $X=10\text{ m}$ ,  $Y=1\text{ m}$  (discharge area).

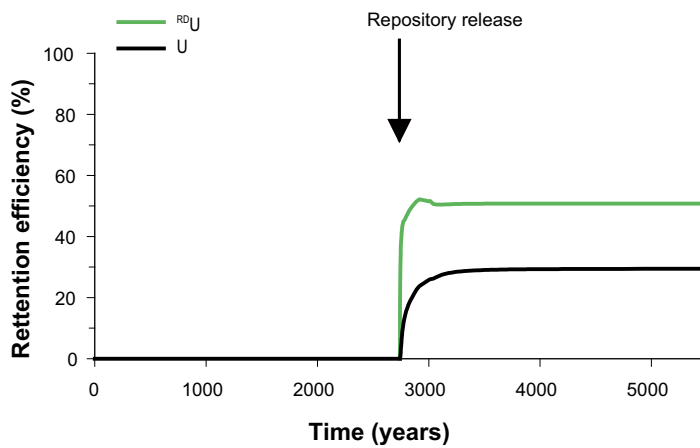


**Figure 5-45.** Computed retention efficiency for natural ( $U$ ) and repository-derived ( $^{RD}U$ ) strontium along the simulation time. Monitoring point  $X=10\text{ m}$ ,  $Y=1\text{ m}$  (discharge area).

The retention efficiency for repository-derived uranium reaches a value of 50% that is kept until the end of the simulation time (Figure 5-45). The retention efficiency of natural uranium is kept null until repository release, since saturation of amorphous uraninite is not reached, and after repository release retention efficiency of natural uranium is 30%. The saturation of amorphous uraninite is triggered by the increment of uranium concentration due to repository release. From this moment, both, natural and repository-derived uranium start to precipitate together as amorphous uraninite.

The calculation of the retention efficiencies of the clay system shows that the retention capacity of this sediment is different for the 4 radionuclides derived from repository release (Figure 5-46). Caesium is again the most effectively retained radionuclide, while radium is not retained in the solid phase.

### 5.2.6 Sensitivity analysis

The sensitivity analysis carried out for the clay system is based on the same criteria as in the till system (see in section 4.4). Figure 5-47 shows the evolution of strontium concentration at the discharge area of the clay deposit, for the reference case and three alternative scenarios developed for sensitivity analysis.

None of the three alternative scenarios significantly influences the natural strontium concentration at the discharge area. Nevertheless, the repository-derived strontium concentration is influenced by the lower CEC case. In this case, the repository-derived strontium concentration is  $1 \times 10^{-4}$  mol/L higher than in the reference case, reflecting that the lower density of cation exchange sites prevents a greater immobilisation of strontium in the illite interlayer.

A lower CEC in the illite interlayer also affects the caesium sorption (Figure 5-48). At the beginning of the simulation period, the reference case predicts a higher natural caesium concentration than the lower CEC case. This apparently contradictory result is explained by the fact that, at the beginning of the simulation period, the inflow of deep groundwater triggers the release of caesium that was previously retained in the planar sites of the illite interlayer. Since in the lower CEC case there is a lower cation exchange site density in the modelled domain, the amount of natural caesium released into solution by the planar sites of illite (per unit volume of water) is lower than in the reference case.

At the end of the simulation, the lower CEC case leads to a higher repository-derived caesium concentration which reflects the progressive decrease of the retention capacity of the clay system, due to a lower cation exchange site density with respect to the reference case.

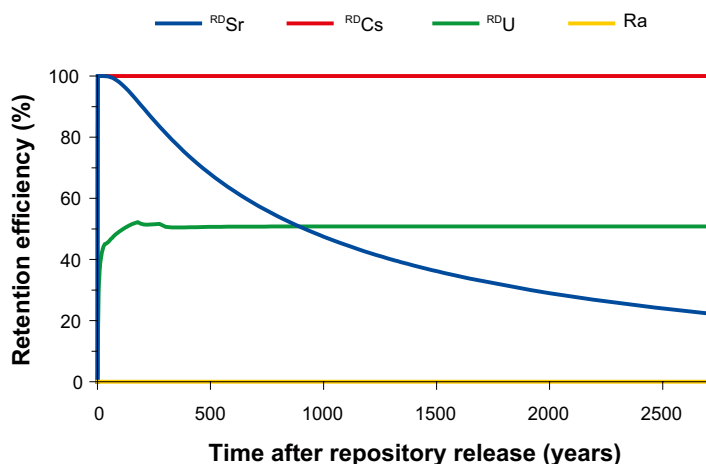


**Figure 5-46.** Computed retention efficiencies for strontium, caesium, uranium and radium, derived from repository release. Monitoring point  $X=10$  m,  $Y=1$  m (discharge area).

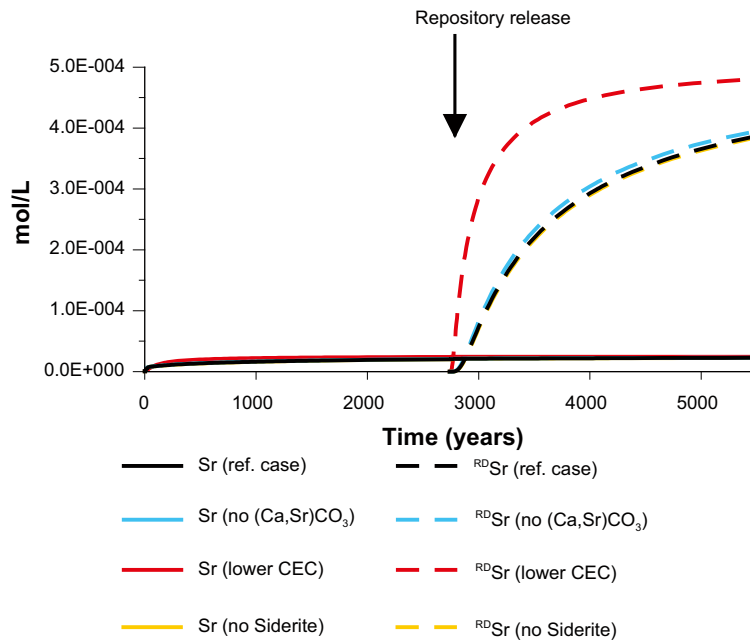


**Figure 5-47.** Predicted evolution of natural (*Sr*) and repository-derived ( $^{RD}Sr$ ) strontium concentration along the simulation time, at the discharge area (Monitoring point:  $X=10$  m,  $Y=1$  m). It is seen that only the lower CEC case influences repository-derived strontium concentration at the discharge area.

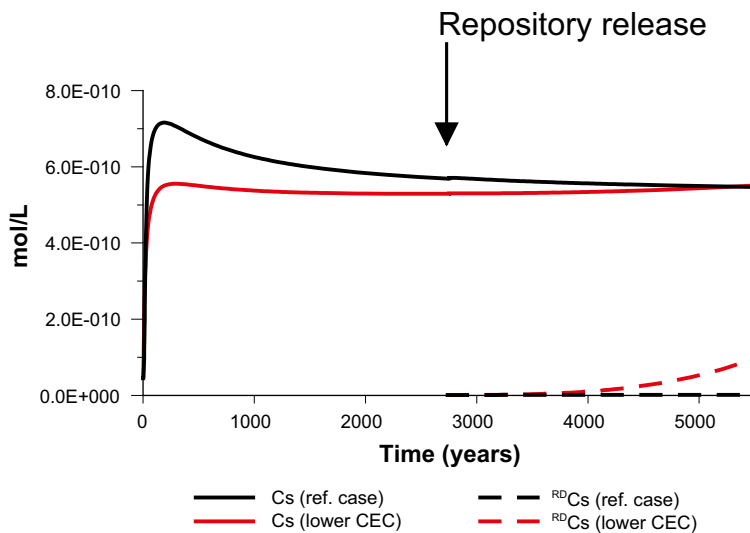


**Figure 5-48.** Predicted evolution of natural (*Cs*) and repository-derived ( $^{RD}Cs$ ) caesium concentration along the simulation time, at the discharge area (Monitoring point:  $X=10$  m,  $Y=1$  m). A lower CEC influences both natural and repository-derived caesium concentration at the discharge area.

Figure 5-49 shows the evolution of uranium concentration at the discharge area of the clay deposit, for the reference case and four alternative scenarios developed for sensitivity analysis. When the clay porewater has a concentration of humic acids of  $10^{-1}$  mol/L, the concentration of  $^{RD}U$ , at the discharge area reaches its highest value. As higher the concentration of humic acids higher will be the concentration of aqueous complexes of uranium and humic acids, and therefore the mobility of  $^{RD}U$  is enhanced.

In this context it would be expected that when no humic acids are present the release of  $^{RD}U$  would be lower than in the reference case. Nevertheless it is seen the opposite in Figure 5-49, which means that other parameters influence uranium mobility. In the case without humic acids it is seen that the pH reached in the geochemical quasi-steady state is slightly higher than in the reference case, and  $p_e$  is slightly lower than in the reference case. Besides, in the case without humic acids other aqueous uranium complexes may be impeding the precipitation of amorphous uraninite, like sulphate and carbonate complexes that are important under these geochemical conditions.

When siderite precipitation is not allowed, the aqueous carbonate concentration in the clay porewater is slightly higher. Consequently the concentration of aqueous uranium carbonates is higher. Under these conditions the release of  $^{RD}U$  is higher than in the reference case.

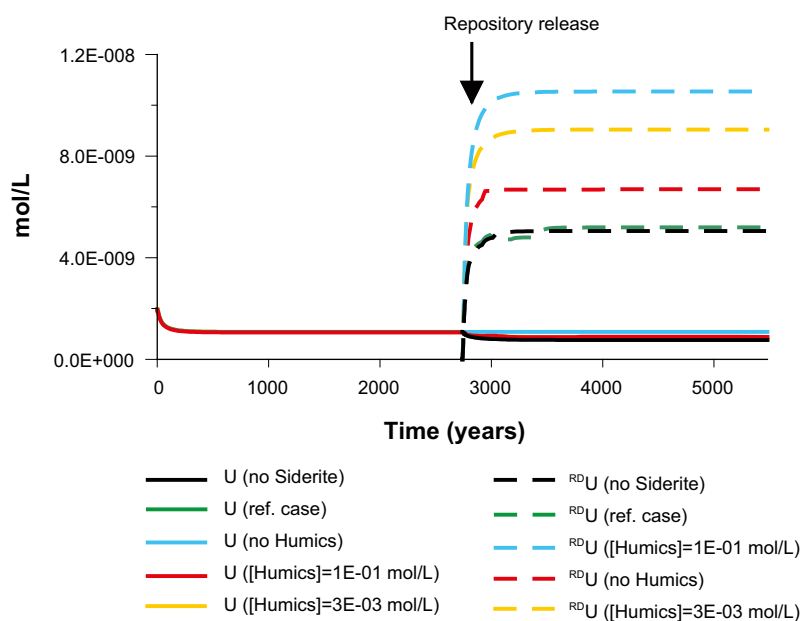


**Figure 5-49.** Predicted evolution of natural ( $U$ ) and repository-derived ( $^{RD}U$ ) uranium concentration along the simulation time, at the discharge area (monitoring point:  $X=10$  m,  $Y=1$  m). All the alternative cases influence  $^{RD}U$  concentration at the discharge area.



## 6 Distribution coefficient ( $K_d$ )

### 6.1 Applicability of $K_d$ models

The numerical models developed in the present work are reactive transport numerical calculations that couple the transport of solutes through porous media, governed by the groundwater flow equation and the advection-dispersion equation, with local thermodynamic equilibrium between aqueous and solid species. In these numerical models, the local thermodynamic equilibrium between aqueous and solid species accounts for the following reactions:

- Aqueous complexation,
- Mineral precipitation/dissolution (including pure phases and solid solutions),
- Cation exchange,
- Surface complexation.

In the present numerical simulations, the geochemical processes that influence solute mobility (including the studied radionuclides) were modelled under the so called “component additivity” (CA) approach, i.e. assuming that each sorbent in a complex mineral assemblage (like the ones modelled here) has unique surface sites with particular sorption properties, where the important linkage between surface and aqueous species is retained through the coupling of mass action equations /Davis et al. 1998, and references therein/.

This approach is obviously more complex than a constant  $K_d$  or isotherm approach, but it is much more reliable when modelling complex near-surface systems like the ones modelled here, because they are affected by changes in key geochemical parameters such as pH, pe, ionic strength, and the carbonate system. These changes may have a strong influence on the  $K_d$  value.

$K_d$  experimental values are applicable only to the geochemical conditions under which they were measured. Any change in a geochemical parameter may have a large effect on the  $K_d$  value. Thus, a  $K_d$  model is difficult to apply meaningfully to an environment with temporally and/or spatially variable geochemical conditions /NEA 2005/.

The results of the numerical simulations developed for the near-surface systems of Forsmark reflect the  $K_d$  sensitivity to changes in key geochemical parameters, since the  $K_d$  value calculated from model outputs varies with time and space in each modelled domain (the till and clay systems), as it will be shown later in section 6.2. It is worth mentioning, though, that  $K_d$  values obtained from our models agree with experimental values. For comparison purposes,  $K_d$  values obtained from the reactive transport simulations were used in a  $K_d$  numerical model. The results are shown in section 6.3.

### 6.2 $K_d$ values from model outputs

A  $K_d$  value of a given solute, in each node of the modelled domain, and at any time step can be calculated from output data of the reactive transport numerical models developed for the till and clay systems. If the concentration of a given solute retained in the solid phase (also known as sorbate) is expressed in mol/kg of rock and the concentration of this solute in the aqueous phase is expressed in mol/L of water, then the  $K_d$ , expressed in L/kg, is calculated from the following equation /Appelo and Postma 2005/:

$$K_d = \frac{[sorbate]_{(mol / kg\_of\_rock)}}{[solute]_{(mol / L\_of\_water)}} \quad (\text{equation 6-1})$$

From the outputs of the reactive transport numerical models we obtain the concentration of a given solute in the aqueous and solid phases, expressed in mol/L of water, in every node of the modelled domain. To convert the concentration of the sorbed species (sorbate) in the solid phase, from mol/L of water to mol/kg of solid, we use the following equation:

$$[sorbate]_{(mol/kg\_of\_rock)} = [sorbate]_{(mol/L\_of\_water)} \times \frac{\phi}{\rho_{bulk\_rock}} \quad (\text{equation 6-2})$$

Where  $\phi$  stands for total porosity of rock (dimensionless), and  $\rho_{bulk\ rock}$  stands for the bulk rock density, expressed in kg/L.

The total porosity of the till is 0.25, and the total porosity of the clay is 0.2 /Johansson et al. 2005/. The till and clay bulk densities are not reported but from literature it is possible to estimate a till bulk density of 1.95 kg/L, and a clay bulk density of 2.00 kg/L. From all these values the concentration of sorbates was converted into mol/kg of rock. Then, the  $K_d$  of a given solute in the modelled domains was calculated.

### 6.2.1 Reference case #1: The till system

As stated above, tracing radionuclides released from the repository was made by labelling each studied radionuclide, meaning that  $^{RD}Sr$ ,  $^{RD}Cs$  and  $^{RD}U$  are derived from repository release, and Sr, Cs, and U are the naturally occurring species. Since the geochemical processes that are simulated in the reactive transport models do not discriminate between distinct isotopes of the studied radionuclides as explained in section 4.3.1, the  $K_d$  of labelled and unlabelled species must be the same, for a given time step, and at a given node of the modelled domain.

The greater changes of  $K_d$  for natural and repository-derived species are expected in the area close to the deep groundwater inflow point, during the approach to the geochemical quasi-steady state. In Figure 6-1 it is seen that only in the beginning of the simulation, when greater geochemical changes occur, the  $K_d$  values of Sr, U and Cs vary significantly. After this initial stage, the  $K_d$  values of these radionuclides are relatively stable. This evolution will be analysed in detail in Figure 6-2, Figure 6-3, and Figure 6-4.

In Figure 6-1 it is observed that  $K_d$  of natural and repository-derived species is the same, although the aqueous concentration of each natural and repository-derived species is considerably different. These results confirm that numerical calculations do not lead to a false isotopic fractionation.

Figure 6-1 also shows that the aqueous concentration of  $^{RD}U$  does not reach a higher concentration than the naturally occurring U. This is mainly due to two reasons: (1) the aqueous concentration of  $^{RD}U$  in the inflowing deep groundwater ( $1.73 \times 10^{-8}$  mol/L), that simulates repository release, is smaller than the natural aqueous concentration of U that occurs in the till deposit ( $2.27 \times 10^{-8}$  mol/L); and (2) the  $Fe(OH)_3$  that is present in the till deposit readily adsorbs the incoming uranium.

The  $K_d$  of the studied radionuclides varies along the simulation period due to the inflow of the deep groundwater (Figure 6-2, Figure 6-3, and Figure 6-4). These variations are related to:

- Mixing of the till groundwater and deep groundwater. The two waters have different concentrations of solutes, and different redox potential and pH. The mixing leads to concentration and dilution of solutes in the till system, depending on the relative concentration of solutes in both waters.
- Local thermodynamic equilibrium. Changes in the aqueous concentration of solutes imply changes in the composition of the solid phase.

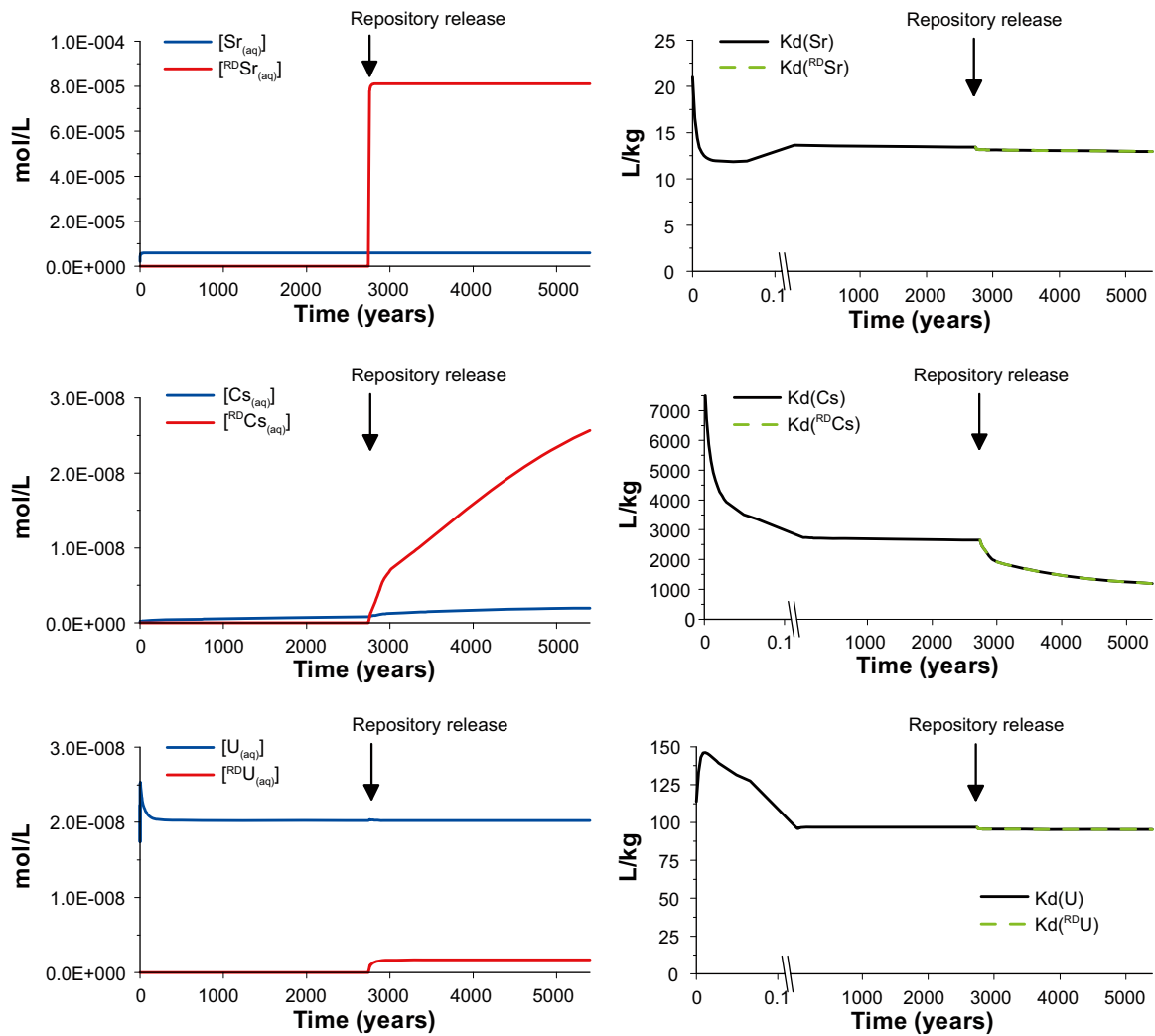


**Figure 6-1.** Predicted evolution of aqueous concentration of natural (Sr, Cs, and U) and repository-derived ( $^{RD}\text{Sr}$ ,  $^{RD}\text{Cs}$ , and  $^{RD}\text{U}$ ) radionuclides and the respective  $K_d$  value in the till system. Although the concentrations of natural and repository-derived radionuclides are considerably different, the  $K_d$  value for each pair is the same, meaning that no isotope fractionation occurs. Monitoring point:  $X= 20.1 \text{ m}$ ;  $Y= 0.2 \text{ m}$  (close to the deep groundwater inflow point).

The inflow of the deep groundwater in the till deposit leads to a decrease of the  $K_d(\text{Sr})$  along time and space (Figure 6-2); this means that the solid concentration/aqueous concentration ratio decreases. Before the deep groundwater intrusion, the till domain has an homogeneous  $K_d(\text{Sr})$  of 20 L/kg, and after the deep groundwater intrusion the  $K_d(\text{Sr})$  in the till domain becomes heterogeneous, ranging from 20 L/kg in the area unaffected by the deep groundwater intrusion, to 12 L/kg in the vicinity of the deep groundwater inflow point.

Deep groundwater has a higher strontium concentration than porewater from the till deposit, and its intrusion leads to an enrichment of Sr in the illite and  $(\text{Ca},\text{Sr})\text{CO}_3$  solid solution. Although the added strontium is retained in the solid phase,  $K_d$  of strontium decreases along time in the area affected by deep groundwater intrusion. The local equilibrium calculations developed for each time step lead to retention of the added strontium in the solid phase lower than the increment of strontium in the aqueous phase. Therefore, the accumulated difference between the amount of Sr retained in the solid phase and the concentration of aqueous Sr becomes wider with time, leading to the distribution of  $K_d(\text{Sr})$  values observed in Figure 6-2.

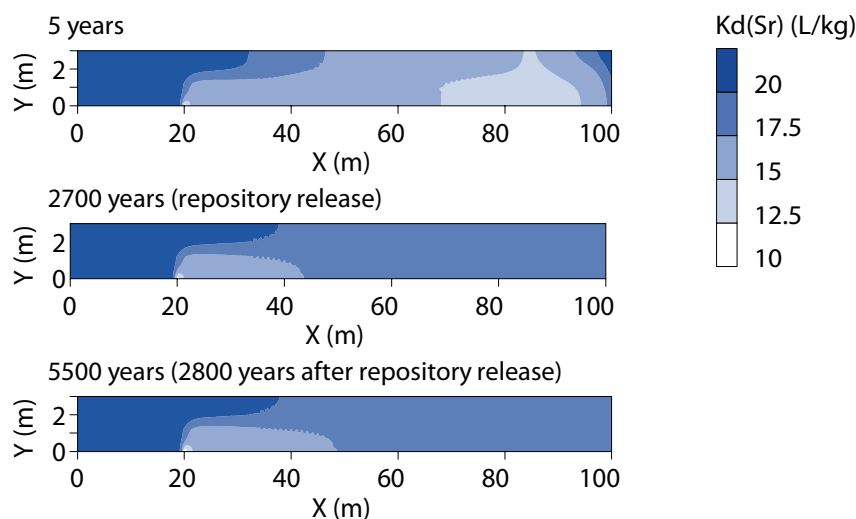


**Figure 6-2.** Predicted evolution of  $K_d(\text{Sr})$  along the simulation time. In the beginning of the simulation period the  $K_d$  varies with time, since major geochemical changes occur in this period. From 2,700 years until the end of the simulation (5,500 years), relatively small geochemical changes occur, and hence  $K_d$  varies little.

The inflow of the deep groundwater in the till deposit also leads to a decrease of the  $K_d$  of caesium from an homogenous value of 7,950 L/kg to an heterogeneous distribution that ranges from 7,950 L/kg in the area close to the till groundwater inflow, to 2,000 L/kg in the vicinity of the deep groundwater inflow point (Figure 6-3).

Deep groundwater has a much higher caesium concentration than the till deposit, and its intrusion leads to a remarkable enrichment of caesium in the FES of illite (see section 5.1.2). Although this retention is relatively efficient, retention of caesium in the solid phase is lower than the increment of caesium in the aqueous phase that results from the local equilibrium calculated for each time step, and therefore  $K_d(\text{Cs})$  decreases along the simulation time.

The inflow of the deep groundwater in the till deposit leads to an initial increase of the  $K_d(\text{U})$  followed by a decrease (Figure 6-4). Initially the till deposit has an homogeneous  $K_d(\text{U})$  of 114 L/Kg, and during the first 5 years of reactive transport simulation there is a dilution of the aqueous concentration of uranium because deep groundwater has a lower uranium concentration than the till deposit, as seen in section 5.1.2.

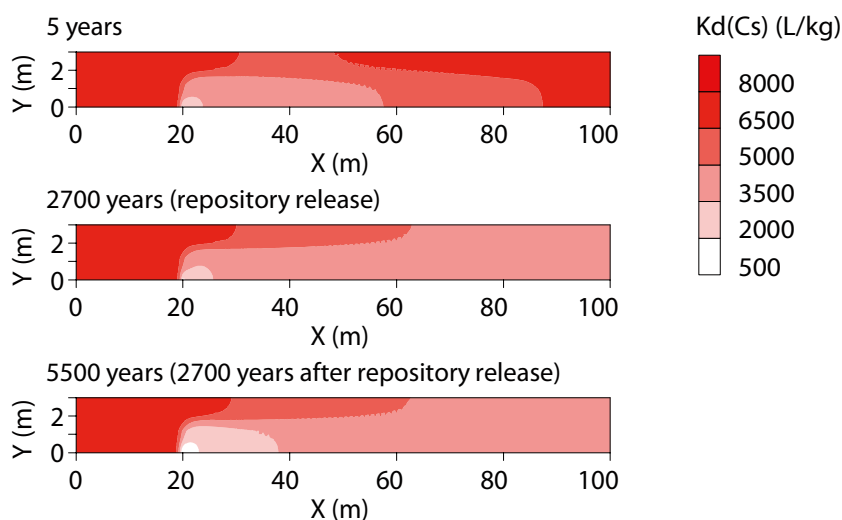


**Figure 6-3.** Predicted evolution of  $K_d(\text{Cs})$  along the simulation time. In the beginning of the simulation period the  $K_d$  varies with time, since major geochemical changes occur in this period. From 2,700 years until the end of the simulation (5,500 years), relatively small geochemical changes occur, and hence  $K_d$  varies little.

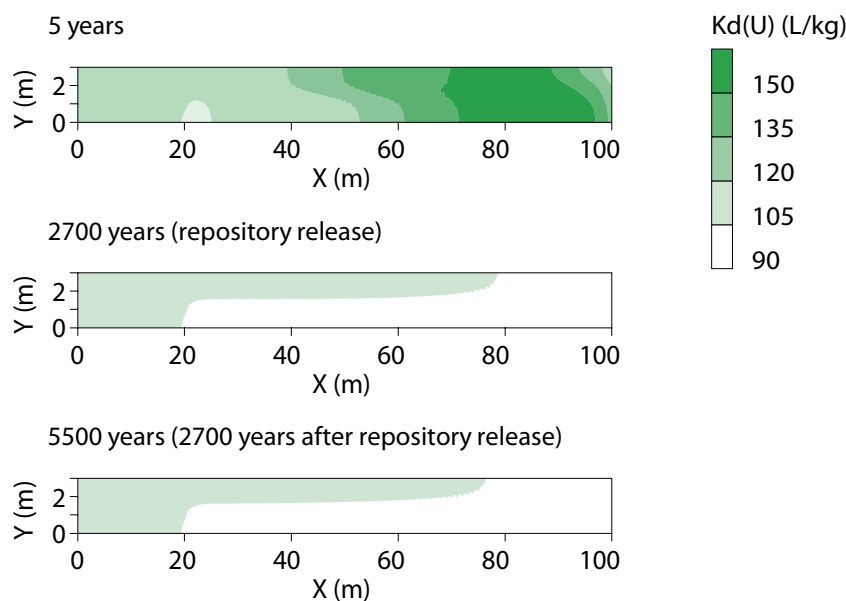


**Figure 6-4.** Predicted evolution of  $K_d(U)$  along the simulation time. Major geochemical changes occur at the beginning of the simulation period, and therefore, the  $K_d$  varies with time. From 2,700 years until the end of the simulation (5,500 years), relatively small geochemical changes occur; and hence  $K_d$  does not change much.

The dilution of U induced by the inflow of deep groundwater causes the initial  $K_d(U)$  increment in the modelled domain (darker green area in Figure 6-4). Thereafter,  $K_d(U)$  progressively decreases, and the resulting till domain has a heterogeneous  $K_d(U)$  that ranges from 114 L/kg close to the till groundwater inflow, to 90 L/kg in the vicinity of the deep groundwater inflow point.

The analysis of the evolution of Kd for Sr, U and Cs with time and space shows that the changes of the Kd value with time only occur at the beginning of the simulations, as observed in Figure 6-1. For longer periods of time, Kd of these radionuclides varies very little with time, but still varies in space (Figure 6-2, Figure 6-3, and Figure 6-4).

It is worth mentioning that the spatial distribution and temporal evolution of the  $K_d$  of radionuclides derived from repository release ( $^{87}\text{Sr}$ ,  $^{137}\text{Cs}$ ,  $^{235}\text{U}$ ) is equal to the  $K_d$  of the natural radionuclides (Sr, Cs, U), from the moment when repository release is simulated (2,700 years), until the end of the simulation period (5,500 years), as previously shown in Figure 6-1.

The  $K_d$  value of each radionuclide obtained from the reactive transport models agrees with experimental values reported in the related literature. In /OECD 1992/, the experimental values reported for Sr vary between 5 L/kg in marls to 500 L/kg in clayey materials. The calculated  $K_d$  for Sr varies between 10 and 22 L/kg (Figure 6-2). In /OEDC 1992/, the experimental values reported for Cs range from 20 L/kg in marls to 10,000 L/kg in shales and clays. The calculated  $K_d$  values obtained for Cs are from 500 to 8,000 L/kg (Figure 6-3), which are in the range of the reported values. In /OECD 1992/, the experimental  $K_d$  values reported for U vary between 5 L/kg to 5,000 L/kg, both in clayey materials. The  $K_d$  values calculated for U in the till system vary between 90 and 155 L/kg (Figure 6-4). These values fall in the variability range reported for clayey materials.

The analysis of the  $K_d(\text{Ra})$  close to the deep groundwater inflow point is shown in Figure 6-5, where it is observed an increment of  $K_d(\text{Ra})$ . Since the till porewater is in equilibrium with barite ( $\text{BaSO}_4$ ), the inflowing deep groundwater that is richer in sulphate and carries Ra, triggers the precipitation of  $(\text{Ba,Ra})\text{SO}_4$  which retains Ra in the vicinity of the deep groundwater inflow point.

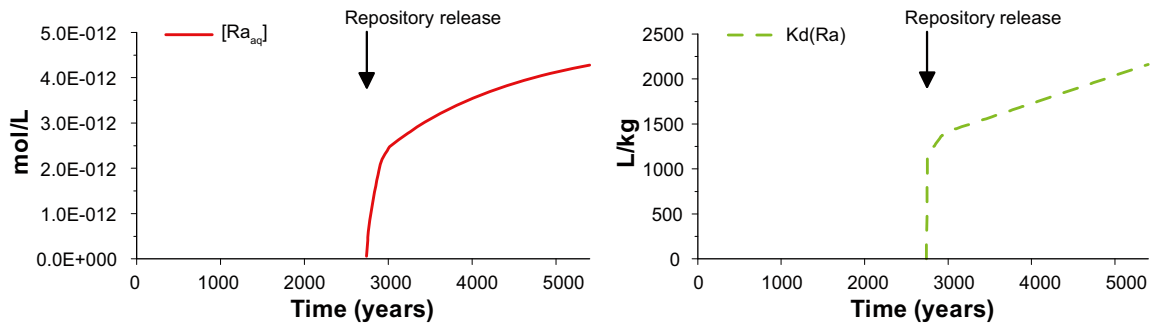


**Figure 6-5.** Evolution of aqueous concentration of Ra and the respective  $K_d$  value, along the simulation time. Monitoring point:  $X=20.1$  m;  $Y=0.2$  m (close to the deep groundwater inflow point).

The range of  $K_d$  values obtained for Ra, from model outputs (600 to 3,600 L/kg, see Figure 6-6) falls in the variability range reported in /OECD 1992/ (between 5 and 30,000 L/kg in sandy to clayey sediments).

### 6.2.2 Reference case #2: The clay system

As already described for reference case #1, the more significant changes in  $K_d$  are expected in the area close to the deep groundwater inflow point and at the beginning of the simulation period, when major geochemical changes occur (Figure 6-7). Also, no isotopic fractionation is introduced by the labelling of repository derived radionuclides.

The naturally occurring concentrations of Sr, Cs and U in the clay porewater are considerably lower than the concentrations of  $^{RD}Sr$ ,  $^{RD}Cs$ , and  $^{RD}U$ , derived from repository release. Therefore, in the vicinity of the deep groundwater inflow, the concentration of repository-derived radionuclides exceeds that of naturally occurring radionuclides (Figure 6-7).

In Figure 6-7 it is seen that when repository-derived uranium is introduced in the clay system, the total concentration of uranium ( $^{RD}U$  + natural U) increases, despite that the concentration of natural uranium in the monitoring point slightly decreases. This increase in total uranium concentration leads to the precipitation of amorphous uraninite, decreasing the concentration of natural uranium.

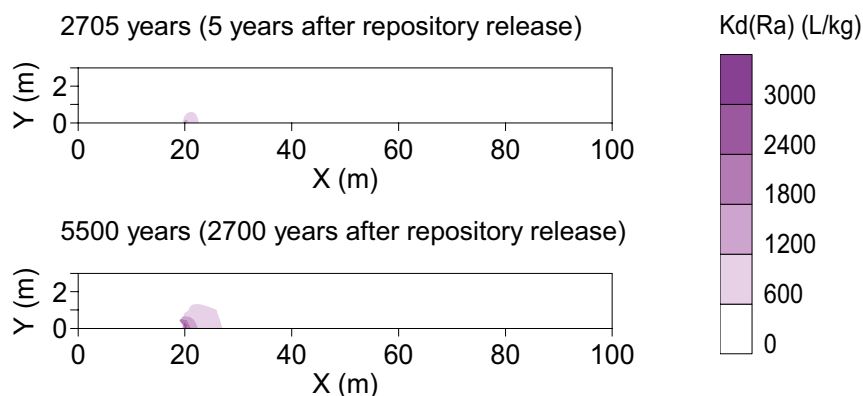


**Figure 6-6.** Predicted evolution of  $K_d(Ra)$  along the simulation time. Ra is readily retained via co-precipitation in a  $(Ba,Ra)SO_4$  solid solution, in the vicinity of the deep groundwater inflow point, so that Ra is not dispersed through the solid phase of the remaining domain. In the area where no Ra is retained in the solid phase,  $K_d$  value is null.

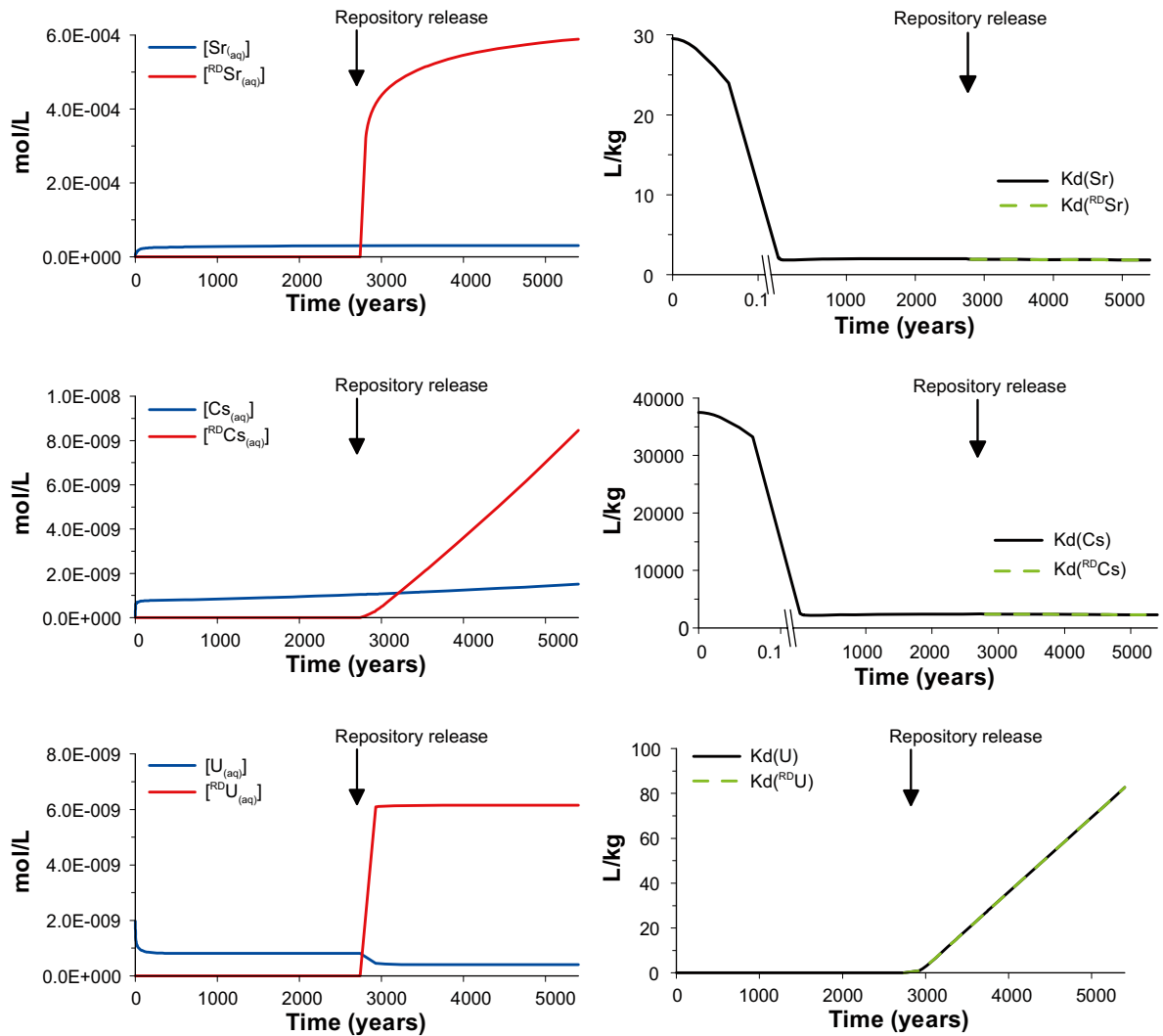


**Figure 6-7.** Predicted evolution of aqueous concentration of natural (Sr, Cs, and U) and repository-derived ( $^{RD}Sr$ ,  $^{RD}Cs$ , and  $^{RD}U$ ) radionuclides, and the respective  $K_d$  value, along the simulation time. Although the concentrations of natural and repository-derived radionuclides are considerably different, the  $K_d$  value for each pair is the same, meaning that no isotope fractionation occurs. Monitoring point:  $X= 9.9$  m;  $Y= 0.2$  m (close to the deep groundwater inflow point).

Since there is no uranium minerals precipitated in the system prior to repository release, and thereafter amorphous uraninite precipitates (containing both  $^{RD}U$  and natural U) until the end of the simulation,  $K_d(U)$  and  $K_d(^{RD}U)$  increase significantly following a linear trend from the moment of repository release. Because the aqueous concentration of uranium becomes constant once uraninite starts to precipitate, and precipitated uranium increases,  $K_d(U)$  and  $K_d(^{RD}U)$  increase linearly.

The inflow of the deep groundwater in the clay deposit leads to a decrease of the  $K_d$  of Sr from an homogeneous value of 35 to an heterogeneous  $K_d(Sr)$  distribution that ranges from 2 L/kg close to deep groundwater inflow point to 35 L/kg in the area far from the deep groundwater inflow (Figure 6-8), meaning that the solid concentration/aqueous concentration ratio decreases.

Deep groundwater has a strontium concentration higher than the clay deposit, and its intrusion leads to an enrichment of Sr in the illite and  $(Ca,Sr)CO_3$  solid solution, but at the same time mixing of clay porewater with deep groundwater occurs which increases aqueous strontium concentration. Therefore, if  $K_d(Sr)$  decreases along time, in the area affected by deep groundwater intrusion, it means that the increment of the aqueous concentration of Sr is more important than the incorporation of Sr in the solid phase, as already observed for the till system.

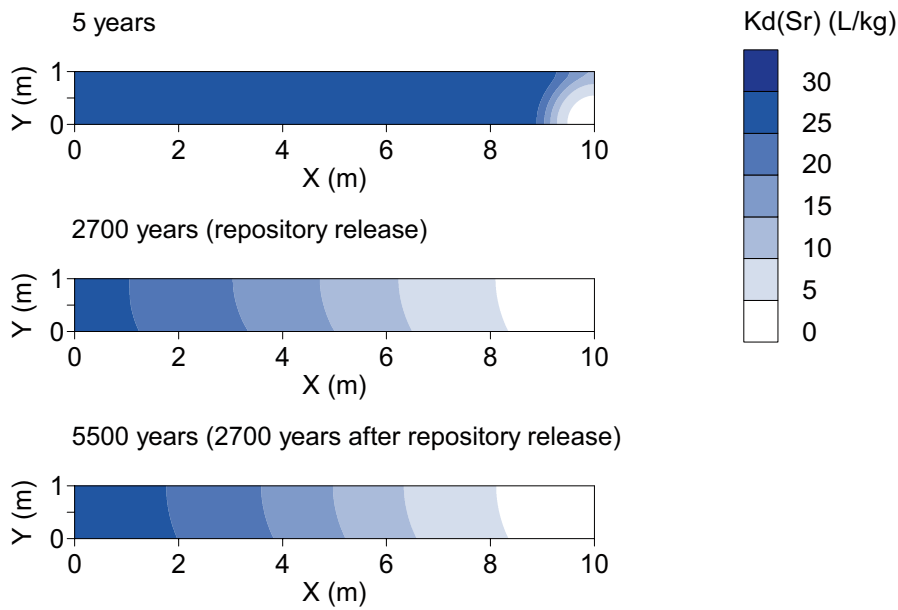


**Figure 6-8.** Predicted evolution of  $K_d(\text{Sr})$  along the simulation time. Major changes in  $K_d$  occur at the beginning of the simulation period.

Figure 6-9 shows the evolution of  $K_d$  for Cs, along the simulation time, in the clay system. The inflowing deep groundwater has a much higher caesium concentration than the clay deposit which leads to an efficient retention of Cs in the FES of illite. Although this retention is important, the increment of the aqueous concentration of caesium is higher than the increment of caesium concentration in the solid phase, and therefore  $K_d(\text{Cs})$  decreases along time.

Before the simulation of repository release, U is not retained in the solid phase of the clay deposit, and therefore  $K_d(\text{U})$  is null. After repository release, the inflow of an uranium-enriched deep groundwater leads to the precipitation of  $\text{UO}_2 \cdot 2\text{H}_2\text{O}(\text{am})$ . From this time, the inflow of the deep groundwater in the clay deposit leads to an increase of the  $K_d$  of U from 0 to 480 L/kg in the vicinity of deep groundwater inflow point (Figure 6-10).

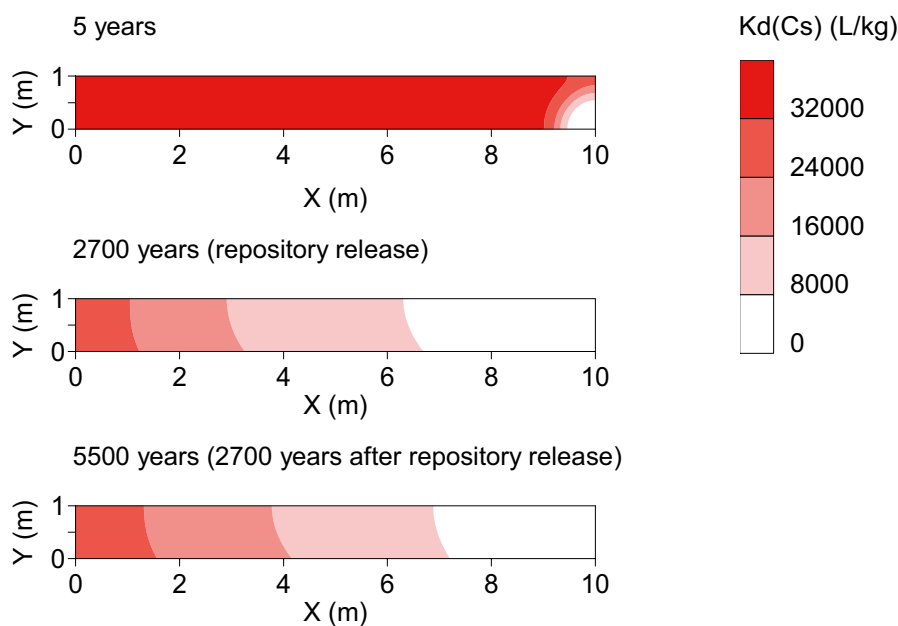


**Figure 6-9.** Predicted evolution of  $K_d(\text{Cs})$  along the simulation time.



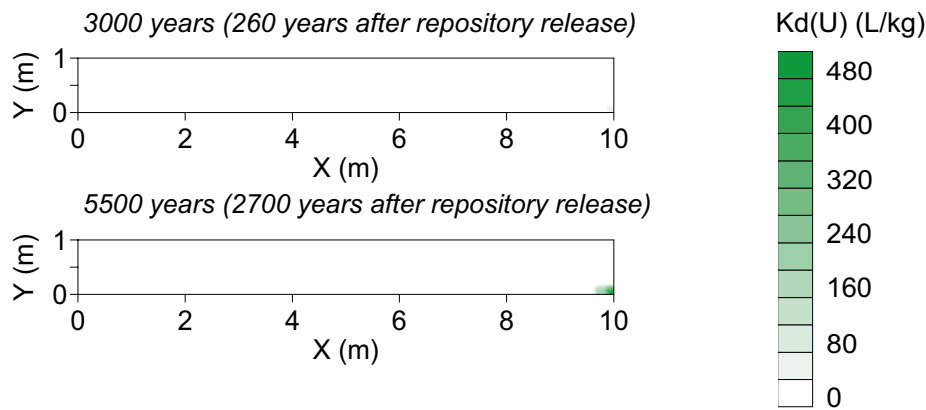


**Figure 6-10.** Predicted evolution of  $K_d(U)$  along the simulation time.

The clay porewater is naturally undersaturated in barite ( $SI = -1.26$ ), and although deep groundwater has a relatively high  $SO_4^{2-}$  concentration, its intrusion does not allow the saturation of the clay porewater on barite. Therefore, Ra is not retained in the solid phase of the clay system.

### 6.3 Application of $K_d$ -based numerical models in the near-surface deposits at Forsmark

$K_d$ -based numerical simulations have been performed using the same domains as in the reactive transport models. These simulations are done for comparative purposes, i.e. to check whether these numerical models are able to generate the same results as the reactive transport simulations previously developed.

$K_d$ -based numerical models have been applied only to those radionuclides that naturally occur in the solid phase of the modelled near-surface deposits. In the till domain, only strontium, caesium and uranium are present in the solid phase of the till deposit prior to the simulation of repository release, and therefore a  $K_d$  characteristic of the till deposit may be estimated for these radionuclides.

In the clay system, only strontium and caesium are initially present in the solid phase, and therefore  $K_d$  models were applied only to these radionuclides.

#### 6.3.1 Reference case #1: The till deposit

Before the inflow of deep groundwater into the till deposit, the modelled system is geochemically homogeneous, and the  $K_d$  of strontium is 20 L/kg. This value is calculated by dividing the concentration of strontium in the solid phase by its concentration in the aqueous phase (both values are outputs of the numerical simulations), as explained in section 6.2. These data are obtained directly from the outputs of the numerical simulations, for every node of the modelled domain. The  $K_d$  value of 20 L/kg has been applied in a  $K_d$ -based model with a time period of 5,500 years.

Figure 6-11 compares the concentration of natural strontium at the discharge area of the till deposit calculated in the reference case (reactive transport model) and in the  $K_d$ -based model. For long periods ( $> 100$  years) the models lead to identical results, but at the beginning of the simulation period the  $K_d$ -based model is not able to reproduce the strontium release predicted by the reference case which results from the major geochemical reactions that occur in this period.

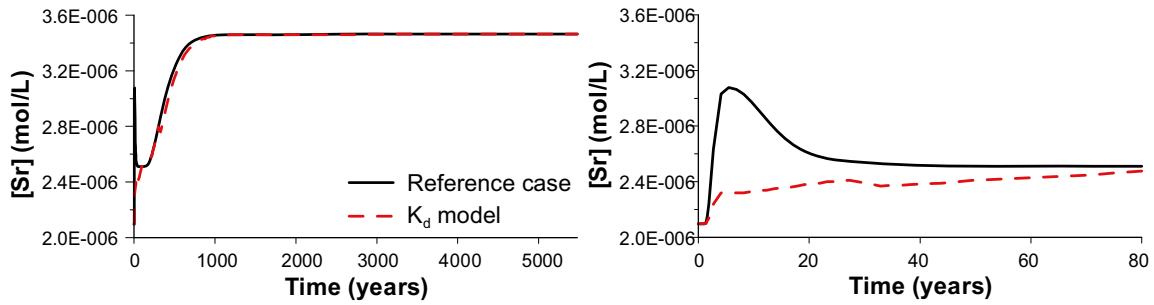


**Figure 6-11.** Predicted evolution of natural strontium concentration calculated in the reference case (reactive transport model) and in the  $K_d$ -based model at the discharge area of the till deposit (Monitoring point:  $X=80$  m;  $Y=3$  m). The initial strontium concentration predicted by both models is  $2.1 \times 10^{-6}$  mol/L.

The  $K_d$  of caesium in the homogeneous till domain, before the inflow of deep groundwater, is 7,950 L/kg. This value has been applied in a  $K_d$ -based model. The results of the  $K_d$ -based model show that the caesium concentration at the discharge area is stable along the whole simulation, while in the reactive transport simulations caesium concentration increases during the first 20 years, and then stabilizes until the end of the simulation (Figure 6-12).

The  $K_d$  of uranium in the homogeneous till domain, before the inflow of deep groundwater, is 114 L/kg. This value has been applied in a  $K_d$ -based model. In Figure 6-12, natural uranium concentration at the discharge area of the till deposit calculated using the reactive transport model is compared with the results of the  $K_d$ -based model. At the discharge area, the  $K_d$ -based model predicts a stable uranium concentration along the whole simulation, whereas in the reactive transport model uranium concentration is affected by the geochemical processes that occur in the first 50 years. At longer simulation times, uranium concentration stabilizes in a slightly lower concentration value than the  $K_d$ -based model.

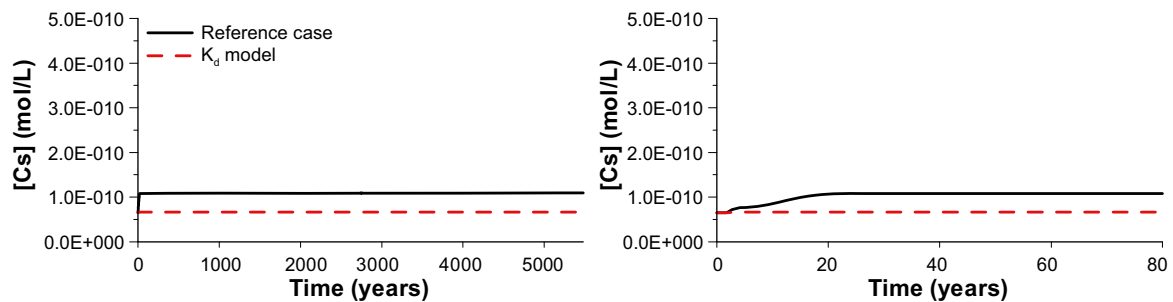


**Figure 6-12.** Predicted evolution of natural caesium concentration calculated in the reference case (reactive transport model) and the  $K_d$ -based model, at the discharge area of the till deposit (Monitoring point:  $X=80$  m;  $Y=3$  m). The initial caesium concentration predicted by both models is  $6.5 \times 10^{-11}$  mol/L.

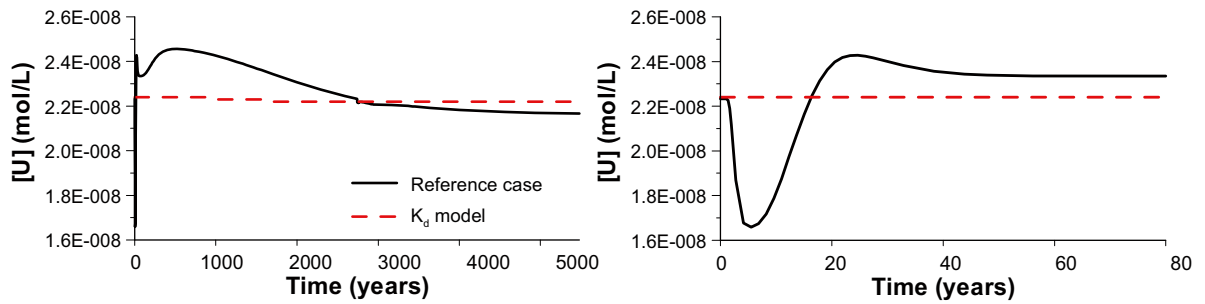


**Figure 6-13.** Predicted evolution of natural uranium concentration calculated in the reference case (reactive transport model) and the  $K_d$ -based model, at the discharge area of the till deposit (Monitoring point:  $X=80$  m;  $Y=3$  m). The initial uranium concentration predicted by both models is  $2.2 \times 10^{-8}$  mol/L.

### 6.3.2 Reference case #2: The clay deposit

Before the intrusion of deep groundwater into the clay deposit, the  $K_d$  of strontium is 30 L/kg. This value has been applied in a  $K_d$ -based model, for the clay system. This value is slightly higher than the  $K_d$  value obtained for strontium in the till deposit, due to the higher content of illite in the clay deposit.

In Figure 6-14 the natural strontium concentration at the discharge area is plotted from data of the reactive transport and  $K_d$ -based models. For long periods ( $> 4,000$  years) both models provide similar results. However, at the beginning of the simulation period the  $K_d$ -based model is not able to reproduce the strontium release resulting from the major geochemical reactions that occur in this period.

Before the inflow of deep groundwater, the  $K_d$  of caesium in the homogeneous clay domain is 37,500 L/kg. This value has been applied in a  $K_d$ -based model. The concentration of caesium at the discharge area, calculated using the  $K_d$  approach differs significantly from that obtained in the reactive transport model (Figure 6-15). In the  $K_d$ -based model, caesium concentration is stable along the whole simulation, while in the reactive transport model this concentration increases at the beginning of reactive transport, and then stabilizes in a higher concentration value than in the  $K_d$ -based model.

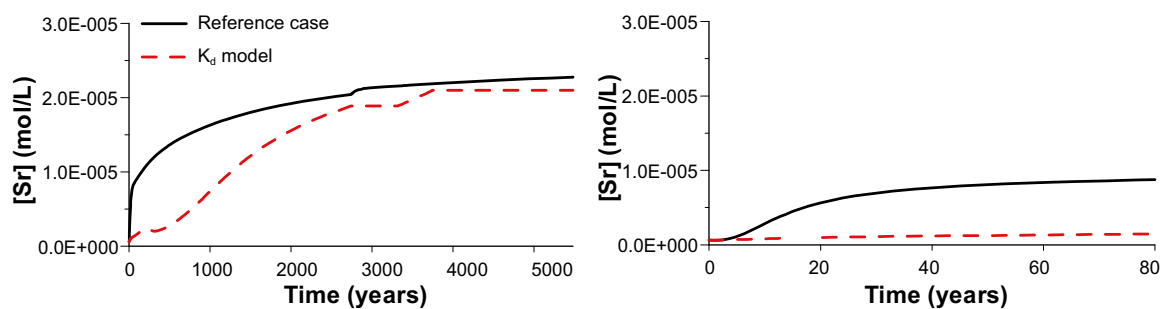


**Figure 6-14.** Predicted evolution of natural strontium concentration calculated in the reference case (reactive transport model) and the  $K_d$ -based model, at the discharge area of the clay deposit (Monitoring point:  $X=10$  m;  $Y=1$  m). The initial strontium concentration predicted by both models is  $6.2 \times 10^{-7}$  mol/L.

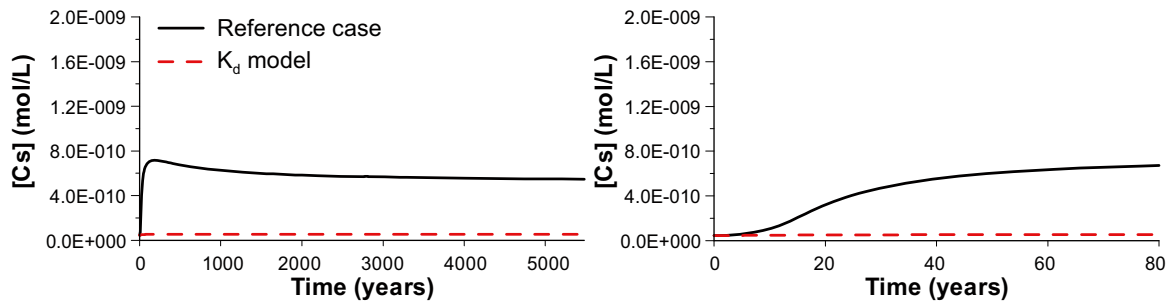


**Figure 6-15.** Predicted evolution of natural caesium concentration calculated in the reference case (reactive transport model) and the  $K_d$ -based model, at the discharge area of the clay deposit (Monitoring point:  $X=10$  m;  $Y=1$  m). The initial caesium concentration predicted by both models is  $4.5 \times 10^{-11}$  mol/L.

The differences observed between the  $K_d$ -based models and the reactive transport models reflect the influence of the  $K_d$  value to be applied in the  $K_d$ -based models. In a  $K_d$ -based model a single  $K_d$  value is used in the calculations, while in the reactive transport simulations different  $K_d$  values can be calculated at different locations within the modelled domain. The larger the range of  $K_d$  values calculated from the reactive transport simulations, the larger the differences between  $K_d$ -based models and reactive transport models.

This is especially significant in the case of Cs for the clay system, as shown in Figure 6-9, where differences of calculated  $K_d$  values are up to 4 orders of magnitude. These differences reflect the difficulty of applying a single  $K_d$  value, obtained from an homogeneous system, to a simulation where it is imposed an important change, like the increment of radionuclide concentration that was used to simulate repository release.

It is seen that only for Sr in the till system, the  $K_d$ -based model is able to reach the same results as the ones attained in the reactive transport models, at the end of the simulation period. From the attained results, it is concluded that the inflow of deep groundwater induces remarkable geochemical changes compared to the initial geochemical state of each system.

## 7 Conclusions

The main objective of the work presented in this report has been the refinement of the geochemical initial and boundary conditions of the numerical models developed in /Grandia et al. 2007/, in order to approach the natural occurring geochemical conditions of the near-surface systems present at Forsmark. In addition, a sensitivity analysis of the key geochemical processes that influence the mobility of the studied radionuclides has also been developed.

The refinement of the geochemical conditions and setup of the alternative cases for the sensitivity analysis is based on site specific data from the SKB database of Forsmark v.1.2 Site descriptive model. An important effort has been devoted to construct a sound conceptual model based on the present-day state-of-the-art knowledge of thermodynamic and geochemical behaviour of radionuclides.

In /Grandia et al. 2007/ it was concluded that Quaternary deposits in Forsmark are able to effectively retain radionuclides transferred from deep bedrock. The results of the reactive transport model indicate that near-surface systems at Forsmark constitute a geochemical reactive barrier able to retain radionuclides by several key processes.

Hydraulic parameters, namely diffusion coefficient and dispersivities, are subject to some degree of uncertainty. A sensitivity analysis should be developed in order to assess the influence of the values of these parameters on the results of the numerical simulations.

The simulation of the till and clay systems during 2,700 years with the natural concentrations of strontium, caesium, uranium, and the other solutes that characterize till porewater, clay porewater and deep groundwater, allowed both modelled domains to reach a relatively stable geochemical state. This geochemical steady state reflects more closely the natural occurring conditions of the till and clay deposits that are being modelled.

During the approach to the geochemical steady state, it is seen that the inflow of deep groundwater in the till deposit leads to a considerable increment of strontium and caesium concentrations at the discharge area, due to mixing of deep groundwater and till porewater, and also to the gradual decrease of retention capacity of the till domain. On the other hand, natural uranium concentration increases after the advective travel time of 5 years due to ferrihydrite dissolution, triggered by deep groundwater inflow. Thereafter, the concentration of uranium progressively decreases to a value similar to the initial uranium concentration in the till porewater.

In the clay system, the approach to the geochemical steady state, leads to an increment of strontium and caesium concentrations, and a decrease of uranium concentration at the discharge area. The increase of strontium and caesium concentrations is due to the combined effect of mixing between deep groundwater and clay porewater, and geochemical reactions that influence the mobility of both radionuclides. On the other hand, the decrease of uranium concentration is exclusively due to dilution, since no geochemical reactions involve uranium during the approach to the geochemical steady state of the clay deposit.

After the approach to the geochemical steady state, repository release is simulated by increasing the concentration of strontium, caesium, uranium, and radium in the inflowing deep groundwater.

In the till and clay deposits, the simulation of repository release leads to a remarkable increment of strontium concentration at the respective discharge areas, which reflects the combined effect of mixing and the relatively limited capacity of illite and  $(Ca,Sr)CO_3$  solid solution to retain the added strontium.

Uranium, caesium and radium releases from the till deposit are slightly increased after repository release. The relatively small increase of uranium concentration is due to the interaction between three processes: (1) mixing of deep groundwater affected by repository release and till porewater; (2) release of uranium into solution due to dissolution of ferrihydrite; (3) and adsorption of uranium to the remaining moles of ferrihydrite. On the other hand, the relatively small increment of caesium concentration is mainly due to an effective retention of this radionuclide in the solid phase of the till deposit. Finally, the small increment of radium concentration, at the discharge area of the till deposit, is due to the combined effect of dilution and retention of radium via precipitation of  $(\text{Ba,Ra})\text{SO}_4$  solid solution.

After repository release, the increment of caesium and uranium concentrations at the discharge area of the clay deposit is relatively small. In the case of caesium, the observed small increment is mainly due to an effective retention of this radionuclide in the illite interlayer, while for uranium, it is due to the low uranium concentration gradient between clay porewater and deep groundwater affected by repository release, and the retention of uranium via precipitation of amorphous uraninite. The evolution of radium release from the clay deposit after repository release is exclusively attributed to mixing of deep groundwater and clay porewater, since no retention of radium occurs in the solid phase of the clay system.

The sensitivity analysis developed for strontium in the till deposit reveals that the range of geochemical variability tested, does not influence much the strontium retention in the till deposit, while for caesium, when a lower CEC is considered, the till deposit becomes progressively unable to retain natural and repository-derived caesium.

The sensitivity analysis developed for strontium in the clay deposit reveals that when a CEC of 20 meq/L is considered, the retention capacity of repository-derived strontium progressively decreases, at the end of the simulation time. In the sensitivity analysis developed for caesium, it is seen that a lower CEC leads to a lower release of natural caesium from the Type II sites of illite during the approach to the geochemical steady state. After repository release, the lower CEC case leads to higher release of repository-derived caesium, due to the a lower density of FES of illite.

The sensitivity analysis developed for uranium reveals that higher concentrations of humic acids in the clay porewater impede precipitation of amorphous uraninite, leading to higher release of uranium. When no humic acids are present, other aqueous complexes are favoured, like carbonate and sulphate complexes, and, contrary to what would be expected  $^{238}\text{U}$  release increases. Finally, when siderite precipitation is not allowed, the slightly higher  $\text{pH}$  of the clay porewater inhibits the precipitation of amorphous uraninite, leading to higher concentration of  $^{238}\text{U}$  at the discharge area.

After repository release, the quantitative assessment of retention efficiency of the till system reveals that repository-derived caesium is the most effectively retained radionuclide (100% retention efficiency), while retention of repository-derived strontium and uranium becomes progressively lower. Radium retention decreases during the first years after repository release, and then approaches a steady state of 30% retention efficiency.

In the clay system, the quantitative assessment of retention efficiency after repository release reveals that repository-derived caesium is readily retained in the solid phase (100% retention efficiency). Retention of repository-derived strontium decreases sharply along the simulation time, and the retention efficiency for repository-derived uranium quickly reaches a stable value of 50%. Radium is not retained in the solid phase of the clay system, since barite saturation is not reached during the simulation time.

The distribution coefficients ( $K_d$ ) calculated for the four radionuclides under study, from the outputs of reactive transport simulations developed for the till and clay systems, are in the range of  $K_d$  values reported for these radionuclides, which reflects the reliability of the numerical models developed here.

In the till deposit,  $K_d$  of strontium is between 10 and 20 L/kg,  $K_d$  of caesium is between 1,500 and 8,000 L/kg,  $K_d$  of uranium is between 90 and 115 L/kg, and  $K_d$  of radium is between 0 and 3,400 L/kg. In the clay deposit,  $K_d$  of strontium is between 2 and 30 L/kg,  $K_d$  of caesium is between 1,500 and 37,500 L/kg, and  $K_d$  of uranium is between 0 and 450 L/kg. The distinct  $K_d$  ranges for each radionuclide and in each modelled domain reflect the different geochemical processes that retain each radionuclide in the solid phase, and the different geochemical conditions of the till and clay systems.

The spatial and temporal evolution of  $K_d$  predicted by the reactive transport simulations reveals that, although the added radionuclides are retained in the solid phase,  $K_d$  values of these radionuclides decrease in the area affected by deep groundwater intrusion with respect to the initially homogeneous till and glacial clay domains. The local equilibrium calculations developed for each time step lead to a retention of the added radionuclides in the solid phase that is lower than the increment of these radionuclides in the aqueous phase. The accumulated difference between the amount of radionuclides retained in the solid phase and the concentration of these radionuclides in the aqueous phase becomes wider with time, leading to a decrease of  $K_d$  in the area affected by deep groundwater inflow.

The application of  $K_d$ -based models as an alternative to reactive transport models reveals that only for longer periods of simulation (after the approach to the geochemical steady state)  $K_d$ -based models lead to similar results as the ones attained in the reactive transport models. At the beginning of the simulations, when major geochemical reactions occur and influence radionuclides partitioning  $K_d$ -based models are unable to reproduce the evolution of radionuclides concentrations. It is concluded that  $K_d$ -based models should be applied when minor geochemical changes in the system are expected.

## 8 References

- Andersson E, Tudorancea M-M, Tudorancea C, Brunberg A-K, Blomqvist P, 2003.** Water chemistry, biomass and production of biota in Lake Eckarfjärden during 2002. SKB R-03-27, Svensk Kärnbränslehantering AB.
- Appelo C-A-J, Postma D, 2005.** Geochemistry, groundwater and pollution. A.A. Balkema Publishers. The Netherlands.
- Blount C-W, 1997.** Barite solubilities and thermodynamic quantities up to 300°C and 1,400 bars. *American Mineralogist*, 62, 942–957.
- Bradbury M-H, Baeyens B, 2000.** A generalised sorption model for the concentration dependent uptake of caesium by argillaceous rocks. *Journal of Contaminant Hydrology*, 42, 141–163.
- Bruno J, Sandino A, 1989.** The solubility of amorphous and crystalline schoepite in neutral to alkaline aqueous solutions. *Mat. Res. Soc. Symp. Proc.*, 127, 871–878.
- Bruno J, Stumm W, Wersin P, Brandberg F, 1992.** On the influence of carbonate in mineral dissolution: Part 1. The thermodynamics and kinetics of hematite dissolution in bicarbonate solutions at T=25°C. *Geochimica et Cosmochimica Acta*, 56, 1139–1148.
- Casas I, Bruno J, Cera E, Finch R-J, Ewing R-C, 1997.** Characterization and dissolution behaviour of a becquerelite from Shinkolobwe, Zaire. *Geochimica et Cosmochimica Acta*, 61, 3879–3884.
- Choppin G-R, Shanbhag P-M, 1981.** Binding of calcium with humic acid. *J. Inorg. Nucl. Chemistry*, 43, 921–922.
- Cole T, Bidoglio G, Soupioni M, O’Gorman M, Gibson N, 2000.** Diffusion mechanisms of multiple strontium species in clay. *Geochimica et Cosmochimica Acta*, 64, 385–396.
- Cox J-D, Wagman D-D, Medvedev V-A, 1989.** CODATA Key Values for Thermodynamics, Hemisphere Publishing Corp., New York, USA.
- Davis J A, Coston J A, Kent D B, Fuller C C, 1998.** Application of the surface complexation concept to complex mineral assemblages. *Environ. Sci. Technol.*, 32, 2820–2828.
- Duro L, Grivé M, Cera E, Domènech C, Bruno J, 2006a.** Update of a thermodynamic database for radionuclides to assist solubility limits calculation for performance assessment. SKB TR-06-17, Svensk Kärnbränslehantering AB.
- Duro L, Grivé M, Cera E, Gaona X, Domènech C, Bruno J, 2006b.** Determination and assessment of the concentration limits to be used in SR-Can. SKB TR-06-32, Svensk Kärnbränslehantering AB.
- Fuller C-C, Bargar J-R, Davis J-A, Piana M-J, 2002.** Mechanisms of uranium interactions with hydroxyapatite: Implications for groundwater remediation. *Environ. Sci. Technol.*, 36, 158–165.
- Guillaumont R, Fanghänel J, Neck V, Fuger J, Palmer D-A, Grenthe I, Rand M-H, 2003.** Chemical Thermodynamics 5. Update on the Chemical Thermodynamics of Uranium, Neptunium, Plutonium, Americium and Technetium. NEA OECD, Elsevier.
- Grandia F, Sena C, Arcos D, Molinero J, Duro L, Bruno J, 2007.** Quantitative assessment of radionuclide retention in the near-surface system at Forsmark. Development of a reactive transport model using Forsmark 1.2 data. SKB R-07-64, Svensk Kärnbränslehantering AB.



- Grandia F, Merino J, Bruno J, 2008.** Assessment of the radium-barium co-precipitation and its potential influence on the solubility of Ra in the near-field. SKB TR-08-07, Svensk Kärnbränslehantering AB.
- Grivé M, 2005.** The linkage between uranium, iron and carbon cycling. Processes at interfaces: evidences from combined solution chemical and spectroscopic studies. PhD. Thesis, Universitat Politècnica de Catalunya, 341 pp.
- Hedenström A, 2004.** Forsmark site investigation: Investigation of marine and lacustrine sediment in lakes. Stratigraphical and analytical data. SKB P-04-86, Svensk Kärnbränslehantering AB.
- Hummel W, Berner U, Curti E, Pearson F J, Thoenen T, 2002.** Nagra/PSI Chemical Thermodynamic Data Base 01/01. ISBN: 1-58112-620-4, 565 pp.
- Johansson P-O, Werner K, Bosson E, Berglund S, Juston J, 2005.** Description of climate, surface hydrology, and near-surface hydrogeology. Preliminary site description. Forsmark area – version 1.2. SKB R-05-06, Svensk Kärnbränslehantering AB.
- Kipp K-L, 1997.** Guide to the revised heat and solute transport simulator HST3D-Version 2. U.S. Geological Survey Water-Resources Investigations Report, 97-4157, 149 pp.
- Krestou A, Xenidis A, Panias D, 2004.** Mechanism of aqueous uranium (VI) uptake by hydroxyapatite. *Minerals Engineering*, 17, 373–381.
- Köhler S J, Dufaud F, Oelkers E H, 2003.** An experimental study of illite dissolution kinetics as a function of pH from 1.4 to 12.4 and temperature from 5 to 50°C. *Geochimica et Cosmochimica Acta*, 67-19, 3583–3594.
- Langmuir D, Riese A-C, 1985.** The thermodynamic properties of radium. *Geochimica et Cosmochimica Acta*, 49, 1593–1601.
- Li W-C, Victor D-M, Chakrabati C-L, 1980.** Effect of pH and uranium concentration on interaction of uranium(VI) and uranium (IV) with organic ligands in aqueous solutions. *Anal. Chem.*, 52, 520–523.
- NEA, 2005.** NEA sorption project – Phase II. Interpretation and prediction of radionuclides sorption onto substrates relevant for radioactive waste disposal using thermodynamic sorption models. *Radioactive Waste Management*. OECD publications.
- Nguyen N-S, Silva R-J, Weed H-C, Andrews Jr J-E, 1992.** Standard Gibbs free energies of formation at the temperature 303.15K of four uranyl silicates: soddyite, uranophane, sodium boltwoodite and sodium weeksite. *J. Chem Thermodyn*, 24, 1, 359–376.
- Nordstrom D-K, Plummer L-N, Langmuir D, Busenberg E, May H-M, Jones B-F, Parkhurst D-L, 1990.** Revised chemical equilibrium data for major water-mineral reactions and their limitations. In R.L. Bassett and D. Melchior, (eds.), *Chemical modelling in aqueous systems II: Washington D.C., American Chemical Society Symposium Series 416*, Chapter 31, 398–413.
- OECD, 1992.** Radionuclide sorption from the safety evaluation perspective. Disposal of radioactive waste. Proceedings of the Nuclear Energy Agency workshop organized by the OECD.
- Outridge P-M, Stern G-A, Hamilton P-B, Percival J-B, McNeely R, Lockhart W-L, 2005.** Trace metal profiles in the varved sediment of an Arctic lake. *Geochimica et Cosmochimica Acta*, 69, 4881–4894.
- Parkhurst D-L, Appelo C-A-J, 1999.** User's guide to PHREEQC (version 2)- A computer program for speciation, batch-reaction, one-dimensional transport and inverse geochemical calculations. U.S. Geological Survey Water Resources investigations report 99-4259.

- Parkhurst D-L, Kipp K-L, Engesgaard P, Charlton S-R, 2004.** PHAST – A program for simulating ground-water flow, solute transport, and multicomponent geochemical reactions. U.S. Geological Survey Techniques and Methods 6-A8, 154 pp.
- Percival J-B, Hunt P, Wyergangs M, 2001.** Mineralogical investigations of Canadian till and lake- and stream-sediment reference materials: Part 1. Standardized X-ray diffraction and scanning electron microscope methods. Geol. Surv. Can. Curr. Res. 2001-E9, 8 p.
- Pérez I, Casas I, Torrero M-E, Cera E, Duro L, Bruno J, 1997.** Dissolution studies of soddyite as long-term analogue of oxidative alteration of spent nuclear fuel matrix. Mater. Res. Soc. Symp. Proc., 465, 565–572.
- Plummer L-N, Busenberg E, 1982.** The solubilities of calcite, aragonite and vaterite in CO<sub>2</sub>-H<sub>2</sub>O solutions between 0°C and 90°C, and an evaluation of the aqueous model for the system CaCO<sub>3</sub>-CO<sub>2</sub>-H<sub>2</sub>O. *Geochimica et Cosmochimica Acta* 46–6: 1011–1040.
- Poinssot C, Baeyens B, Bradbury M-H, 1999.** Experimental and modelling studies of caesium sorption on illite. *Geochimica et Cosmochimica Acta*, 63, 3217–3227.
- Robbie R-A, Waldbaum D-R, 1968.** Thermodynamic properties of minerals and related substances at 298.15°K (25°C) and one atmosphere (1.013bars) pressure and at high temperatures, U.S. Geological Survey Bulletin, 1259.
- SKB, 2005a.** Description of surface systems. Preliminary site description. Forsmark area – version 1.2. SKB R-05-03, Svensk Kärnbränslehantering AB.
- SKB, 2005b.** Preliminary site description. Forsmark area – version 1.2. SKB R-05-18, Svensk Kärnbränslehantering AB.
- SKB, 2006.** Long-term safety for KBS-3 repositories at Forsmark and Laxemar – a first evaluation. Main Report of the SR-Can project. SKB TR-06-09, Svensk Kärnbränslehantering AB.
- Seaman J-C, Meehan T, Bertsch P-M, 2001.** Immobilization of cesium-137 and uranium in contaminated sediments using soil amendments. *Journal of Environmental Quality*, 30, 1206–1213.
- Shanbhag P-M, Choppin G-R, 1981.** Binding of uranyl by humic acid. *J. Inorg. Nucl. Chem.* 43, 3369–3372.
- Sohlenius G, Bergman T, Snäll S, Lundin L, Lode E, Stendahl J, Riise A, Nilsson J, Johansson T, Göransson M, 2006.** Oskarshamn site investigation. Soils, Quaternary deposits and bedrock in topographic lineaments situated in the Laxemar subarea. SKB P-06-121, Svensk Kärnbränslehantering AB.
- Stumm W, Morgan J-J, 1996.** Aquatic Chemistry. John Wiley and Sons.
- Tesoriero A J, Pankow J F, 1996.** Solid solution partitioning of Sr<sup>2+</sup>, Ba<sup>2+</sup>, and Ca<sup>2+</sup> to calcite. *Geochimica et Cosmochimica Acta*, 60-6, 1053–1064.
- Tournassat C, Gailhanou H, Cruzet C, Braibant G, Gautier A, Lassin A, Blanc P, Gaucher E-C, 2007.** Two cation exchange models for direct and inverse modelling of solution major cation composition in equilibrium with illite surfaces. *Geochimica et Cosmochimica Acta*, 71, 1098–1114.
- Tröjbom M, Söderbäck B, 2006.** Chemical characteristics of surface systems in the Forsmark area. Visualisation and statistical evaluation of data from shallow groundwater, precipitation, and regolith. SKB R-06-19, Svensk Kärnbränslehantering AB.
- Waite T-D, Davis J-A, Payne T-E, Waychunas G-A, Xu N, 1994.** Uranium (VI) adsorption to ferrihydrite: Application of a surface complexation model. *Geochimica et Cosmochimica Acta*, 58, 5465–5478.
- Van Geen A, Robertson A-P, Leckie J-O, 1994.** Complexation of carbonate species at the goethite surface: Implications for adsorption of metal ions in natural waters. *Geochimica et Cosmochimica Acta*, 58, 2073–2086.